

**PLASTIC OPTICAL FIBER COATED WITH ZINC OXIDE
FOR RELATIVE HUMIDITY SENSING APPLICATION**

ZURAIDAH BINTI HARITH

**INSTITUTE FOR ADVANCE STUDIES
UNIVERSITY OF MALAYA
KUALA LUMPUR**

2019

**PLASTIC OPTICAL FIBER COATED WITH ZINC
OXIDE FOR RELATIVE HUMIDITY SENSING
APPLICATION**

ZURAI DAH BINTI HARITH

**THESIS SUBMITTED IN FULFILMENT OF THE
REQUIREMENTS FOR THE DEGREE OF DOCTOR OF
PHILOSOPHY**

**INSTITUTE FOR ADVANCE STUDIES
UNIVERSITY OF MALAYA
KUALA LUMPUR**

2019

UNIVERSITY OF MALAYA
ORIGINAL LITERARY WORK DECLARATION

Name of Candidate: Zuraidah Binti Harith

Matric No: HHE130001

Name of Degree: Doctor of Philosophy

Title of Project Paper/Research Report/Dissertation/Thesis (“this Work”):

Plastic Optical Fiber Coated with Zinc Oxide for Relative Humidity Sensing
Application

Field of Study: Photonics Engineering

I do solemnly and sincerely declare that:

- (1) I am the sole author/writer of this Work;
- (2) This Work is original;
- (3) Any use of any work in which copyright exists was done by way of fair dealing and for permitted purposes and any excerpt or extract from, or reference to or reproduction of any copyright work has been disclosed expressly and sufficiently and the title of the Work and its authorship have been acknowledged in this Work;
- (4) I do not have any actual knowledge nor do I ought reasonably to know that the making of this work constitutes an infringement of any copyright work;
- (5) I hereby assign all and every rights in the copyright to this Work to the University of Malaya (“UM”), who henceforth shall be owner of the copyright in this Work and that any reproduction or use in any form or by any means whatsoever is prohibited without the written consent of UM having been first had and obtained;
- (6) I am fully aware that if in the course of making this Work I have infringed any copyright whether intentionally or otherwise, I may be subject to legal action or any other action as may be determined by UM.

Candidate’s Signature

Date:

Subscribed and solemnly declared before,

Witness’s Signature

Date:

Name:

Designation

PLASTIC OPTICAL FIBER COATED WITH ZINC OXIDE FOR RELATIVE HUMIDITY SENSING APPLICATION

ABSTRACT

In recent years, plastic optical fiber (POF) has been studied and developed in various applications including sensors as POF-based sensors do not require rare materials to develop and they can be employed at room temperature. In this thesis, relative humidity sensor, employing tapered polymethyl methacrylate (PMMA) fiber and microfiber are proposed and demonstrated. The tapered PMMA fibers are fabricated based on chemical etching method while PMMA microfibers are fabricated using a direct drawing technique. For relative humidity measurement, changes in the behavior of the evanescent field passing through the media, whose refractive indices are influenced by the water molecules absorbed or desorbed. To increase the sensitivity of sensor, the probes are coated with Zinc Oxide (ZnO) nanostructures. ZnO nanostructure materials able to provide a suitable platform for developing relative humidity sensor due to its unique properties such as high catalytic efficiency and strong adsorption ability. Subsequently, ZnO is doped with other group III metal, which is Aluminium (Al) as Al doping is more highly conductive due to its close covalent bond length of Al–O to that of Zn–O. ZnO and Al-doped ZnO are grown using both seeded and non-seeded techniques and they are synthesized using the sol–gel and hydrothermal methods. The measurement is based on intensity modulation technique to detect the changes in relative humidity. These nanostructures on the tapered fiber induce changes of the optical properties in response to an external stimulus. Results show that tapered POF with ZnO and Al-doped ZnO nanostructures enables the increase in sensitivity of fiber for detection of changes in relative humidity. The proposed sensor

provides numerous advantages, such as simplicity of design, low cost of production, higher mechanical strength, and is easier to handle compared with silica fiber-optic.

Keywords: Plastic Optical Fiber, ZnO nanostructures, sol-gel method, hydrothermal method, relative humidity sensor.

University of Malaya

SERAT OPTIK PLASTIK BERSALUT ZINK OKSIDA SEBAGAI APLIKASI PENGESAN KELEMBAPAN RELATIF

ABSTRAK

Kebelakangan ini, serat optik plastik (POF) telah dikaji dan dibangunkan dalam pelbagai aplikasi termasuk sebagai pengesan kerana untuk membangunkan pengesan berdasarkan POF tidak memerlukan bahan-bahan yang jarang digunakan dan boleh direkabentuk pada suhu bilik. Dalam tesis ini, pengesan kelembapan relatif, menggunakan gentian serat tirus polymethyl methacrylate (PMMA) dan gentian serat tirus mikrofiber dicadangkan dan ditunjukkan. Gentian serat tirus PMMA yang direka adalah berdasarkan kaedah punaran manakala mikrofiber PMMA dihasilkan menggunakan teknik tarikan secara langsung. Untuk ukuran kelembapan relatif, perubahan dalam ciri medan evanesen melalui media, yang biasan kepekaan indeks dipengaruhi oleh molekul air yang diserap. Untuk meningkatkan kepekaan pengesan, gentian serat tirus dilapisi dengan zink oksida (ZnO) struktur-nano. Bahan struktur-nano ZnO mampu menyediakan platform yang sesuai untuk membangunkan pengesan kelembapan relatif kerana sifat uniknya seperti kecekapan pemangkin tinggi dan keupayaan penjerapan yang tinggi. Kemudian, ZnO dilaburkan dengan logam kumpulan III yang lain, iaitu Aluminium (Al) kerana Al lebih konduktif disebabkan panjang ikatan kovalen Al-O lebih hampir kepada Zn-O. ZnO dan Al dilaburkan. Al dihasilkan menggunakan teknik pembenihan dan bukan pembenihan ZnO dan mereka disintesis menggunakan kaedah sol-gel dan hidroterma. Pengukuran adalah berdasarkan teknik modulasi intensiti untuk mengesan perubahan kelembapan relatif. Struktur-nano pada gentian serat tirus menyebabkan perubahan sifat optik sebagai tindak balas kepada rangsangan luaran. Keputusan menunjukkan bahawa gentian serat tirus POF dengan ZnO dan Al yang dilaburkan dengan Al membolehkan peningkatan sensitiviti

gentian serat tirus untuk mengesan perubahan kelembapan relatif. Pengesan yang dicadangkan memberikan banyak kelebihan, seperti kesederhanaan reka bentuk, kos pengeluaran yang rendah, kekuatan mekanikal yang lebih tinggi, dan lebih mudah dikendalikan berbanding dengan gentian serat silika.

Kata kunci: Serat optik plastik, struktur nano ZnO, kaedah sol-gel, kaedah hidroterma, pengesan kelembapan relatif.

University of Malaya

ACKNOWLEDGEMENTS

In the name of God, the Most Gracious, the Most Merciful

First and foremost, praise be to Allah swt, with His mercy and blessing, I am able to complete my thesis.

Next, I wish to express my utmost gratitude to my supervisor, Prof. Dr. Sulaiman Wadi Harun and co-supervisor, Prof. Datuk Dr. Harith bin Ahmad. These professors are the prominent figures of their field, and I am very fortunate to learn from the best. I am forever indebted to my supervisors and will always value and appreciate their advices and guidance.

I also want to take this opportunity to thank Dr. Malathy Batumalay. She is my mentor, who is also a dearest friend. She was actually the one who literally dragged me to meet her then supervisor. If it wasn't for her 'push', I might still procrastinate in pursuing my study. Thank you so much Malathy, for constantly providing your assistance and tirelessly encouraging me to move forward. Your positive spirit always inspires me, and I hope our research journey together will continue progressively.

Another person that worth to mention here is my lab mate turns dear friend, Dr. Ninik Irawati. Ninik has always been there for me, every time when I need her. She shares her knowledge, reminds me to update my progress report and helps me a lot, yet, wish for nothing in return. I am forever indebted and will cherish all the memories that I have with her.

There are so many other persons who have been helping me during my studies. My lab mates at Photonic Research Center, especially Dr. Hartini, Dr. Husna, Dr. Anas, Quisar, and Hafiz; my best friends, Mazlia and Mastura, who I constantly share all sort of stories; my superiors, Ms. Chen Wan-Yu and Dr. Tezara Cionita, who understand what I have to go through and always provide their support and I also wish to express my

gratitude to University of Malaya staffs, especially to IPS, IAS and Bursary for their assistance and guidance as well as to my examiners for their constructive comments during my proposal and candidature defense.

Last but not least, the most important persons in my life, who are also my support system: my mother, sisters, brother, my two nephews and niece. I might not share much, be it my achievements or struggle during my study time, but they just know. They understand that I have to ‘work’ extra hours during the weekdays as well as the weekends and do not mind taking over some responsibilities when I am tight with my work. To my father and brother, who are no longer around to witness this achievement, I am sure you will be equally proud, and I dedicate this thesis to both of you.

I am truly thankful to all these people and I pray that Allah swt will protect them from any harm and grant them with all the good things in their lives. This PhD journey has taught me a lot and developed me to be a better learner. One thing for sure, I must keep on learning and moving forward, rest if I must, but don’t ever quit.

Thank You

TABLE OF CONTENTS

ABSTRACT.....	iii
ABSTRAK.....	v
Acknowledgements.....	vii
Table of Contents.....	ix
List of Figures.....	xiii
List of Tables.....	xvii
List of Symbols and Abbreviations.....	xviii
List of Appendices.....	xx
CHAPTER 1: INTRODUCTION.....	1
1.1 Background of Plastic Optical Fiber.....	1
1.2 Background on Zinc Oxide (ZnO) nanostructures.....	2
1.3 Motivation of Study.....	3
1.4 Objectives of Study.....	5
1.5 Dissertation Overview.....	5
CHAPTER 2: LITERATURE REVIEW.....	8
2.1 Introduction to Optical Fiber.....	8
2.1.1 Plastic Optical Fiber.....	10
2.1.2 Polymer Microfiber.....	11
2.2 Fiber Optical Sensor.....	15
2.2.1 Sensing Location.....	16
2.2.2 Operating Principle.....	18
2.2.3 Application of fiber optic sensor.....	19
2.3 Tapered fiber.....	21

2.3.1	Tapering of Plastic Optical Fiber	25
2.4	Evanescent wave and refractive index sensing.....	25
2.5	Zinc Oxide (ZnO)	31
2.6	Doping in ZnO.....	35
2.7	Synthesis of ZnO	35
2.7.1	Sol-gel Immersion Method.....	36
2.7.2	Hydrothermal Method	37
2.7.3	Zinc Oxide Nanostructures for Optical Sensor Applications.....	40
2.8	Humidity	41
2.8.1	Humidity Measurement Parameters	42
2.8.2	Relative Humidity Sensor	43

CHAPTER 3: ZINC OXIDE COATED MULTIMODE TAPERED PLASTIC OPTICAL FIBER FOR HUMIDITY SENSOR..... 48

3.1	Introduction	48
3.2	Preparation of tapered POF through chemical etching process.....	50
3.3	Coating of POF with Zinc Oxide nanostructures for relative humidity sensing ...	52
3.3.1	Coating of unseeded Al-Doped ZnO nanostructures onto the tapered POF.....	53
3.3.2	Experimental arrangement for the relative humidity sensing	55
3.3.3	Sensing performance	56
3.4	RH sensor employing tapered POF coated with seeded Al-Doped ZnO	61
3.5	Comparison with RH sensor employing silica microfiber coated with ZnO Nanostructures	66
3.6	Summary.....	72

CHAPTER 4: GROWTH OF ZINC OXIDE NANORODS ON TAPERED PLASTIC OPTICAL FIBERS VIA HYDROTHERMAL TECHNIQUE FOR RELATIVE HUMIDITY SENSOR.....75

4.1 Introduction 75

4.2 Tapered Plastic Optical Fiber 77

4.3 Synthesis of Zinc Oxide Nanorods on Tapered Plastic Optical Fiber..... 79

 4.3.1 ZnO Seeding Procedure..... 80

 4.3.2 Formation of Nucleation Site on POF 82

 4.3.3 Physical Characterization 84

4.4 Experimental Setup for the Humidity Sensor..... 85

4.5 Sensing performance 87

4.6 Summary..... 91

CHAPTER 5: POLYMER MICROFIBER COATED WITH ZNO NANOSTRUCTURES FOR HUMIDITY SENSING..... 93

5.1 Introduction 93

5.2 Fabrication and characterization of PMMA microfiber 94

5.3 PMMA microfiber for relative humidity sensor..... 99

 5.3.1 Preparation of sensor probe 99

 5.3.2 Experimental setup for the RH measurement..... 101

 5.3.3 Performance of the RH sensor..... 102

5.4 PMMA microfiber based humidity sensor with ZnO nanorods coating 104

5.5 Summary..... 110

CHAPTER 6: CONCLUSION AND FUTURE WORKS 112

6.1 Conclusion 112

6.2 Recommendation for future work..... 118

References.....	119
List of Publications and Papers Presented	131

University of Malaya

LIST OF FIGURES

Figure 2.1: Overview of POF	8
Figure 2.2: Different type of optical fiber	9
Figure 2.3: Basic structure of an optical fiber.....	11
Figure 2.4: Total internal reflection in optical fiber.....	11
Figure 2.5: Schematic diagram of electrospinning process	12
Figure 2.6: Illustration of direct drawing a polymer microfiber	14
Figure 2.7: General structure of an optical sensor	16
Figure 2.8: Illustration for (a) extrinsic and (b) intrinsic types of fiber optic sensor.....	17
Figure 2.9: Illustration of a tapered fiber optic	22
Figure 2.10: (a) a stationary flame with fixed pulling stages, (b) a stationary flame with independent pulling stages and (c) a moving flame with independent pulling stages	23
Figure 2.11: Illustration of exponentially decaying evanescent field in the cladding	26
Figure 2.12: Illustration of penetration depth for a fiber	27
Figure 2.13: Illustration of the waist length, L for tapered fiber.....	28
Figure 2.14: Structure of tapered fiber with overlay sensitive material.....	29
Figure 2.15: Schematic diagram of ZnO crystal structures (a) cubic rock salt (B1), (b) cubic zinc blend, and (c) hexagonal wurtzite (B4)	31
Figure 2.16: Wurtzite structure of Zinc Oxide.....	32
Figure 2.17: Example of ZnO of 1D structures.....	33
Figure 2.18: Example of ZnO of 2D structures.....	34
Figure 2.19: Example of ZnO of 3D structures.....	34
Figure 2.20: Reaction pathway for the production of metal oxide nanostructures in the sol-gel method.....	36
Figure 2.21: Classification of Optical Fiber Humidity Sensor	45

Figure 3.1: Microscopic image of the (a) un-tapered PMMA fiber (with diameter of 1 mm) and (b) Tapered PMMA fiber (with diameter of 0.45 mm), with etching technique	51
Figure 3.2: FESEM images of (a) un-doped ZnO nanostructures and (b) Al doped ZnO nanostructures coated onto the tapered POF	54
Figure 3.3: Experimental setup for the proposed relative humidity sensor using a tapered POF coated with un-doped ZnO and Al-doped ZnO nanostructures	56
Figure 3.4: Output voltage against relative humidity for the proposed tapered POF with Al-doped ZnO nanostructure at different doping concentration	57
Figure 3.5: Output voltage against relative humidity for the proposed tapered POF with un-doped ZnO and Al-doped ZnO nanostructure	58
Figure 3.6: FESEM image of Al doped ZnO nanostructures obtained with seeding method	62
Figure 3.7: Output voltage against relative humidity for the proposed tapered POF with seeded Al-doped ZnO nanostructure at different doping concentration	63
Figure 3.8: Output voltage against relative humidity for the proposed tapered POF with un-doped ZnO and Al-doped ZnO nanostructure (non-seeded method)	64
Figure 3.9: FESEM image of ZnO nanostructures coated on silica microfiber.....	67
Figure 3.10: Experimental setup for the proposed RH sensor using a silica microfiber coated with ZnO nanostructures as a probe	68
Figure 3.11: Output voltage against relative humidity for the proposed tapered POF and silica microfiber coated with non-seeded ZnO nanostructure.....	69
Figure 3.12: Output voltage against relative humidity for the proposed tapered POF and silica microfiber coated with seeded ZnO nanostructure.....	70
Figure 4.1: Schematic diagram of tapered fiber.....	78
Figure 4.2: Microscope images of the (a) original un-tapered and (b) tapered POF	78
Figure 4.3: Hydrothermal techniques procedure for synthesis ZnO nanorods on tip of POF	79
Figure 4.4: Process of the preparation of 1 mM ZnO nanoparticle solution.....	80
Figure 4.5: Preparation of the pH-controlled solution using NaOH	81
Figure 4.6: Alkaline process of ZnO nanoparticles solution by NaOH.....	82

Figure 4.7: Dip and dry process	83
Figure 4.8: Drop and dry method in seeding process.....	83
Figure 4.9: Morphology of ZnO nanorods.....	85
Figure 4.10: Morphology of ZnO nanostructures (a) non-seeded method (b) seeded method.....	85
Figure 4.11: FESEM image of ZnO nanorods at higher magnification.....	85
Figure 4.12: Schematic diagram for the proposed humidity sensor.....	87
Figure 4.13: Output voltage against relative humidity for the proposed tapered POF with ZnO nanorods.....	88
Figure 4.14: Performance of proposed sensor for both sol-gel and hydrothermal method	89
Figure 5.1: Schematic illustration of the polymer microfiber fabrication by direct drawing method from molten PMMA. (a) A cylindrical silica fiber is approaching the molten PMMA (b) The fiber tip is immersed into the molten PMMA (c) The fiber conglutinated PMMA is being drawn out. (d) A PMMA microfiber is formed.....	95
Figure 5.2: Microscope image of the fabricated PMMA microfiber (a) PMMA microfiber is formed between the molten PMMA and the fiber tip (b) the middle part of the PMMA microfiber as a 632 nm laser is launched into the microfiber	96
Figure 5.3: PMMA microfibers with three different waist diameters (a) 9 μm (b) 11 μm and (c) 13 μm	97
Figure 5.4: Schematic diagram of an optical waveguiding in a single PMMA microfiber with two ends coupled with silica microfibers.....	98
Figure 5.5: The transmitted output power from the PMMA microfiber against its length	98
Figure 5.6: FESEM image of ZnO nanostructure coated on PMMA microfiber.....	100
Figure 5.7: Experimental setup for humidity sensor using PMMA microfiber	101
Figure 5.8: Output power against relative humidity for PMMA microfiber with and without ZnO nanostructure coating.....	103
Figure 5.9: Repeatability of the sensors	103
Figure 5.10: FESEM image of the PMMA microfiber coated with ZnO nanorods.....	106

Figure 5.11: The output power of the ASE against relative humidity for PMMA microfiber without ZnO nanorods coating for three different runs..... 107

Figure 5.12: The output power of the ASE against relative humidity for PMMA microfiber coated with ZnO nanorods coating for three different runs 108

Figure 5.13: Output power against relative humidity for PMMA microfiber with and without ZnO nanorods coating..... 109

University of Malaya

LIST OF TABLES

Table 2.1: Comparison of extrinsic and intrinsic optical sensor.....	17
Table 2.2: Different microfiber structure.....	20
Table 3.1: Performance of the proposed RH sensor at different doping concentration..	60
Table 3.2: The performance of the proposed RH sensor for un-doped ZnO and Al-doped ZnO	60
Table 3.3: The performance of the proposed RH sensor at different doping concentration	65
Table 3.4: The comparison of performances between seeded ZnO and proposed RH sensor for seeded Al-doped ZnO.....	65
Table 3.5: The comparison of performances between non-seeded and proposed seeded RH sensor for Al-doped ZnO.....	65
Table 3.6: The performance comparison for both RH sensors with non-seeded ZnO....	72
Table 3.7: The performance comparison for both RH sensors with seeded ZnO nanostructure.....	72
Table 4.1: The comparison of performances between sol – gel and hydrothermal method for growing ZnO	91
Table 5.1: Performance of the humidity sensor using PMMA microfiber with and without ZnO nanostructures coating	104
Table 5.2: Performance of the humidity sensor using PMMA microfiber with and without ZnO nanorods coating.....	110
Table 6.1: Morphologies Al-Doped ZnO for different synthetization methods	113
Table 6.2: Morphologies of ZnO for different synthetization methods.....	115
Table 6.3: Overview of the results for the proposed sensors using POF	117
Table 6.4: Overview of the results for the proposed sensors using PMMA Microfiber	117

LIST OF SYMBOLS AND ABBREVIATIONS

For example:

n	:	Refractive index
n_{cl}	:	Refractive index for cladding
n_{co}	:	Refractive index for core
Al	:	Aluminium
ASE	:	Amplified Spontaneous Emission
B	:	Boron
$C_6H_{12}N_4$:	HMTA
$COCl_2$:	Phosgene
EMI	:	Electromagnet interference
EW	:	Evanescence wave
FESEM	:	Field emission scanning electron microscopy
Ga	:	Gallium
GaN	:	Gallium nitrate
H_2O	:	Dihydrogen monoxide
He-Ne	:	Helium Neon
HMTA	:	Hexamethylenetetramine
In	:	Indium
MF	:	Microfiber
NaCl	:	Sodium chloride
OSA	:	Optical Spectrum Analyzer
Pb	:	Lead
PDMS	:	Polydimethylsiloxane
PMKR	:	Polymer Microfiber Knot Resonator

PMMA	:	Polymethyl methacrylate
POF	:	Plastic Optical Fiber
PS	:	Polystyrene (PS)
PVA	:	Poly Vinyl Alcohol
RH	:	Relative humidity
RI	:	Refractive index
SMKR	:	Silica Microfiber Knot Resonator
Sn	:	Stannum (Tin)
TIR	:	Total internal reflection
Zn (O ₂ CCH ₃) ₂	:	zinc acetate dehydrate
Zn(NO ₃) ₂	:	zinc nitrate hexahydrate
ZnO	:	Zinc oxide

University of Malaya

LIST OF APPENDICES

Appendix A: Sample of data	132
Appendix B: Sample of statistical analysis	133

University of Malaya

CHAPTER 1

INTRODUCTION

1.1 Background of Plastic Optical Fiber Sensor

Plastic optical fiber (POF) is a type of fiber that made of polymers, including polymethylmethacrylate (PMMA), poly-styrene, polycarbonates and per-fluorinated materials. Most of the commercial POFs use PMMA as the core material, with typical core and cladding indices of 1.49 and 1.41, respectively (Shin & Park, 2013). POFs are complementing glass fibers in short-haul communications links, because they are easy to handle, flexible, and economical. However, POFs also possess some good qualities such as flexibility and capability to resist impacts and variations (Zubia & Arrue, 2001), high elastic strain limits, high fracture toughness, high flexibility in bending, high sensitivity to strain and potential negative thermo-optic coefficients (Peters, 2011). In addition, unlike silica-based fibers that will break under a strain of only 5%, POF will not break with strains over 50% (Gravina, Testa, & Bernini, 2009). These interesting physical and mechanical merits, together with the recent advances of polymer technology, POFs offer broader potential in sensor designs. To date, fiber-optic sensors have been widely used to monitor a wide range of environmental parameters such as position (Mehta et al., 2003), vibration (Conforti et al., 1989), strain (Kersey, 1996), temperature (Li et al., 2006), humidity (Kronenberg et al., 2002), viscosity (Haidekker et al., 2006), chemicals (Wolfbeis, 2005), pressure (Rajan et al., 2013), current (Bohnert et al., 2007), electric field (Vohra et al., 1991) and several other environmental factors.

To enhance the performance of a POF as sensor, a certain length of the fiber needs to be tapered. Tapering process involves a chemical etching method and this is done in

order to reduce the waist diameter of the fiber. Recently, tapered optical fibers have attracted many interests especially for sensing applications (Batumalay et al., 2013; Rahman et al., 2011). This is due to a higher portion of evanescent field travels inside the cladding in the tapered fiber, thus, the travelling wave characteristics become more sensitive to the physical ambience of its surrounding. Tapering will enhance the interaction between the light guided in the fiber and the surrounding medium, as the fraction of evanescent wave has become stronger at the tapered region. Besides that, sensitive material can be coated onto the tapered region and this will enhance the sensitivity of the sensor due to different refractive index between the core and the cladding. Many works have been reported in tapered POF as sensor such as Bariáin et al. (2000), Batumalay et al. (2014), Corres et al. (2006), Rahman et al. (2011) and Tian et al. (2011).

1.2 Background on Zinc Oxide (ZnO) nanostructures

ZnO is an II-IV compound semiconductor, whose covalence is on borderline between ionic and covalent semiconductors. Apart from that, ZnO has a direct wide band, which is ~ 3.3 eV at 300 K. With that direct wide band, semiconductor ZnO is attractive for short-wavelength light emitting devices while, as an oxide semiconductor, it is highly interesting for a range of sensors (Yakimova, 2012). Recently, ZnO nanostructures have been widely used for sensing applications because of their high sensitivity to the chemical environment (Schmidt-Mende & MacManus-Driscoll, 2007). In addition, ZnO can be synthesized to variety of nanometric structure, that can be categorized to one- (1D), two- (2D), and three-dimensional (3D) structures. Example of 1D structures is nano-rods, -needles, -helixes, -springs and -rings, -ribbons, tubes -belts, -wires and -combs, and this make this group as the largest category. The unique properties of ZnO and the ease of ZnO nanostructure fabrication make this material extremely interesting for applications

and the high surface area and strong adsorption ability the nanostructures possess are an added advantage for sensing applications (Yakimova, 2012).

The different morphologies of ZnO can be obtained through different synthetization methods. Depending on the precursors used, as well as the synthesis conditions, synthetization methods can be classified to metallurgical and chemical methods (Kolodziejczak-Radzimska & Jesionowski, 2014). Aqueous solution growth has also attracted great interest as this method allows growth of nanowires and other nanostructures at low temperatures (Schmidt & Macmanus, 2007).

Due to the richest nanostructures that can be synthesized from ZnO, it offers wider applications, especially in sensors. For instances, ZnO nanostructures can be employed as gas sensors (Carotta et al., 2009; Choopun et al., 2009; Ma et al., 2011; Wang et al., 2006; Wang et al., 2012), humidity (Chang et al., 2010; Erol et al., 2010; Zhang et al., 2005), pH (Chiu et al., 2012; Fulati et al., 2009), urea (Ali et al., 2012) and other biosensors (Arya et al., 2012; Wang et al., 2006; Wei et al., 2010; Zhao et al., 2010).

1.3 Motivation of Study

Tapered POF has garnered much interest in many applications, especially in sensors design due to its merits such as easy to handle, immunity to electromagnetic interference, flexibility and resistance to impact and vibrations. The reduced diameter waist within the tapered fiber enable large fraction of evanescent field of the propagating mode within the fiber to extend into external environment. In addition, the deposition of a sensitive material onto the tapered region affects the interaction between the light propagating in the fiber and the external medium, hence controlling the transmission spectrum. The coating of the sensitive material can be exploited for different type of measurands, depending on the response to an external stimulus. To date, ZnO has been

studied widely due to their variety of morphologies and availability of simple and low-cost processing (Djurišić et al., 2010). ZnO is also suitable for optical applications due to its direct wide bandgap (~3.3 eV) material with a large exciton binding energy of 60 meV (Schmidt & Macmanus, 2007). Apart from that, ZnO is piezoelectric due to its non-central symmetry, which is a key property for electromechanical sensors and transducers (Fortunato et al., 2009). The synthesis of ZnO enables the tailoring of various nanostructures that open up to possibilities for more applications including sensors and the morphologies may be correlated with the performance of the proposed sensors. Therefore, different techniques have been applied to synthesize ZnO, namely sol-gel and hydrothermal method. Different synthesis techniques applied will change the morphology of ZnO, hence, affect the performance of the sensor. When ZnO nanostructures are used as the sensitive material and coated on the tapered fiber, it can enhance the performance of the fiber. As reported by Nagata et al., (2007), the newly deposited cladding had a refractive index slightly above the refractive index of the core and in the presence of a detection medium, the refractive index decreases to values below the core. The changes in refractive indices cause an enhancement in the power output of the system.

This thesis proposes and demonstrates a relative humidity sensor based on tapered POF and polymer microfiber coated with ZnO nanostructures. The working principle of the sensors is based on a simple intensity modulation technique, which utilizes tapered polymethyl methacrylate (PMMA) fiber and microfiber. The ZnO nanostructures are synthesized using two different methods and the different morphologies of the nanostructures are recorded, in correlation with the performance of the sensor. The proposed sensors are easy to fabricate and inexpensive and ZnO can be synthesized without the need of high temperature and complex vacuum environment, yet, able to detect changes in relative humidity. In this work, ZnO is fabricated using sol-gel and

hydrothermal methods, and then coated on the tapered fibers and microfibers. The performance of the relative humidity sensors is investigated.

1.4 Objectives of Study

The aims of this work are to explore ZnO nanostructures coated on the tapered plastic optical fiber and polymer microfiber employing different synthesizing techniques and investigate the response to detecting changes in relative humidity. In order to achieve those, few objectives have been proposed in order to guide the research directions:

- i. To synthesize Al-doped ZnO nanostructures with sol-gel method.
- ii. To synthesize ZnO nanostructures with different techniques, namely sol-gel and hydrothermal method.
- iii. To develop a relative humidity sensor employing tapered POF and polymer microfiber coated with ZnO nanostructures.

1.5 Thesis Overview

This thesis comprises of six main chapters, providing a comprehensive study on ZnO nanostructures coated on tapered plastic optical fibers and polymer microfiber for relative humidity sensing. The current chapter presents a brief background in plastic optical fiber sensor and ZnO nanostructures as well as motivation and the objectives of this research.

Chapter 2 provides a literature review on POF with various fabrication methods, followed by ZnO nanostructures, its synthesizing techniques as well as the application as relative humidity sensor, together with other works related to the sensor.

Chapter 3 reports on the zinc oxide coated multimode tapered plastic optical fiber for humidity sensor. Here, the fabrication to taper the fiber is elaborated. The

synthetization of ZnO doped with aluminium using sol-gel for both non-seeded and seeded techniques as well as the morphologies of the obtained nanostructures are discussed and contrasted. The performance of the proposed sensor is analyzed. In addition, the performance of the proposed sensor is compared with silica microfiber and the performance of the sensors is assessed and discussed.

Chapter 4 appraises hydrothermal method to synthesize ZnO nanostructures. Step by step taken to grow ZnO nanorods is shown and explained. The morphology obtained is investigated and compared with sol-gel method, as discussed in previous chapter. The performance of the ZnO nanorods that are coated on the tapered plastic optical fiber is evaluated and contrasted with previous proposed sensor.

Chapter 5 presents polymer microfiber coated with ZnO nanostructures for relative humidity sensing. Here, the fabrication of the polymer fiber that uses direct-drawing method is shown and explained. Sol-gel method, for both non-seeded and seeded method is employed to synthesize ZnO nanostructures. The microfibers are then coated with these ZnO nanostructures and the morphologies of ZnO is investigated. The performance of relative humidity utilizing these microfibers are discussed and elaborated. It is found that the proposed sensors are able to detect changes in relative humidity.

The findings in this study are concluded in Chapter 6. It also gives a summary and review of the results and analysis of this study. Further research work is also recommended.

The novelty of the study includes:

1. Synthetization of Aluminium (Al) Doped ZnO via Sol-Gel Method

It is found that Al-doped ZnO can be synthesized using non-seeded method and the morphology of the nanostructures are enhanced when seeded technique is applied.

2. Synthetization of ZnO via Sol-Gel and Hydrothermal Method

ZnO nanostructures are synthesized using sol-gel method, for both non-seeded and seeded technique. It is also observed that the morphologies of ZnO nanostructures have significantly improved. Hydrothermal method is also applied to synthesize ZnO nanostructures and the morphology is further improved. The nanorods are more apparent and highly distributed on the fiber.

3. Development of simple Relative Humidity Sensors

The tapered POF and the polymer microfiber are coated with ZnO nanostructures that are synthesized using different techniques. The proposed fibers are able to detect changes in relative humidity. The performances of the sensors vary, depending on the sensitive material that is coated on the fibers.

CHAPTER 2

LITERATURE REVIEW

2.1 Introduction to Optical Fiber

Fiber optic or optical fiber is a flexible and transparent fiber that made of silica or plastic. These fibers refer to the medium related with the transmission of information of light pulses along the fiber. There are two main materials of optical fiber, namely glass and plastic. Glass optical fiber mostly made from silica. Plastic optical fiber (POF) or polymer optical fiber is made from polymer such as polymethyl methacrylate (PMMA) and perfluorinated material. Figure 2.1 shows the overview of POF.

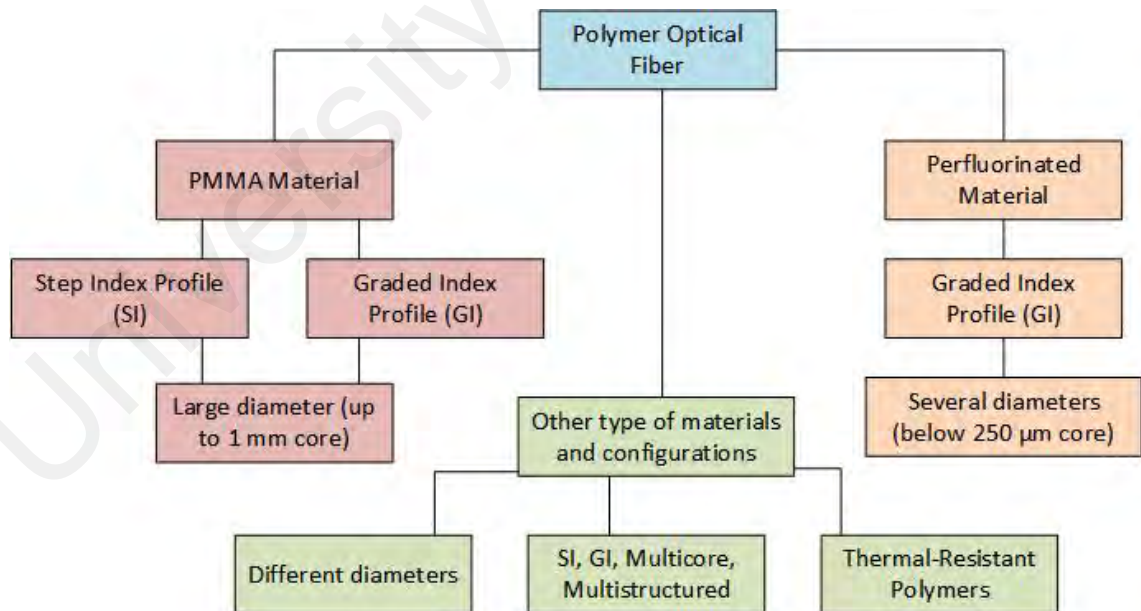


Figure 2.1: Overview of POF

Optical fibers are divided into two groups called single mode and multimode, and index of refraction profile can be differentiated to step index and gradient index. Step index fibers have a constant index profile over the whole cross section, while gradient index fibers have a nonlinear, rotationally symmetric index profile, which falls off from the center of the fiber outwards (Fidanboyly & Efendioğlu 2009). Figure 2.2 shows the different types of fibers.

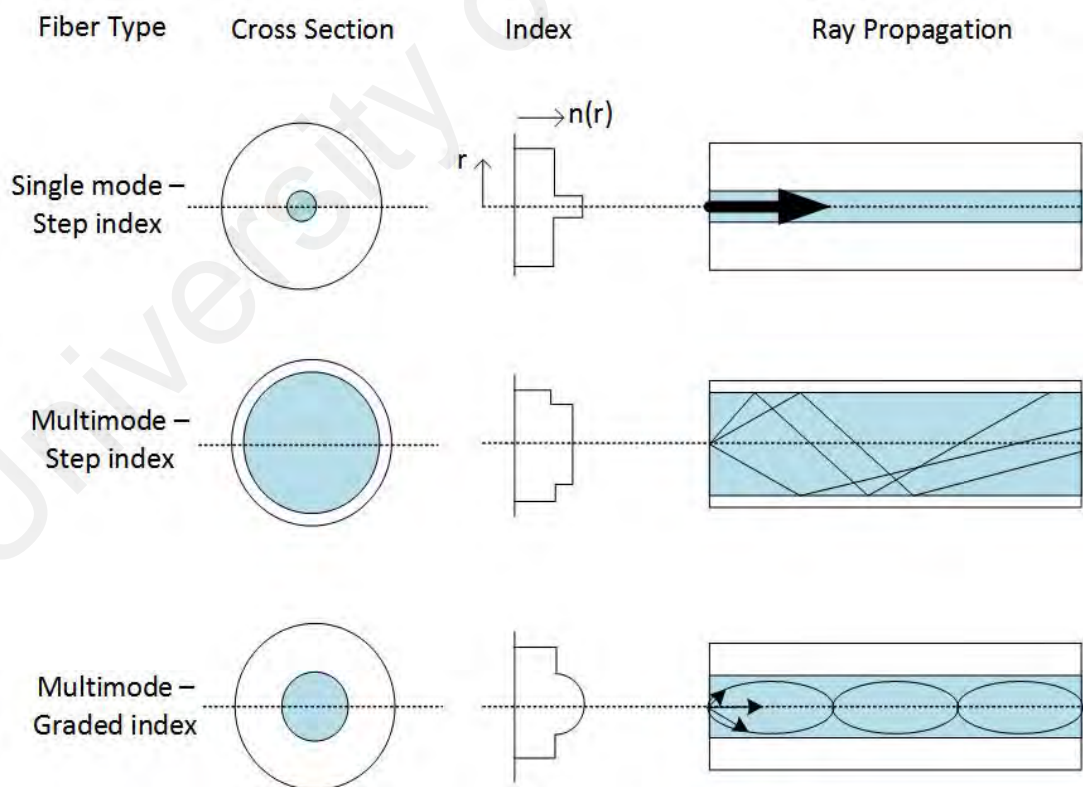
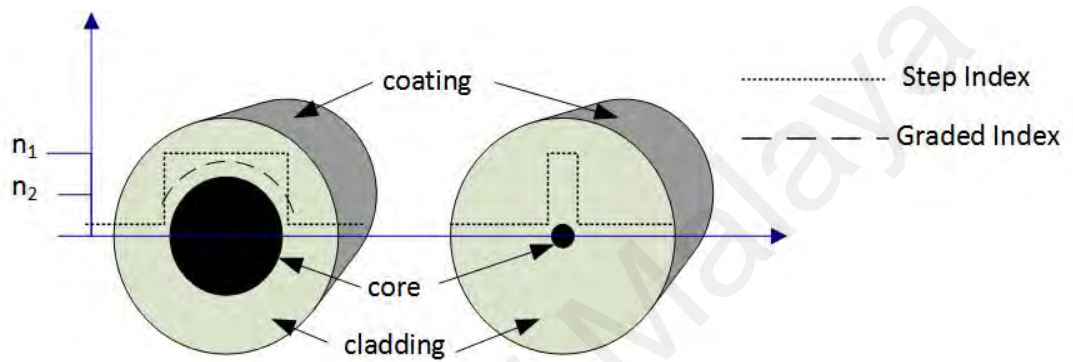


Figure 2.2: Different type of optical fiber

2.1.1 Plastic Optical Fiber

PMMA core was first introduced in 1960s. Earlier days, unlike silica, POF was less favored due to its high attenuation (Bilro et al., 2012). However, POF has received great deals of attention in some application when Professor Koike at Keio University developed the graded-index plastic optical fibers and later achieved a low-attenuation perfluorinated fibers (Zubia & Arrue, 2001). To date, they are abundantly available for various applications such as medium for telecommunication, sensors and power transmission. G. Jiang, et al. (1997) employed step index (SI) POF to carry out pulse broadening measurements under different launching conditions and they reported that the equilibrium mode distribution (EMD) condition can be achieved in an SI POF. In Cennamo et al. (2013) work, they used POF based on surface plasmon resonance (SPR) at the interface between test medium and a thin gold layer deposited on a photoresist buffer spin coated on the plastic fiber core or directly on the fiber core, which is useful for biosensing application.

The basic structure of a POF consists of a core, cladding and coating (buffer), as shown in Figure 2.3. The core is generally made of glass and it is a cylindrical rod of a dielectric waveguide that transmits light along its axis, by the process of total internal reflection and the dielectric material conducts no electricity. The core is surrounded by a layer of material of a lower refractive index called cladding, both of which are made of dielectric materials. The refractive index difference between core and cladding provide total internal reflection and confine the optical signal in the core, as shown in Figure 2.4. Cladding layer is made of plastic or glass and its main functions are to reduce loss of light from the core to surrounding air as well as reduce scattering loss at the surface of the core. Apart from that, the cladding protects the fiber from absorbing surface contaminants and it also adds the mechanical strength of the fiber. The coating enclosed the cladding by

adding an additional layer and this will provide the additional protection from any physical damage.

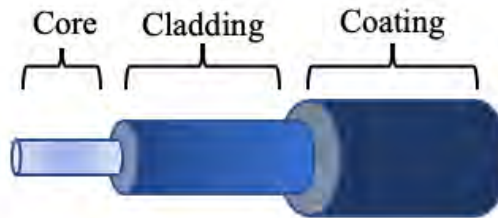


Figure 2.3: Basic structure of an optical fiber

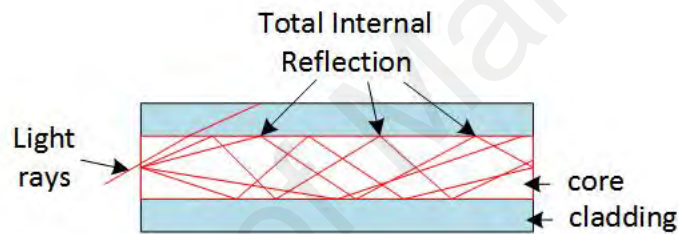


Figure 2.4: Total internal reflection in optical fiber

2.1.2 Polymer Microfiber

Optical microfibers are optical fiber taper with uniform waist region size comparable to the wavelength. It is a cylindrical optical waveguide, generally made of amorphous materials. Optical microfibers also known as optical fiber microwires, optical fiber nanowires, optical nanofibers, nanotapers, sub-wavelength optical fibers and photonic nanowires.

Optical microfibers can be fabricated via three main techniques: (i) heat and pull, (ii) etching and (iii) direct draw from bulk. The reduced diameter to tens or hundreds of nanometers makes the fibers more attractive. Optical microfibers guide light with low

optical loss due to its high-index contrast between the fibers' material (such as glass or polymer) and surrounding (such as air or water). Apart from that, optical microfibers offer excellent mechanical flexibilities, tight optical confinement and large fractional evanescent fields. These characteristics open up to new possibilities of miniaturizing platform for optical sensing with special advantageous including faster response, higher sensitivity and low power consumption (Lou et al., 2014).

As for polymer microfiber, to achieve a microfiber with a diameter of micro or nanometer, two main fabrication techniques have been reported, namely electrospinning and non-electrospinning techniques. In electrospinning technique, electrostatic force is used whereby for non-electrospinning, mechanical force is used for the formation of fibers.

There are three primary components for a typical electrospinning: a high-voltage power supply, a syringe with pumps, and a grounded collector. The schematic diagram for the electrospinning process is shown in Figure 2.5.

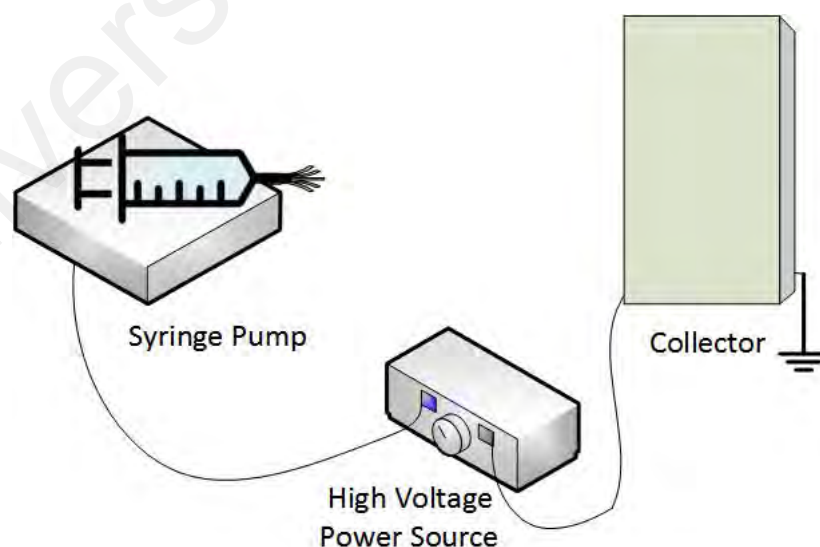


Figure 2.5: Schematic diagram of electrospinning process

The polymer solution is pumped through a capillary connected to the syringe. When the high voltage is applied to the system, an electric field is created between the tip of the capillary and the collector plate. When the surface tension in the liquid droplet is overcome by the force of the electric field, the droplet is distorted, forming a conical cone or Taylor cone (Bognitzki et al., 2001). The distortion leads to an electrically charged jet injection that move towards the collector, thus forming thin fibers. If the collector is a rotating collector, aligned polymer fibers are generated. Megelski et al., (2002) employed electrospinning method to produce fibers using a variety of solvents to investigate the influence of polymer/solvent properties on the fiber surface morphology. It was found that when a nanoporous morphology, is combined with the exceptionally small diameters (10-1000 nm) of the smallest fibers, it can give rise to an extremely large surface area ($\sim 100-1000 \text{ m}^2/\text{g}$). The surface area of these small fibers can easily surpass that of silica gel ($400 \text{ m}^2/\text{g}$) if a nanoporous texture is added. On the other work, Lin et al., (2010) demonstrated a direct approach for fabricating nanoporous polymer fibers via electrospinning. Polystyrene (PS) fibers with micro- and nanoporous structures both in the core and/or on the fiber surfaces were electrospun in a single process by varying solvent compositions and solution concentrations of the PS solutions. This process able to generate nanoporous polymer fibers with accurately controllable specific surface area and pore volume directly.

The use of high electrical voltage in an electrospinning technique can cause an excessive use of energy, hence, higher cost is required for the process. As such, mechanical force can provide an alternative to the electrical force, when the nanofilament is drawn from the polymer solution. In addition, much wider range of polymers and solvents can be applied to the process, because electrical conductivity is not a significant parameter (Lee et al., 2018). One of the optimal mechanical force approaches is a direct drawing technique. This technique not only can avoid the high cost and excessive use of

energy in the production, but also able to fabricate polymer microfibers with excellent surface qualities that are highly desired for low-loss wave guiding.

Direct drawing of polymer solutions to fabricate microfiber is done at room temperature. The illustration of direct drawing a polymer microfiber is as shown in Figure 2.6. Firstly, polymer bulk material is dissolved in a certain solvent to form a homogenous polymer solution. Then, a droplet of the polymer solution is pick up and place upon a substrate (e.g., a glass slide) by a certain tip (e.g., tungsten probe). With the evaporation of the solvent, the viscosity of the solution gradually increases to an appropriate value for drawing. Finally, the tip is withdrawn with a speed of 0.1–1 m/s, and a polymer microfiber can be formed with excellent geometric uniformity. The diameter of the drawn polymer microfiber can be roughly controlled by the drawing speed and the solution concentration.

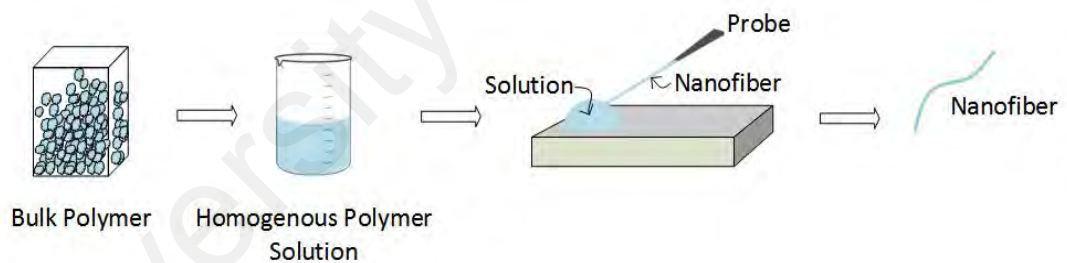


Figure 2.6: Illustration of direct drawing a polymer microfiber

Ong et al., (2015) demonstrated a direct drawing technique in fabricating polymer microfiber using molten polymethylmethacrylate (PMMA) that requires no solvent and polymer state is manipulated through temperature control. Here, a hotplate is used to melt PMMA as well as to keep the temperature constant during the drawing of the fiber. For PMMA, it is vital to maintain the viscosity at the desired level, therefore, the heating of

the hot plate must be controlled within the temperature range between glass transition temperature and melting temperature of polymer. First, a silica fiber with diameter about 125 μm is assembled and its tip is immersed into the molten PMMA. Then the fiber tip is retracted from the molten polymer with a speed of $0.1\text{--}1\text{ms}^{-1}$, leaving a PMMA microfiber extending between the molten PMMA and the tip. The extended PMMA microfiber is quickly quenched in air and finally, a bare PMMA microfiber is formed. The microfiber produced has high surface smoothness and length uniformity.

2.2 Fiber Optical Sensor

An advancement in polymer technology has enabled POF to be applied as a sensor. The main advantages of optical fiber sensor are their inherent safety due to its electrically passive operation as well as high immunity to electromagnetic interference (EMI) due to the dielectric nature of a fiber sensor system. Apart from that, its optical metrology allows the development of much lesser cost system compared to the conventional technologies, hence, garnered more scientific interest. Fiber optic sensors are capable of measuring a wide variety of parameters including strain, temperature, internal and applied loads, deflection, liquid level and more.

Generally, fiber sensors can be classified as intensity-based or phase-modulated-based. Most POF sensors are based on intensity variation detection (Bilro et al., 2012) and the experimental setup consists of an optical source, optical fiber, sensing or modulator element (which transduces the measurand to an optical signal), optical detector and processing electronics. Figure 2.7 depicts the general structure of an optical fiber system.

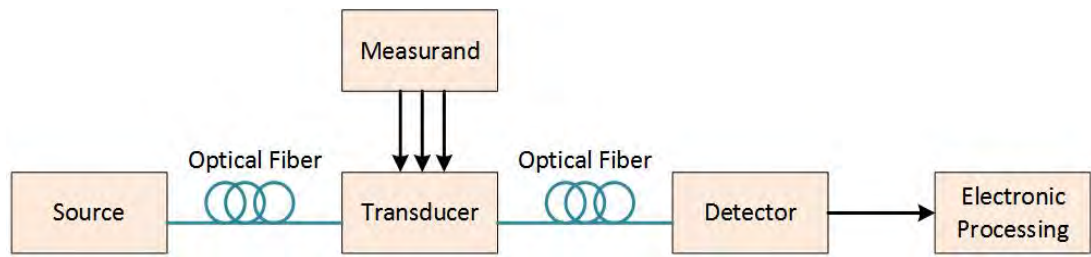
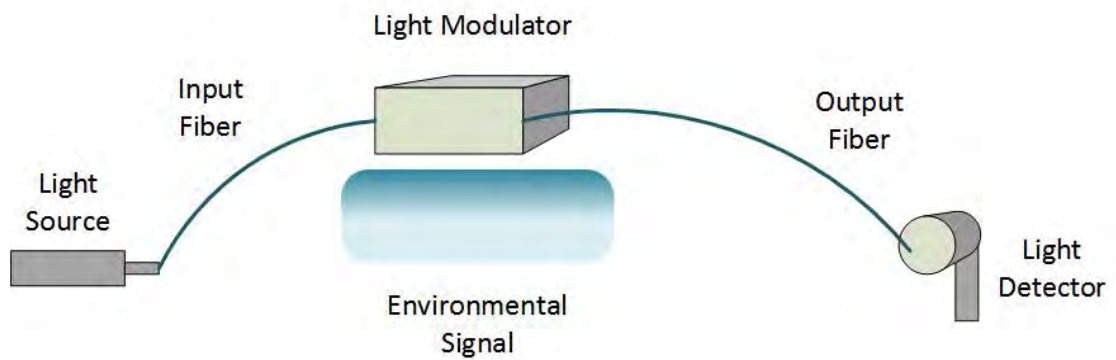


Figure 2.7: General structure of an optical sensor

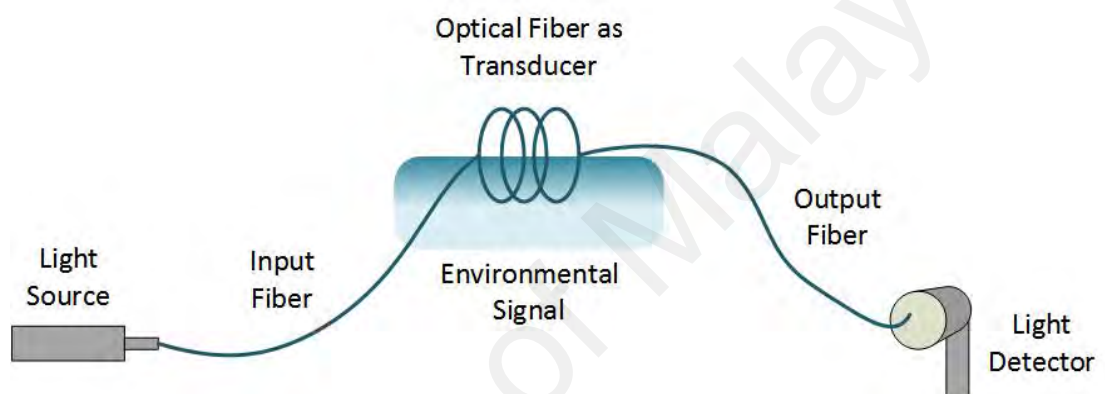
Fiber optic sensor can be classified further to three main categories: sensing location, operating principle, and application.

2.2.1 Sensing Location

Based on the sensing location, depending on where the transduction of light and measure takes place, either inside or outside the fiber, there are two basic types of sensors, namely intrinsic and extrinsic type. In intrinsic system, the modulation of optical signal occurs while the light is guided within the fiber and the fiber itself is sensitized to the measurand field. For extrinsic system, the light leaves the fiber, passes through some external transduction element, and is then recoupled back into the fiber and the external transduction element is the one that responsive to the measurand. Figure 2.8 shows the illustration for intrinsic and extrinsic types of fiber optic sensor and the comparison between these two types of sensor is as listed in Table 2.1, as reported by Ahuja & Parande (2012).



(a)



(b)

Figure 2.8: Illustration for (a) extrinsic and (b) intrinsic types of fiber optic sensor

Table 2.1: Comparison of extrinsic and intrinsic optical sensor
(Ahuja & Parande, 2012)

Extrinsic	Intrinsic
<ul style="list-style-type: none"> • Applications: Temperature, pressure, liquid level and flow • Less sensitive • Easily multiplexed • Ingress/egress connection problems • Easier to use • Less expensive 	<ul style="list-style-type: none"> • Applications: Rotation, acceleration, strain, acoustic pressure and vibration • More sensitive • Tougher to multiplex • Reduces connection problems • More elaborate signal demodulation • More expensive

2.2.2 Operating Principle

Based on the operating principle or modulation and demodulation process, a fiber optic sensor can be classified as an intensity, a phase, a frequency, or a polarization sensor. As a physical medium, fiber optic is subjected to perturbation of one kind or the other at all times. Its geometrical (size, shape) and optical (refractive index, mode conversion) will experience changes to a larger or lesser extent depending upon the nature and the magnitude of the perturbation (Gholamzadeh & Hooman, 2008).

Intensity based sensor requires the use of multimode large core fibers due to the need of more lights, and they rely on signal that are undergoing some loss. One method to do this is by applying a force that bends the fiber which results in attenuation of the signal and the values obtained is then converted using an apparatus. Another method that can cause attenuation to the fiber is through absorption or scattering of the target. Few mechanisms can be used to produce measurand-induced change in optical intensity propagated by an optical fiber such as micro bending loss, attenuation, and evanescent fields.

Micro bending is defined as the mechanical perturbation of a multimode fiber waveguide that causes a redistribution of light power among the many modes in the fiber, and light intensity will decrease with mechanical bending. As for evanescent type of sensor, the sensing is done by stripping a section of the cladding of the fiber and proportioning a very sensitive region within the fiber. The intensity of the propagating electromagnetic field is then can be perturbed by the external medium coated on the surface due to the penetration of the evanescent field into the medium. In other word, this type of sensor utilizes the light energy that leaks from core to cladding. With variety of materials that can be coated on the stripped section of the fiber, there will be diverse possibilities for the fiber system to measure other physical measurand, such as

temperature (Yoon et al., 2012), relative humidity (Wu et al., 2011) and pH of aqueous solution (Lee et al., 2002).

2.2.3 Application of fiber optic sensor

Fiber optic sensors can offer many advantageous, compared to the conventional sensor system. Among the criteria of fiber optics are lightweight and compact, therefore, the sensor will be able to handle difficult measurement conditions. As reported by Tennyson et al. (2001), it was found that fiber optic sensor is more durable than electric strain gauges when both sensors were embedded in concrete members. In other work, Rosolem et al. (2013) employed fiber optic sensor and proposed a water level sensor based on fiber bending effect associated to the use of an elastomeric membrane. The proposed water level monitoring not only low in cost, but also simple and reliable. Wang & Chen (2011) introduced the fiber-optic evanescent wave fluorescence sensor for determining penicillin G, and the proposed sensor able to provide a naturally built-in higher signal to noise ratio. There are many other advantageous of fiber optic sensors such as immunity to electromagnetic interference, resistant to high temperatures and chemically reactive environment, as well as ability to monitor a wide range of physical and chemical parameters. As mentioned earlier, fiber optic sensors have been used in bridges, dams and biomedical. There are also several reports on utilizing fiber optic sensors in other measurement of physical properties like displacement (Kuang et al., 2010), temperature (Zhang et al., 2010), vapors (Bariáin et al., 2000) and velocity (Leal-Junior et al., 2018).

Similarly, microfiber has unique geometry, with low dimension and large surface-to-volume ratio, as well as versatility for electrical and optical detection. These advantageous properties have garnered much interest in sensor application, especially in physical, chemical and biological sensing (Irawati et al., 2017).

Generally, there are two main types configuration of microfiber that can be manipulated as sensors: (i) non-resonator and (ii) micro resonator microfiber (MF).

Table 2.2 list the different structures for both of the microfiber sensor.

Table 2.2: Different microfiber structure

(a) (Alder et al., 2000), (b) (Gu & Tong, 2008), (c) (Qin et al., 2008), (d) (Yu Zhang et al., 2010), (e) (Wo et al., 2012), (f) (Tian et al. 2008), (g) (Kou et al., 2010), (h) (Chen et al., 2013), (i) (Zhaobing & Yam, 2009), (j) (Xu et al., 2008), (k) (Jiang et al., 2006), 2014), and (l) (Xu et al., 2007)

Non-Resonator MF		Micro Resonator
(a) Tapered core and cladding	(f) Abrupt-MF based Michelson interferometer	(j) Loop
(b) Evanescently coupled MF	(g) MF tip	(k) Knot
(c) Surface coated MF	(h) Uncoupled MF coil	(l) Coil
(d) MF with Bragg grating	(i) Abrupt Mach-Zehnder interferometer	
(e) MF based Mach-Zehnder interferometer		

Tapered core and cladding microfiber is the most common configuration, whereby it exploits the strong evanescent field of the guided mode to interact with the surrounding medium. As for the evanescently coupled microfiber, Gu & Tong, (2008) reported a polymer single-nanowire optical sensor for humidity detection. The nanowire was drawn from solvated polymers and are evanescently coupled to nanoscale fiber tapers for optical launching and signal collection. The proposed sensor exhibited high sensitivity and fast response. On other work, Hernandez-Romano et al. (2015) demonstrated and fabricated microfiber mode interferometer embedded in Polydimethylsiloxane (PDMS). The

polymer is used to protect the material, in order to eliminate issues with regards to degradation or contamination of the microfiber. The interferometer was built with a fiber taper with appropriate geometry and dimension. The proposed sensor was used as a temperature sensor, and due to its strong dependence of the interfering modes on the external refractive index and the high-optic coefficient of the polymer, the sensor possessed a sensitivity of 3101.8 pm/°C. Apart from that, the sensor was easy to fabricate, robust and has a good mechanical strength.

2.3 Tapered fiber

Fiber optic is well known for its admirable uniformity and other physical properties in term of strength and flexibility and fiber optic sensors have attracted much interest in providing sensor technology which can produce sensors that are lightweight, small, easily multiplexable, and immune to electromagnetic interference, require no electrical power at the sensing point, and in most cases have the potential to be produced at low cost (Kersey, 1996). However, in a fiber with uniform diameter, the evanescent field will decay to almost zero in the cladding. Hence, the light propagation cannot interact with fiber's outer surroundings. In order to make the sensing for fiber optic is possible, one way is to ensure an interaction between the light propagated in the fiber and its outer surrounding take place. This can be done by exposing the evanescent field of the transmitted light and tapered fiber is a good solution to this.

Fiber tapering is a process of reducing the fiber diameter in order to change their light coupling or light propagation properties. Tapered fiber consists of three segments; (i) a taper waist segment with small and uniform diameter and (ii) two conical transition regions with gradually changed diameter, as identified in Figure 2.9.

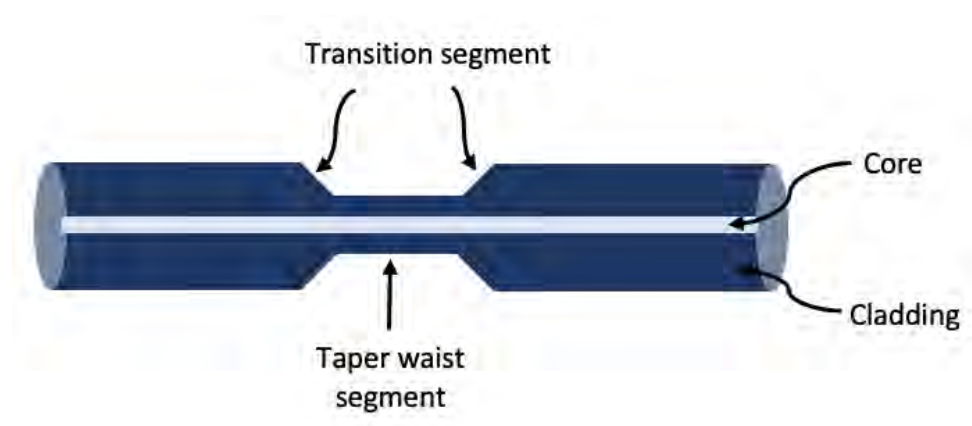


Figure 2.9: Illustration of a tapered fiber optic

Heat pulling or chemical etching method can be used to reduce the waist diameter of the fiber optic. The main difference between the two methods is that, for heat pulling, it maintains the geometrical ratio between cladding and core, while chemical etching will remove part of the cladding (Corres et al., 2007).

The heat-and-pull techniques make use of mass conservation by stretching a fiber which is being heated. There are four main variations to this technique: “flame brushing”, “microheater brushing”, “drawing tower” and “self-modulated taper-drawing”.

Heat pulling method has been applied to silica fiber for many years and the typical fabrication setup comprises of fiber holders and a heating source. For flame brushing technique, the fiber optic is placed on the fiber holders that are fixed on the translation stages and the heating source will be fixed or travelled under the tensioned optical fiber. There are three different ways of fabrication that can applied: (i) a stationary flame with fixed pulling stages, (ii) a stationary flame with independent pulling stages and (iii) a moving flame with independent pulling stages, as shown in Figure 2.10.

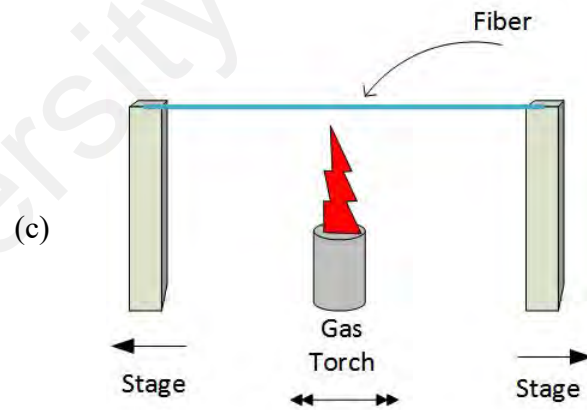
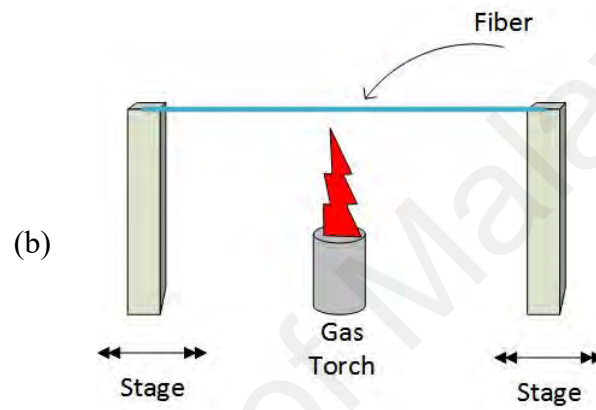
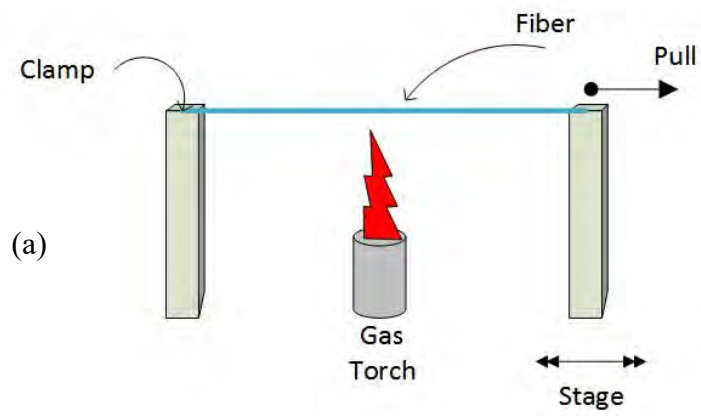


Figure 2.10: (a) a stationary flame with fixed pulling stages, (b) a stationary flame with independent pulling stages and (c) a moving flame with independent pulling stages

In the first set up, the flame is kept stationary under the fiber while the bottom stage performs a bidirectional motion which simulates a moving flame. The top stage, on the other hand, moves in only one direction and pulls on the fiber. As for the second set up, the two stages are controlled to synchronously perform bidirectional motion while the flame is kept stationary under the fiber. During the fabrication process, flame brushing is done through the reciprocal movements of these two stages, while the fiber is elongated by increasing the separation between them. Meanwhile, for the third set up, three translation stages are utilized. One stage is used to oscillate the flame position along the fiber, while two stages are used to pull on either end of the fiber. Therefore, for heat pulling method, it is important that parameters such as heating length, pulling speed and temperature to be monitored and controlled as tapered fiber with different shapes and properties can be fabricated.

Microheater brushing replaces the heating source in the flame brushing to microheater whereby the resistive element can be adjusted, hence, controlling the current flow through it will control the temperature. This technique can be used to produce microfibers from low-softening-temperature glasses, such as compound silicate and non-silicate glasses. In drawing tower approach, the process to fabricate microfiber similar to conventional way of producing optical fiber (Ismaeel et al., 2013). In this technique, fiber is continuously fed in a vertical furnace, while a microfiber is pulled at the other furnace opening. The diameter of the microfiber can be set by controlling the relative feed and pull speed. Self-modulated taper-drawing is a two-step process and it is able to produce small taper up to 10 nm. The first step is to taper the fiber to a diameter of few micrometers using the flame brushing technique. Secondly, the fiber separated into halves, and one of them is wrapped onto a hot sapphire rod that is heated by a flame positioned at a distance from the fiber and pulled to sub-micrometric to its final diameters.

2.3.1 Tapering of Plastic Optical Fiber

To taper POF, chemical etching is the most suitable as heat pull method can cause breakages, uneven profile and most of the time, total melting of the fiber as POF has low ductility. Chemical etching method requires acetone, de-ionized water and sandpaper. Firstly, acetone solution is applied to the tapering section of the POF. During this time, it is vital that no tension is applied to the fiber as the section becomes susceptible to brittle stress fracture. One way is to apply acetone on the fiber using a cotton bud to rapidly expose the cladding to the solvent, with a de-stressed fiber is supported in a straight line. A milky white surface around the outer cladding of the plastic fiber can be observed during this process. Then, the section of the fiber is neutralized with de-ionized water, in order to stop the solution process while keeping the cladding soft enough. The surface is then smoothed with sandpaper for about 8-10 seconds. This process is repeated until the tapered fiber has reached the desired stripped region length of the waist diameter. A microscopic is used to identify any areas of cladding remaining in place and hence can be removed by repeating the entire process. The core will remain in its original condition even with the exposure to the solvent provided that the exposure times are limited as described. The use of fresh solvent for each process ensures a much more consistent taper surface finish across the samples provided. This chemical etching is a gradual process, hence, it is simpler to monitor the diameter of the tapered waist physically or optically.

2.4 Evanescent wave and refractive index sensing

To ensure total internal reflection in the core, the refractive index of the core is made higher compared to the cladding. The value of refractive index for the core and cladding are 1.492 and 1.402 respectively. Lights that are propagating through the optical

fibers consist of the guided field in the core as well as exponentially decaying evanescent field in the cladding, as shown in Figure 2.11.

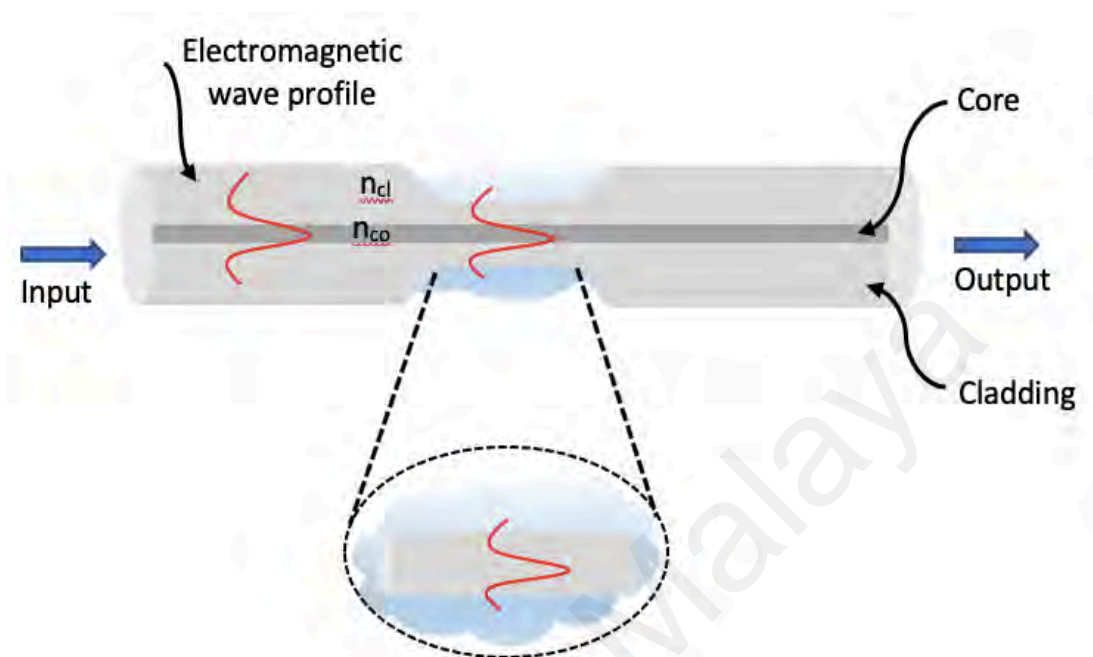


Figure 2.11: Illustration of exponentially decaying evanescent field in the cladding

Leung et al. (2007) showed a mathematical expression of an evanescent field with amplitude that decays exponentially with distance away from the core/cladding interface as:

$$E(x) = E_0 \exp\left(\frac{-x}{d_p}\right) \quad (2.1)$$

where E_0 is the magnitude of the field at the interface, x is distance from the fiber core, starting at $x = 0$ at the core-cladding interface, and d_p is the penetration depth. Penetration depth is defined as the distance of to which the evanescent field extends beyond the core-cladding interface, which is the distance where the evanescent field

decreases to $1/e$ of its value at the core-cladding interface. Figure 2.12 illustrates the penetration depth of a fiber. Mathematically, d_p can be describes as:

$$d_p = \frac{\lambda}{2\pi\sqrt{n_{co}^2 \sin^2 \theta - n_{cl}^2}} \quad (2.2)$$

where λ is the wavelength of the light source, θ is the angle of incidence of the light at the core/cladding interface, n_{co} and n_{cl} are the refractive indices of the core and cladding, respectively (Leung et al., 2007).

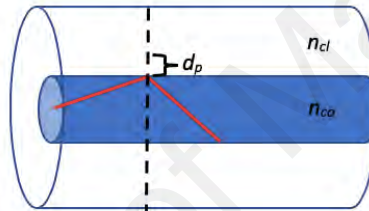


Figure 2.12: Illustration of penetration depth for a fiber

Therefore, the depth to which the cladding is removed from the fiber gives control over the level of interaction with the evanescent field. If the cladding is replaced with a material with different refractive index, the insertion loss of the fiber section will be changed.

As can be seen in Figure 2.9, light enters from the un-tapered region to tapered region at one end thus exciting higher order modes in the tapered region. Then, the fundamental modes and higher order modes coupled together in un-tapered region at the other end to form interferometric pattern due to large difference in indices between air and glass. From Figure 2.11, n_{co} and n_{cl} are the refractive indices of the core and

cladding, respectively. Thus, the resulting intensity at the end of fiber, as shown by Yadav et al. (2014) is given as:

$$I_T = I_{co} + I_{cl} + 2\sqrt{I_{co}I_{cl}}\cos(\Delta\phi) \quad (2.3)$$

where I_{co} is the intensity at the core and I_{cl} is the intensity at the cladding. $\Delta\phi$ is the difference between the two modes, which is the phase of the resultant interferometry intensity pattern, and be described by the following mathematical equation (Yadav et al., 2014):

$$\Delta\phi = \frac{2\pi}{\lambda}(\Delta n)L \quad (2.4)$$

λ is central wavelength of the light and L is the waist length of the tapered segment of the fiber, as shown in Figure 2.13.

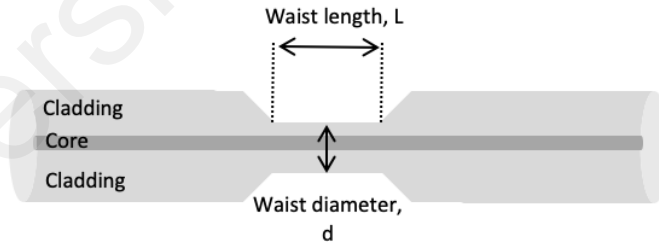


Figure 2.13: Illustration of the waist length, L for tapered fiber

Δn is the difference in the indices and described as the following:

$$\Delta n = n_{eff}^{co} - n_{eff}^{cl} \quad (2.5)$$

where n_{eff}^{co} is the effective index of the core mode and n_{eff}^{cl} is the effective index of the cladding mode (Yadav et al., 2014). By multiplying Δn and L will result in optical path difference of the two interfering modes. Therefore, when the refractive index of the surrounding medium changes, the phase difference, $\Delta\phi$, will also change and will then leads to a shift in the transmission spectrum (Yadav et al., 2014).

Refractive index change is frequently demonstrated as an approach for evanescent wave sensing. The measuring or sensing of refractive index is one of importance scientific technique since the refractive index is a fundamental material property for which its accurate measuring is crucial in many cases. Figure 2.14 shows the refractive index based on a tapered fiber coated with modified cladding sensitive material.

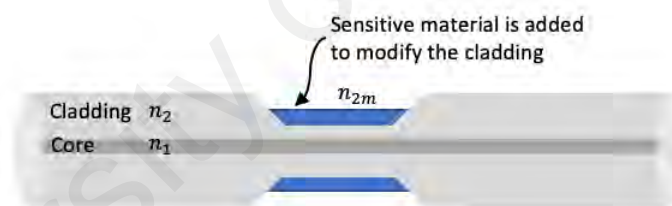


Figure 2.14: Structure of tapered fiber with overlay sensitive material

The refractive index of the modified cladding material (n_{2m}) can be considered in two situations either having lower or higher refractive index than core (n_1). Therefore, two basic types of fiber-optic intrinsic sensors can be designed according to the difference of refractive indices between the fiber core and cladding (Yuan & El-Sherif, 2003). If the modified cladding, n_{2m} has a lower refractive index than core, n_1 , the incident ray bends away from normal and greater than critical angle. Then the total reflection condition is met (Thyagarajan & Ghatak 2007). On the other hand, if modified cladding, n_{2m} has a

higher refractive index than core n_1 , the incident ray bends towards to normal and less than critical angle, part of the optical power is refracted into the cladding, and another part is reflected back into the core (Elosua et al., 2006). The partial leaky-mode sensor is constructed based on the intensity modulation induced by the absorption of the refracted rays and evanescent field in the modified cladding (Yuan & El-Sherif, 2003). In principle, as long as the refractive index of the overlay material chose is close to effective index of the propagating modes along the fiber, hence, any overlay material can be used depending on the objectives and the analyte to be measured.

Numerous applications of evanescent wave's sensors have been reported. For example, Gaston et al. (2003) have developed a sensitive and versatile evanescent wave-sensing system featuring polished optical fiber-based sensor designs with low-cost light sources for temperature, relative humidity, and pH measurements. The output power change in the proposed sensor is based on the interaction of the evanescent field in side-polished standard single mode fibers with the external medium or overlay. Single U-bend plastic-clad silica fiber also can be employed as evanescent wave sensor, as reported by Khijwania et al. (2005). Bending the fiber in the sensing region leads to a larger interaction with evanescent light, whereby a small portion of the optical power in the guided modes, extended to the cladding region, interacts with the coated sensing thin film of PVA and COCl_2 . On the other work, Xiong et al. (2013) investigated the feasibility of coiled optical sapphire fiber sensors based on evanescent absorption spectroscopy in the infrared range for the quantitative determination of H_2O content in deuterium oxide. The coiling of the fiber enables the enhancement of the sensitivity of evanescent absorption sensors by converting lower order modes into higher order modes.

2.5 Zinc Oxide (ZnO)

To date, a great deal of interest on ZnO has been exhibited from numerous researches and publications. This can be due to its direct wide band, which is ~ 3.3 eV at 300 K, a characteristic that has a potential in optoelectronics applications (Wang, 2004). Even though some optoelectronics applications employ gallium nitrate (GaN), another wide gap material ($E_g \sim 3.4$ eV at 300 K), ZnO is some advantageous over GaN, among which are the availability of fairly high quality ZnO bulk single crystals and a large exciton binding energy (~ 60 meV) (Ozgun et al., 2010). Apart from that, ZnO-based devices require less cost to produce as it has much simple crystal-growth technology.

ZnO is an II-IV compound semiconductor, whose covalence is on borderline between ionic and covalent semiconductors used for many applications especially for electronics, optoelectronics and sensor. The crystal structures shared by ZnO are wurtzite (B4), zinc blende (B3), and rock salt (B1), as shown by the schematic diagram in Figure 2.15. At ambient conditions, the thermodynamically stable phase is wurtzite. The zinc-blende ZnO structure can be stabilized only by growth on cubic substrates, and the rock salt (NaCl) structure may be obtained at relatively high pressures.

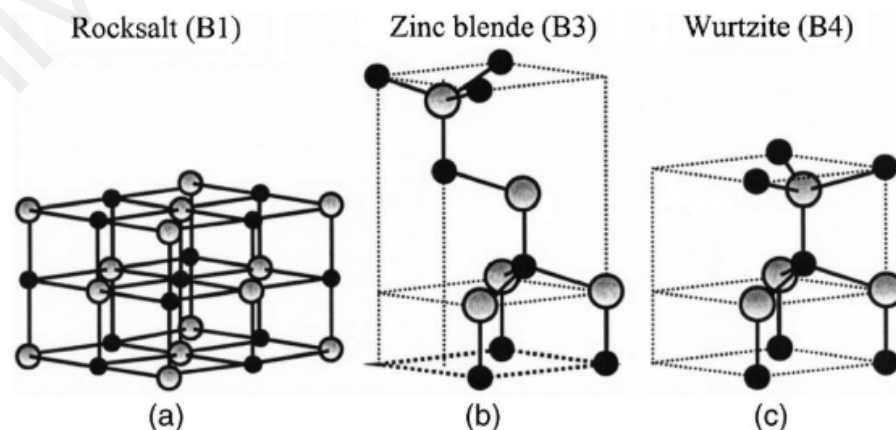


Figure 2.15: Schematic diagram of ZnO crystal structures (a) cubic rock salt (B1), (b) cubic zinc blend, and (c) hexagonal wurtzite (B4)
(Özgül et al., 2005)

Generally, ZnO is a hexagonal wurtzite structure (refer to Figure 2.16) with lattice parameters $a = 0.3296$ and $c = 0.52065$ nm, exhibiting partial polar properties (Baruah & Dutta, 2009). Each zinc atom is surrounded by four oxygen atoms, which are located at the corners of a nearly regular tetrahedron. The structure has alternating planes implicated of tetrahedral coordinated Zn^{2+} and O^{2-} ions attached along c-axis, where the ends are terminated with either polar or non-polar surfaces.

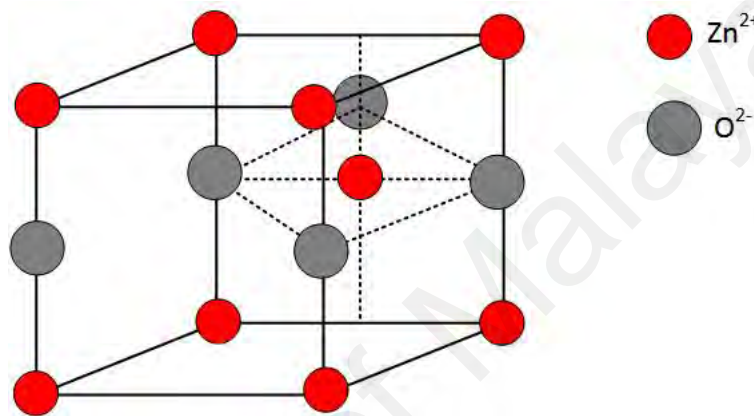


Figure 2.16: Wurtzite structure of Zinc Oxide

Apart from wide gap material, the high stable non-centro-symmetric hexagonal wurtzite structure possessed by ZnO leads to a relatively large piezoelectric coefficient, high modulus of elasticity and high piezoelectric tensor, and key property for electromechanical sensor and transducers (Fortunato et al., 2009).

ZnO can be applied in many new potential areas of nanotechnology due to its variety of nanometric structure. ZnO can be categorized into one- (1D), two- (2D), and three-dimensional (3D) structures. 1D structures comprise of nano-rods, -needles, -helices, -springs and -rings, -ribbons, tubes -belts, -wires and -combs, and this makes this group as the largest. Example of 1D structures is as shown in Figure 2.17.

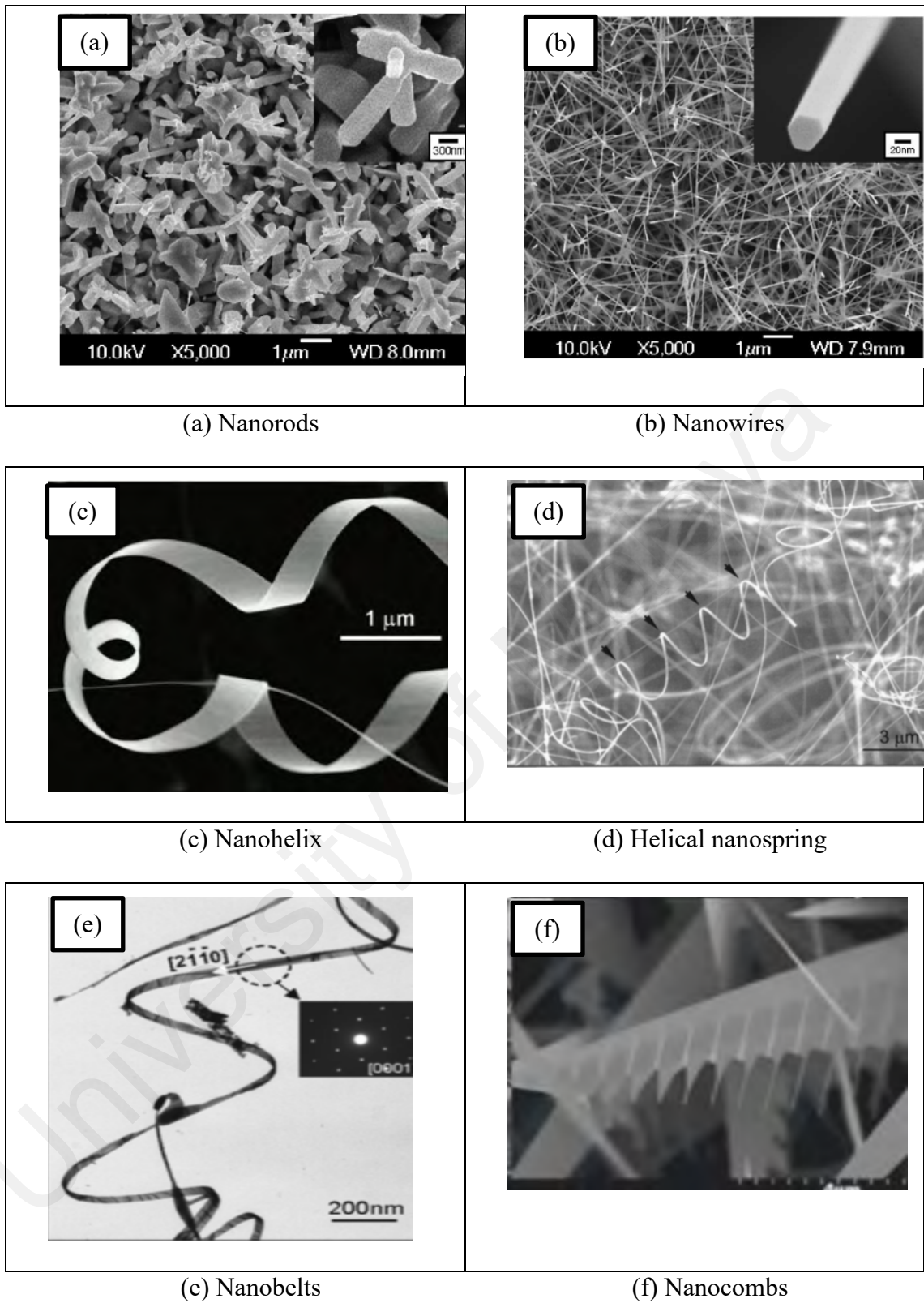


Figure 2.17: Example of ZnO of 1D structures

(a) Nanorods (Zhang et al., 2005), (b) Nanowires (Zhang et al., 2005), (c) Nanohelix (Gao et al., 2006), (d) Helical nanospring (Kong & Wang, 2004), (e) Nanobelts (Kong & Wang, 2004) and (f) Nanocombs (Wang et al., 2006)

On the other hand, example of 2D structures of ZnO are nanoplate/nanosheet and nanopellets while 3D structures of ZnO include flower, dandelion, snowflakes, coniferous and urchin-like. Figure 2.18 and 2.19 show the example of 2D and 3D structures of ZnO respectively.

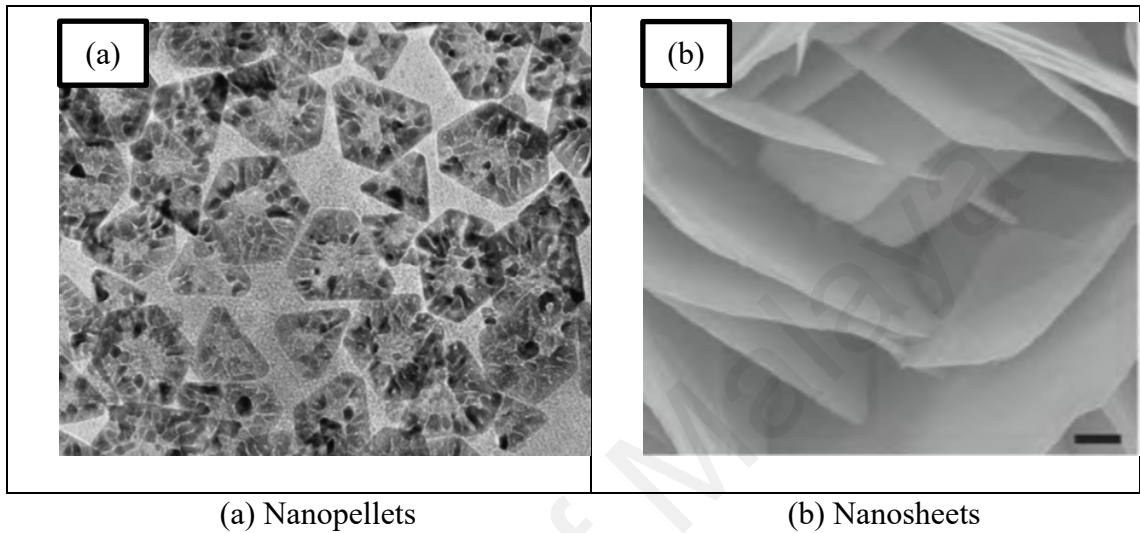


Figure 2.18: Example of ZnO of 2D structures
(a) Nanopellets (Huang et al., 2013) and (b) Nanosheets (Sun et al., 2014)

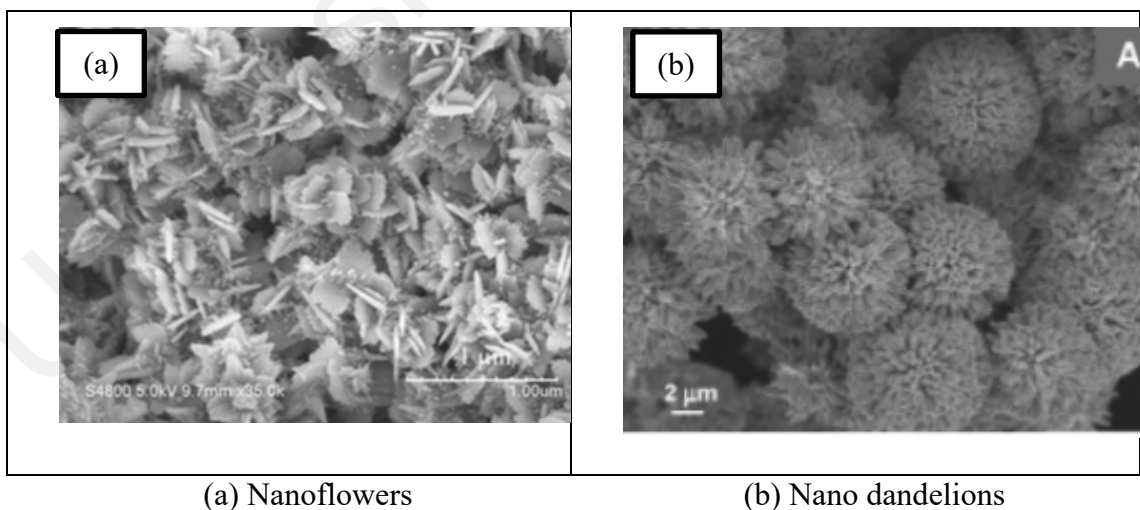


Figure 2.19: Example of ZnO of 3D structures
(a) Nanoflowers (Huang et al., 2013) and (b) Nano dandelions (Liu & Zeng, 2003)

2.6 Doping in ZnO

ZnO can be doped with other elements as it offers an alternative method to adjust the electrical, optical and magnetic properties of ZnO (Schmidt-Mende & MacManus-Driscoll, 2007). Among typical dopants that have been employed in order to increase the conductivity of ZnO are group III (B, Al, In, Ga) and group IV (Pb, Sn). Among which, Aluminium (Al) doping produces highly conductive as well as good quality films with high transparency in the visible spectral region due to the close covalent bond length of Al–O (0.192 nm) to that of Zn–O (0.197 nm), as reported by Mridha & Basak (2007). In addition, Al has the lowest resistivity, which is $\sim 10^{-4} \Omega\text{cm}$ and $\sim 90\%$ of transmittance in visible range. These properties have attracted much research in photonic applications. Kim et al., (2002) demonstrated Al doped ZnO films deposited by PLD on glass substrates. It was found that the optical properties such as optical band gap, refractive index, plasma wavelength of Al doped ZnO films were strongly affected by Al-doping amount. The optical band gap increased with an increase in carrier concentration as a result of Al-doping. The sensitivity of proposed sensor also improved when ZnO is doped with other materials, as reported by (Md Sin et al. (2011) and Jiaqiang et al. (2006), and morphology of ZnO can also be modified with doping, as reported by Mondal et al. (2013).

2.7 Synthesis of ZnO

The variety of ZnO nanostructures morphologies can be obtained through different methods. Depending on the precursors and synthesis conditions, growing ZnO can be divided into metallurgical and chemical methods. Chemical method consists of mechanochemical process, controlled precipitation, sol-gel method, solvothermal and hydrothermal method, method using emulsion and microemulsion environment and any

other method. These methods will determine the properties and the applications of ZnO as reported in detail by Kolodziejczak-Radzimska & Jesionowski (2014).

2.7.1 Sol-gel Immersion Method

The sol-gel process is a wet chemical technique also known as chemical solution deposition, and involves several steps, in the following chronological order: hydrolysis and polycondensation, gelation, aging, drying, densification, and crystallization. This technique is suitable for side-coating of optical fibers or waveguides in evanescent wave sensors because precise control of sensitivity-determining parameters, such as the coating thickness and length, is achievable (MacCraith et al., 1995). Aqueous sol-gel method is when water is used as a reaction medium while non-aqueous sol-gel use organic solvent as reaction medium. Figure 2.20 illustrates the reaction pathway for the production of metal oxide nanostructures in the sol-gel method, as reported by Rao et al. (2017).

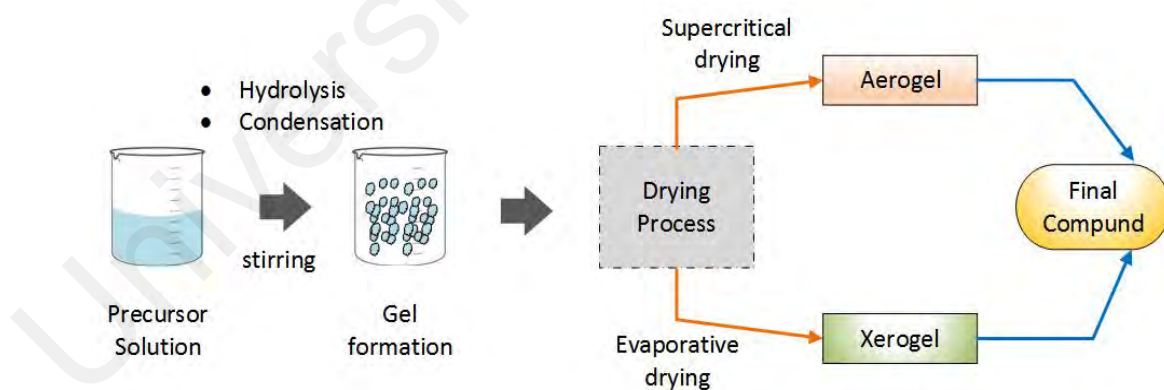


Figure 2.20: Reaction pathway for the production of metal oxide nanostructures in the sol-gel method

As mentioned earlier, the nature of the precursor and the solvent have a significant role in the synthesis process.

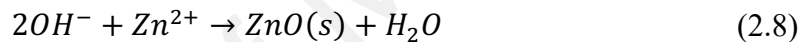
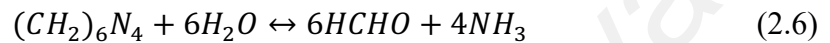
Erol et al. (2010) synthesized ZnO nanoparticles with about 10 nm diameter by sol-gel process. Here, two solutions consisting (1) Sodium hydroxide (NaOH) and Ethanol (C₂H₅OH) and (2) Zinc acetate (Zn(CH₃COO)₂) were stirred at the 70 °C separately. Then, these two solutions were stirred in an ice bath and n-heptane is added to in order to produce ZnO precipitation from the solution. The resulting white products showed that the reaction was completed, hence, the products were centrifugalized and re-dispersed into ethanol. On the other hand, Tai & Oh (2002) utilized sol-gel method to synthesize Al-doped ZnO. Firstly, diethanolamine was dissolved in isopropanol at room temperature. Then, zinc acetate dihydrate (Zn(CH₃COO)₂·2H₂O) was stirred and aluminium nitrate nanohydrate (Al(NO₃)₃·9H₂O) was dissolved in ethanol. The resultant solution was stirred to yield a clear and homogeneous solution. Finally, the solution was let aged for 10 days at room temperature.

2.7.2 Hydrothermal Method

Currently, ZnO have attracted more study in the creation of ZnO nanostructures, growth mechanisms and the investigation of their structural, optical and electronics properties. Apart from that, ZnO also plays an important role in current industry as it possesses characteristic such as anti-bacteria, anti-corrosion, has low electron conductivity and great heat resistance. As mentioned earlier, ZnO particles can be prepared by different methods such as sol-gel, hydrothermal, chemical vapor deposition, thermal decomposition, electrochemical precipitation, chemical precipitation and spray pyrolysis (Kolodziejczak-Radzimska & Jesionowski, 2014). However, hydrothermal method is favored because of its low process temperature, low cost, reliability, repeatability, and simplicity as well as less hazardous (Kolodziejczak-Radzimska & Jesionowski, 2014; Madathil et al., 2007). In addition, the nanoparticles produced using

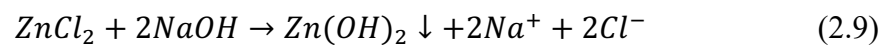
this method show good optical properties and the morphology and size of the nanostructures are easily can be controlled by adjusting the reaction time, annealing time and concentration of seeding solution (Ridhuan et al., 2012).

Often, to grow ZnO, solution of zinc nitrate ($ZnO(NO_3)_2$) and hexamethyltetramine (HMTA) are used and produced in an aqueous environment. Hence, the following equations are obtained (Schmidt-Mende & MacManus-Driscoll, 2007):



Hydroxide ions are formed by the decomposition of HMTA and they react with the Zn^{2+} to form ZnO.

Chen at al. (1999) proposed a synthetization of ZnO with zinc chloride ($ZnCl_2$) and sodium hydroxide (NaOH) reagents. The reaction of the process is as follows:



The white $Zn(OH)_2$ precipitate underwent filtration and washing, and hydrochloric acid (HCl) is used to correct the pH of the solution to the value of 5 – 8. The hydrothermal process takes place in the autoclave at a programmed temperature for a set time, followed by cooling. The end product of the process is zinc oxide, with the following reaction:



ZnO can be synthesized using a number of different methods, hence, it can be grown to different morphologies and offered wide range of application. Baratto et al. (2009) reported a ZnO nanowires synthesized using evaporation-condensation technique and the optical sensor is able to detect the presence of nitrogen dioxide (NO₂). Lupan et al. (2010) used different method to synthesize ZnO nanowires. In their work, ZnO nanowires were synthesized via chemical vapor deposition and the nanowires can be used to sense material in nano-sensors with a higher response to hydrogen gas at room temperature. Apart from ZnO nanowires, ZnO nanorods have large surface area which make them attractive for gas and chemical sensing (Heo et al., 2004). ZnO nanorods can be synthesized via hydrothermal method as reported by Jiaqiang et al. (2006). Here, the ZnO nanorods had a diameter of 40 – 80 nm, with a length of about 1µm and potentially to be used as gas sensors. Subsequently, Yun et al. (2008) synthesized ZnO nanorods using the same hydrothermal method and the outcome was an aligned ZnO nanorods grown on an indium tin oxide substrate. Baruah & Dutta (2009) reported the seeding on the growth and orientation of the ZnO nanorods using hydrothermal method. Seeding with ZnO nanoparticles in colloidal form produced nanorods which were oriented like flowers, while seeding with zinc acetate gave different morphology and orientations based upon the preheating and post annealing temperatures used during the growth of the seed layer. Therefore, hydrothermal method is favored to grow ZnO as it offers most energy-efficient, economic, and environmentally friendly and does not require complex vacuum environment (Baruah & Dutta, 2009). In addition, the morphology of ZnO can be controlled and changed according to the precursor and techniques used, to suit the intended applications.

2.7.3 Zinc Oxide Nanostructures for Optical Sensor Applications

ZnO nanostructures have attracted much interest in various applications especially sensor applications. Ali et al. (2012) demonstrated a simple fabrication procedure for a highly sensitive electrochemical uric acid sensor based on ZnO nano-flake-based structures. The proposed electrochemical nanosensor demonstrates immense surface area to volume ratios which provide a suitable microenvironment for enzyme loading because of its porosity that allows for very good sensitivity. The uricase sensor retained its enzymatic activity due to strong electrostatic interaction between zinc oxide and uricase. Wang et al. (2006) demonstrated a gas sensor fabricated from ZnO nanorods arrays and the nanorods were synthesized on ZnO thin film via hydrothermal approach. The ZnO nanorods exhibited a diameter of 30 – 100 nm with a length around several hundred nanometers. The proposed sensor showed a high sensitivity to hydrogen (H₂) from room temperature to a maximum sensitivity at 250 °C and a detection limit of 20 ppm. Apart from H₂, ZnO nanorods also responded to ammonia (NH₃) and carbon monoxide (CO) exposure. The high sensitivity of the ZnO gas sensor is attributed to the small grain size and high surface to volume ratio associated with the ZnO nanorods.

The biosensor platform requires specific material with advanced structure, electrical and optical properties for the effective signal transformation of biological interaction into physical signal. Among different materials, metal oxides are quite attractive for biosensor applications as they possess all required physical properties (conductivity, luminescence and absorbance) as well as biocompatibility and ZnO is the most interesting metal oxide material (Tereshchenko et al., 2016) .

Research by Liu et al. (2012) reported studies on growth of well-arrayed ZnO nanorods on thinned silica fiber for humidity sensing. Thinning of the silica fiber is done using flame heated method with tapering length of 10 mm for fiber diameters of 5µm,

10 μ m and 20 μ m while the ZnO nanorods was hydrothermally grown on the fiber. The presence of one-dimensional ZnO nanorods with high surface-to-volume ratio boost the optical interaction between the device and ambient environment. Sensitivity of the sensor exceptionally displayed 50-fold increase in terms of unit length compared to nanoparticle-coated fiber sensor, as reported by Kobayakov et al. (2009). Nevertheless, the diameter of the nanorods obtained is in the range of 200 nm – 300 nm which is still big, and the synthesis process has not yet been optimized.

Renganathan et al. (2011) demonstrated an ammonia gas detection based on multimode plastic optical fiber coated with ZnO nanostructures. The tapered fiber was dipped into the nanocrystalline ZnO solution and then dried in air. In addition, the existence of ZnO nanocrystalline altered the total internal reflection at the interface of core/cladding, and the percentage of reflected light at the interface depends upon the refractive index of core and modified cladding. Increasing in ammonia onto the ZnO will degrade the output power of the sensor, due to loss of intensity of the propagating light through the fiber.

2.8 Humidity

Humidity is the presence of water vapor in air (or any other gas). Water vapor is the gaseous state of water; as the temperature of the air increases, more water vapor can be held since the movement of molecules at higher temperatures prevents condensation from occurring. The quantities of humidity can be expressed in several different ways: absolute, specific and relative humidity.

2.8.1 Humidity Measurement Parameters

Absolute humidity is a measure of the actual amount of water vapor in the air, regardless of the air's temperature. The higher the amount of water vapor, the higher the absolute humidity. The unit is given as grams of water vapor per cubic meter volume of air (g/m^3) and expressed as:

$$AB = \frac{m_w}{v} \quad (2.11)$$

where AB is absolute humidity, m_w is the mass of water vapor (gram or grain) and v is the volume of air.

Specific humidity refers to the weight of water vapor contained in a unit weight (amount) of air (expressed as grams of water vapor per kilogram of air). Absolute and specific humidity are quite similar in concept. Relative humidity (RH), expressed as a percent (%), measure the amount of water vapor that air is holding compared to the amount it can hold at a specific temperature. Warm air can possess more water vapor (moisture) than cold air, so with the same amount of absolute/specific humidity, air will have a higher relative humidity. Relative humidity can be expressed as:

$$RH\% = \frac{P_v}{P_s} \times 100 \quad (2.12)$$

where P_v is the actual pressure of moisture content in air and P_s is the saturated pressure of moist air at the same given temperature (both in Bar and KPa).

Relative humidity can also be expressed in term of percent of saturation humidity. Saturation occurs when a gas (or a space) holds the maximum water vapor possible at a given temperature. Saturation humidity can be expressed as:

$$SH = \frac{m_{ws}}{v} \quad (2.13)$$

where SH is the saturation humidity (g/m^3), m_{ws} is the mass of water vapor at saturation and v is the volume of air. Hence, relative humidity can also be expressed as:

$$RH\% = \frac{AB}{SH} \times 100 \quad (2.14)$$

Another quantity that is related to humidity is dew points, and it is expressed in units of temperature. Dew point is defined as a temperature (above 0 °C) at which the water vapor content of the gas begins to condense into liquid water,

2.8.2 Relative Humidity Sensor

Humidity contributes to one of the most commonly required physical quantities. Humidity not only important parameter for air conditioning for human comfort, or combating bacterial growth, but has an important influence on several industrial processes such as electronic, food or pharmaceutical manufacturing, food storage, etc (Ascorbe et al., 2017). All these processes require continuous monitoring of air humidity. In addition, proper humidity levels can be critical to the quality of the product and having the right humidity level can contribute to diminishing energy consumption (Ascorbe et al., 2017). Relative humidity (RH) is commonly used for humidity

measurement because it is generally simpler and thus cheaper and is extensively applied in applications involving indoor air quality and human comfort issues (Farahani et al., 2014). To date, various different RH sensors have been reported, depending on the applications and measurement techniques (Yeo et al., 2008).

The simplest conventional way of measuring humidity is using hygrometer. Depending on the many principles that can be measured, hygrometer can be divided to these four main methods: electrical impedance, condensation, wet- and dry-bulb, and mechanical. In electrical impedance, the hygrometer is based on an electric component that absorbs water vapor according to air humidity and changes the electrical impedance. Condensation principle hygrometer uses cooling to induce controlled condensation and when the temperature is stable, the value is measured and recorded as dew or frost point. Wet- and dry-bulb hygrometer comprises of two thermometers, one of it is a dry bulb and the other bulb is kept wet. The paired temperature values can be used to find humidity using tables or by calculation. As for mechanical hygrometer, the expansion and contraction of the materials used is in proportion to the humidity change. Hygrometer is inexpensive and easy to use, however, it is not suitable for some applications that requires precision, cost, ease of operation, background interference and remote operation, as mentioned by Yeo et al. (2008).

For the past years, optical fiber humidity sensors have attracted much attention, as an alternative to the conventional humidity sensor. Optical fiber humidity sensor is small in size, free from electromagnetic interference, intrinsic safety and remote sensing, as well as offering the potential of distributed sensing using the fiber itself as sensor (Kharaz & Jones 1995; Corres et al., 2008). Ascorbe et al. (2017) demonstrated a classification of optical sensor humidity sensor based on their working principle, as shown in Figure 2.21

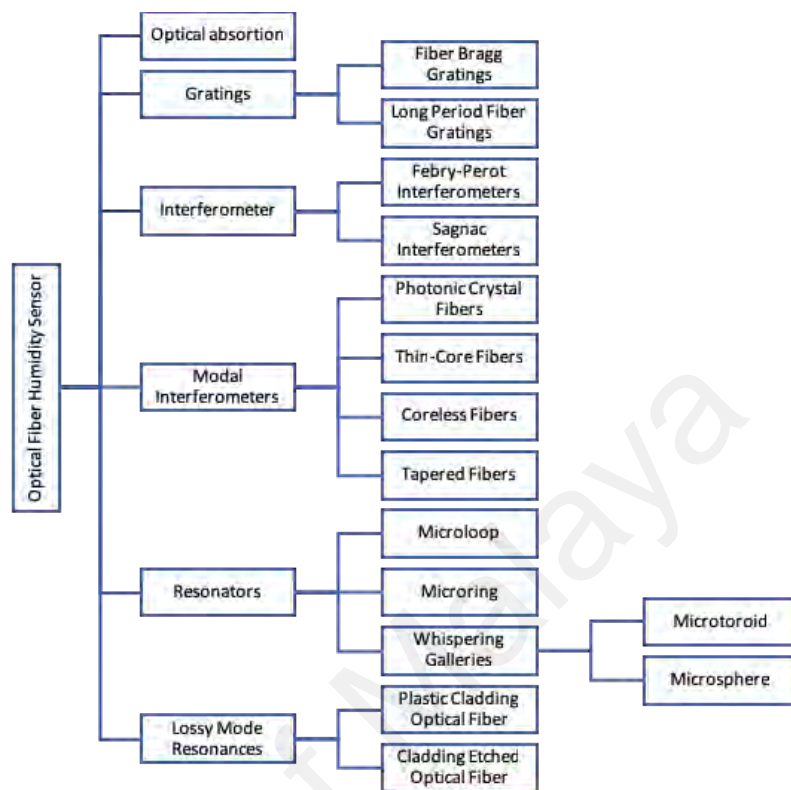


Figure 2.21: Classification of Optical Fiber Humidity Sensor
(Ascorbe et al., 2017)

Gupta (2001) demonstrated a fiber optic humidity sensor based on the moisture dependence absorption of light using U-bent fiber, coated with phenol red doped PMMA film. The proposed sensor is based on the interaction of the evanescent field with the coating used as the sensitive material, providing changes of the transmitted optical power. Measurement of humidity started at 20 % by passing the hot air in the humidity chamber. To increase the value of humidity, a beaker filled with hot water was placed in the chamber. The hot water is used to increase the moisture in the air inside the chamber, hence the humidity. The maximum RH that can be achieved for this experiment was 80%. The output power at each humidity level was measured with power meter. The U-shape used decreases the angle of incident of the ray at the film-core interface, hence, increases the fraction of light in the film. As the bending radius of the probe decreases, the

sensitivity increases. Similarly, type of U-bent fiber has been coated with other variety of potential materials and chemical reagents, in light of their humidity-dependent optical absorption properties. For example, Jindal et al. (2002) employed phosgene (CoCl_2) doped PVA film, Kharaz & Jones (1995) used CoCl_2 doped HEC and gelatin films as the sensitive material and Otsuki et al. (1998) reported the use of Rhodamine B doped HPC film.

Sensitive materials can also be coated on the tapered fiber and this approach has garnered much interest in sensing RH. As mentioned earlier, tapering fiber optic can expose the evanescent field of the transmitted light, ensuring an interaction between the light propagated in the fiber and its surrounding. In fact, ZnO nanostructure materials can also affect the sensitivity and performance of humidity sensor. The variety of morphologies from different synthesis techniques offers wider applications, including humidity sensor.

As reported by Qiu & Yang (2007), ZnO nanotetrapods fabricated have an arm diameter down to 17 nm, and with arm lengths ranging from 50 nm up to a few micrometers. The tetrapod sensor can be operated between 40 % to 100 % of relative humidity. The sensing mechanism for the proposed sensor was based on ionic conduction whereby protons dissociated from water molecules act as charge carriers transporting charge between physisorbed water molecules on the ZnO surface. In another work carried out by Qi et al. (2008), a highly sensitive humidity sensor with rapid response and recovery, which is based on the flower-like ZnO nanorods was reported. Relative humidity was measured based on the dependence of the impedance of the flower-like ZnO nanostructures. It was found that the impedance of the film decreases with increasing the frequency at low RH, and the impedance difference between adjacent two working frequencies becomes progressively smaller with increasing RH. This is because, at higher

frequencies, the adsorbed water cannot be polarized, and the dielectric phenomenon does not appear. Low working frequency can ensure high RH sensitivity and good linearity over the entire RH range.

As reviewed by Farahani et al. (2014), humidity sensors, especially the ones that incorporating nano-scale element, has high potential in enhancing accuracy, reliability, and economic efficiency, and ceramic/polymer are among the most promising material for sensing humidity.

University of Malaya

CHAPTER 3

ZINC OXIDE COATED MULTIMODE TAPERED PLASTIC OPTICAL FIBER FOR HUMIDITY SENSOR

3.1 Introduction

The developments of novel optical fiber devices have become the central focus of optical fiber researches in the past recent years. One in particular are the invention of tapered optical fibers that have led to various impressive applications in microscale and nanoscale photonic devices (Bariáin et al., 2000; Brambilla et al., 2004; Eggleton et al., 2001; Polynkin et al., 2005; Stiebeiner et al., 2010; Tian et al., 2011). These types of waveguides have found profound applications in the fields of biochemical, biomedical, environmental and different area sensors etc. The sensitivity of the fiber is enhanced by enabling the interaction between the evanescent fields in of the sensing fibers with the analyte under investigation. They are able to guide light at visible and infrared wavelengths with low loss (Shi et al., 2006; Wolchover et al., 2007).

To date, comprehensive researches have been conducted on the fabrication, characterization and use of tapered silica-core fibers. However, one practical limitation of using silica-core fibers is that when a section of cladding is removed, the exposed fiber core is very fragile and brittle which further imposes restrictions on sensor design and handling. Alternatively, plastic optical fibers (POFs) such as polymethylmethacrylate (PMMA) may be used as an alternative to silica-core optical fibers due to their comparatively cheaper price, and considerably more flexible structure. POF possess a strain limit of over 50 %, whereas the silica-based fibers are fragile and will break under a strain of only 5 %. The simplicity of use owing to the simple set-up involved and the

absence of expensive termination tooling, make POF an attractive alternative for tapered fiber sensors. Furthermore, they possess good tensile strength, higher numerical aperture, load resistance and lower bend radius limits than standard fibers (Gravina et al., 2009).

POFs have been used extensively in optical sensing applications due to their flexibility, resistance to impacts and vibrations, immunity to electromagnetic interference, and excellent coupling of light from light source to fiber (Bilro et al., 2012; Zubia & Arrue, 2001). Normally, POF-based sensors do not require rare materials to develop and they can be employed at room temperature. POF sensors can be used to detect temperature, strain, pressure and humidity (Yeo et al., 2008). Generally, humidity or moisture content is related to the presence of water in gaseous form and thus most humidity sensors are based on adsorption and desorption processes (Yeo et al., 2008). For optical fiber sensors, changes in the behavior of the evanescent field passing through the media whose refractive indices are influenced by the water molecules absorbed or desorbed, has been used in relative humidity measurement.

POF consists of cladding and core with refractive index of 1.402 and 1.492 respectively. In this work, the cladding of the POF was removed using a chemical etching technique. This was done so that Al-doped ZnO nanostructures can be coated onto the tapered region. ZnO was chosen because it is a wide band gap semiconductor with a gap energy of about 3.4 eV at room temperature, and regularly used as transparent conductive layer without toxic components (Czigany et al., 2009). It is also a unique material that exhibits semiconducting, piezoelectric, and pyroelectric multiple properties. These unique nanostructures unambiguously demonstrate that ZnO is probably the richest family of nanostructures among all materials, both in structures and properties (Gao & Li, 2009). When aluminium (Al) is doped with ZnO, the electrical property of ZnO is improved and the optical or magnetic properties can be altered

(Djurišić et al., 2010). ZnO can be doped with various Group-III metals such as B, Al, In and Ga, among which Al doping produces highly conductive due to the close covalent bond length of Al–O (0.192 nm) to that of Zn–O (0.197 nm) (Mridha & Basak, 2007).

In this chapter, POF was tapered and coated with Al-doped ZnO nanostructures and its behavior towards changes in relative humidity based on the intensity modulation technique was studied. Al – doped ZnO nanostructures coating is carried out using sol-gel immersion method on both seeded and non-seeded fibers. The performance of the proposed POF based RH sensor is also compared with tapered silica microfiber-based sensor.

3.2 Preparation of tapered POF through chemical etching process

The fabrication of tapered POF discussed and demonstrated in this section is done by chemical etching method. The fiber used is a step indexed multimode fiber with an overall cladding diameter of 1 mm, a numerical aperture of 0.51 and an acceptance angle of 61°.

Chemical etching of plastic fibers is very attractive because it has the potential for batch fabrication of a larger number of identical tapered regions. Acetone, de-ionized water and sandpaper were used to taper the fiber. The acetone solution was applied to the PMMA using a cotton bud. The PMMA fiber was then neutralized with de-ionized water. The milky white surface around the outer cladding of the plastic fiber was removed using sandpaper for about 8-10 seconds. This process was repeated until the tapered fiber has reached the desired stripped region length of the waist diameter. A microscopic is used to identify any areas of cladding remaining in place and hence can be removed by repeating the entire process. The core will remain in its original condition even with the exposure

to the solvent provided that the exposure times are limited as described. The use of fresh solvent for each process ensures a much more consistent taper surface finish across the samples provided.

In an earlier work, it was found that waist diameters in the range of 0.40 mm to 0.50 mm showed a good sensitivity to refractive index variation whereas those above 0.55 mm and below 0.40 mm did not demonstrate substantial sensitivity (Muhammad et al., 2013). Figure 3.1 (a) and (b) show the microscope images of the original un-tapered and tapered POF, which have a cladding diameter of 1 mm and 0.45 mm respectively. The total length of the tapered section was 10 mm. Finally, the tapered POF fiber was cleansed again using de-ionized water. The described process of the chemical etching technique is repeatable and does not require high operator skill. Furthermore, the etching process is gradual, which makes it simpler to monitor the waist diameter physically or optically, by measuring the transmitted power.

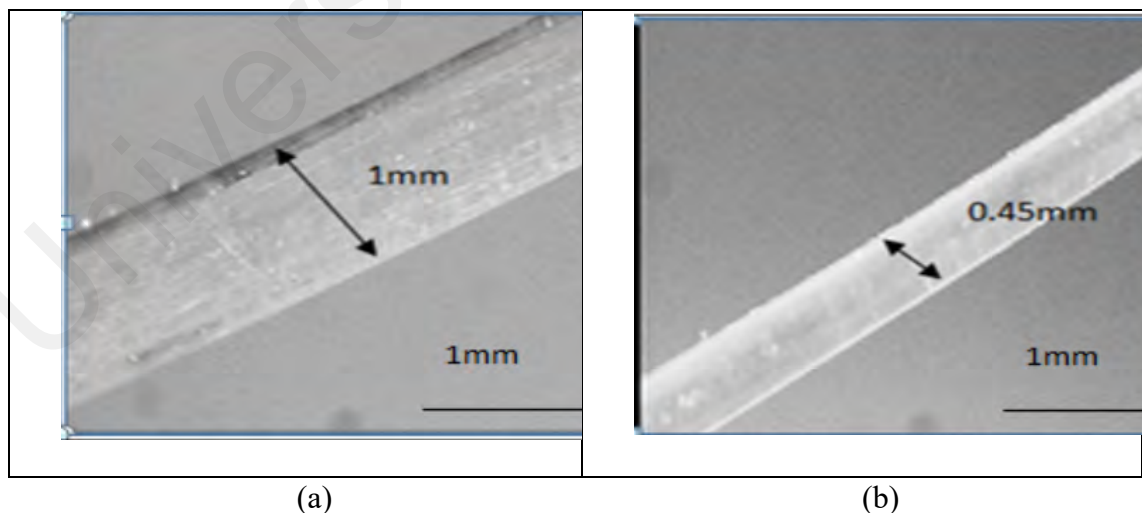


Figure 3.1: Microscopic image of the (a) un-tapered PMMA fiber (with diameter of 1 mm) and (b) Tapered PMMA fiber (with diameter of 0.45 mm), with etching technique

3.3 Coating of POF with Zinc Oxide nanostructures for relative humidity sensing

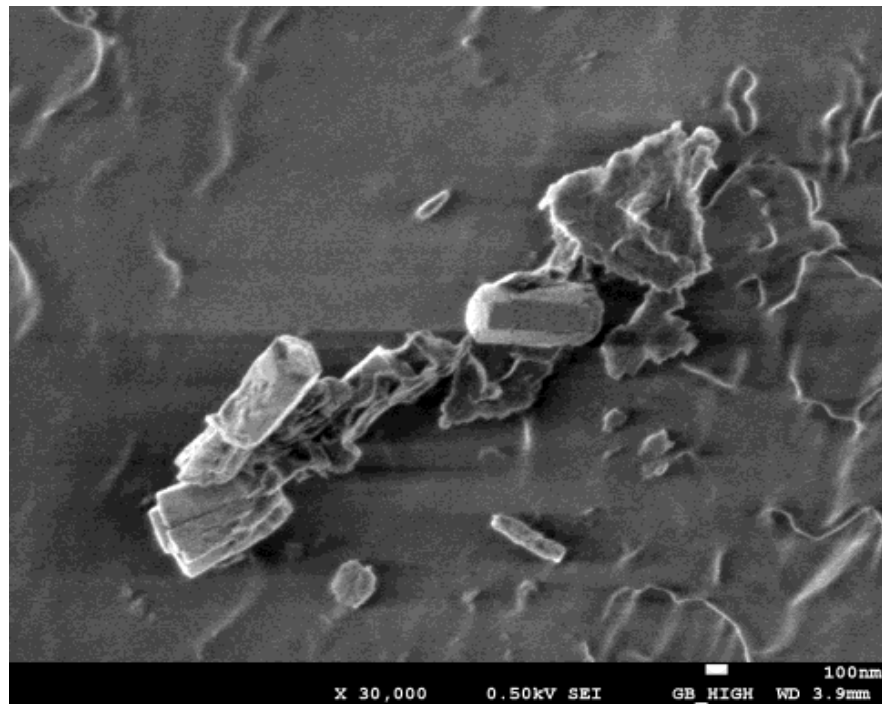
Zinc Oxide (ZnO) is a semiconductor with a bandgap of 3.3 eV and has been a subject of intense interest in recent years for various applications such as communication, biosensor etc (Coleman & Jagadish, 2006; Yakimova, 2012; Zhang et al., 2005). It has a wide range of properties including a range of conductivity from metallic to insulating (including n-type and p-type conductivity), high transparency, piezoelectricity, wide-bandgap semi-conductivity, room-temperature ferromagnetism, and huge magneto-optic and chemical-sensing effects (Schmidt-Mende & MacManus-Driscoll, 2007). The advantages of ZnO are that it can be easily processed by wet chemical etching and has shown an excellent stability under high-energy radiation. In addition, it can be grown in a variety of nanostructured morphologies by various low cost and low temperature methods (Djurišić et al., 2010). These nanostructures have many unique advantages such as high surface area and high sensitivity even at room temperature (Schmidt-Mende & MacManus-Driscoll, 2007). For instance, light coupled to nanostructures enhances the optical interaction between the device and the ambient environment (Y. Liu et al., 2012). Besides, in combination with immobilized enzymes, it can also enhance the direct electron transfer between the enzyme's active sites and the electrons (Ali et al., 2012). Therefore, many new sensors have been developed based on the ZnO nanostructure. For instance, ZnO nanowires grown on the surface of gold coated on flexible plastic substrate has been demonstrated as a good uric acid biosensor (Ali et al., 2012).

The deposition of ZnO nanostructures have been demonstrated on various polymer and silica substrates (Kim et al., 2012; Zubia & Arrue, 2001). Looking at the compatibility of ZnO crystal structure, there is no apparent difference between polymer and silica, as both do not have defined crystal structures. In this chapter, a new sensor for detecting changes in RH is proposed and demonstrated using a tapered POF coated with

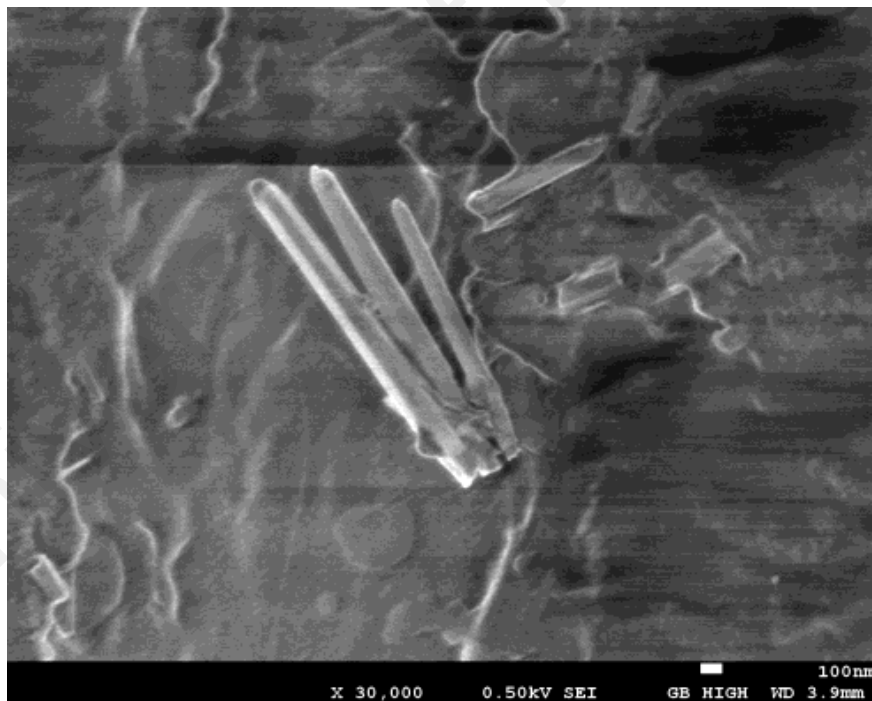
ZnO nanostructures, which is grown using both seeded and non-seeded techniques. The ZnO nanostructures on the tapered fiber induce changes of the optical properties in response to an external stimulus. The measurement is based on intensity modulation technique to detect the changes in RH. In this section, the tapered POF was with Al-doped ZnO nanostructures and its behavior towards changes in relative humidity based on the intensity modulation technique was studied. The performance of the sensor is also investigated with un-doped ZnO nanostructure.

3.3.1 Coating of unseeded Al-Doped ZnO nanostructures onto the tapered POF

The un-doped ZnO and 1 mol% Al-doped ZnO nanostructure were synthesized using the sol-gel method. Aqueous solution of zinc nitrate hexahydrate ($\text{Zn}(\text{NO}_3)_2 \cdot 6\text{H}_2\text{O}$) (0.01 M), hexamethylenetetramine (HMTA; $\text{C}_6\text{H}_{12}\text{N}_4$) (0.01 M) and aluminium nitrate nonahydrate ($\text{Al}(\text{NO}_3)_3 \cdot 9\text{H}_2\text{O}$) are prepared using deionized (DI) water. The solution was stirred until solution temperature rose to 60 °C for 2 hours to obtain clear homogeneous solution and then the solution was kept for aging for 24 hours prior for fiber coating process. The fiber was put in the solution for 15 hours. Finally, the fibers were taken out of solution and cleaned with DI water and dried at 50°C. The fiber was then characterized using Field Emission Scanning Electron Microscope (FESEM) to investigate the morphology of undoped and Al-doped ZnO nanostructures coated tapered fiber. Figure 3.2 shows the FESEM images of undoped ZnO nanostructures and Al doped ZnO nanostructures. From the pictures, it can be seen that the morphology of ZnO will change when it is doped with aluminium. It has been proved and reported by Djurišić et al. (2010).



(a)



(b)

Figure 3.2: FESEM images of (a) un-doped ZnO nanostructures and (b) Al doped ZnO nanostructures coated onto the tapered POF

3.3.2 Experimental arrangement for the relative humidity sensing

Figure 3.3 shows the experimental setup for the proposed sensor to detect changes in relative humidity using the fabricated tapered POF with un-doped ZnO and Al-doped ZnO nanostructures. The setup consists of a light source, an external mechanical chopper, the proposed probe, a highly sensitive photo-detector, a lock-in amplifier and a computer. The input and output ports of the tapered POF are connected to the laser source and photo-detector, respectively. The light source used in this experiment is a He-Ne laser which operates at a wavelength of 633 nm with an average output power of 5.5 mW. It was chopped at a frequency of 113 Hz by a mechanical chopper to avoid the harmonics from the line frequency which is about 50 to 60 Hz. The 113 Hz frequency was chosen as an odd number to prevent multiplication of 50 and 60 Hz. Besides that, it is an acceptable value of output and stability. In addition to that, an increase to the value of chopper frequency causes the output voltage and stability to decrease.

The probes that were used to measure relative humidity in this experiment were fabricated tapered POF coated with un-doped ZnO and Al-doped ZnO nanostructures. Laser source (He-Ne) is launched into the tapered POF placed in a sealed chamber with a dish filled with saturated salt solution. The sealed chamber is constructed with a hole and the tapered POF is introduced through it into the sealed receptacle and suspended to saturated salt solutions in order to simulate different values of relative humidity. In the experiment, the performance of the proposed sensor was calibrated for relative humidity ranging from 50 to 80 % using 1365 data logging humidity-temperature meter. The output lights were sent into the silicon photodetector (818 SL, Newport) and the electrical signal was fed into the lock-in amplifier (SR-510, Stanford Research System) together with the reference signal of the mechanical chopper. The output that resulted from the lock-in amplifier was connected to a computer through an RS232 port interface and the signal was processed using Delphi software. The reference signal from the chopper was matched

with the input electrical signal from the photo-diode. This allows a very sensitive detection system that will remove the noise generated by the laser source, photo-detector and the electrical amplifier in the photo-detector.

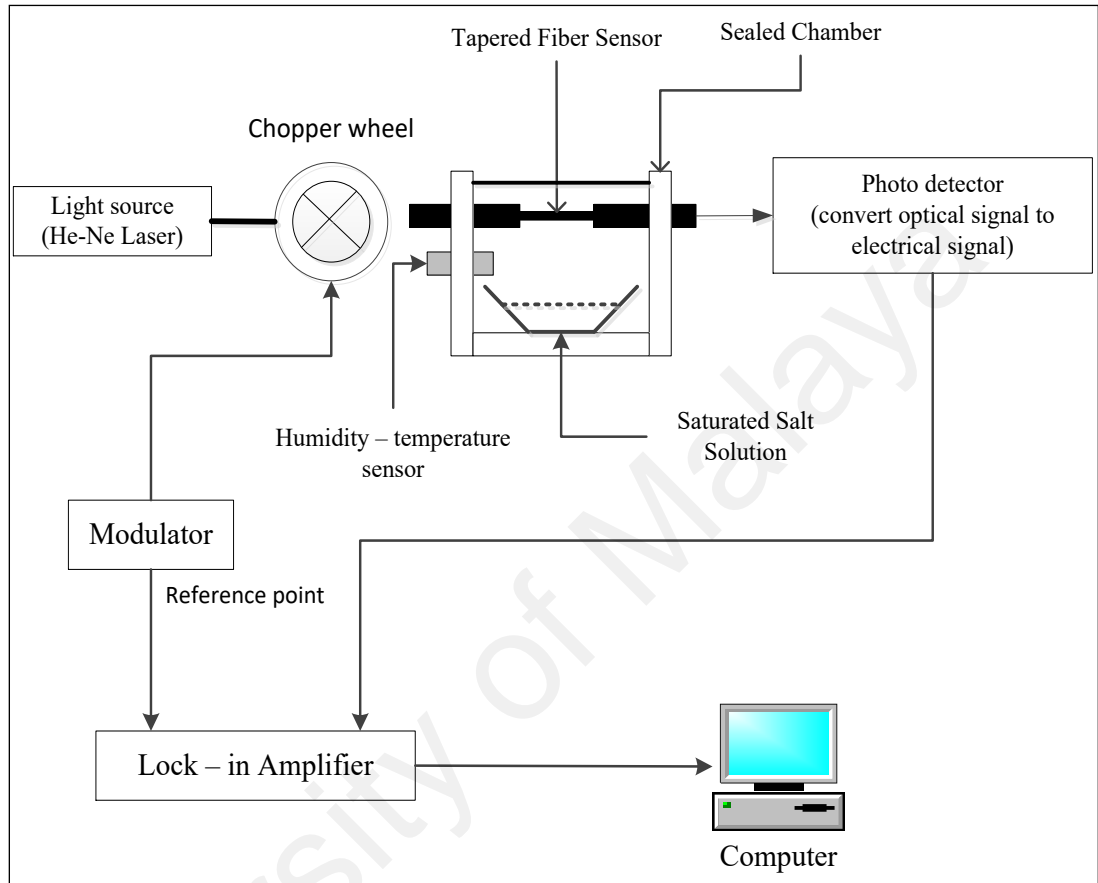


Figure 3.3: Experimental setup for the proposed relative humidity sensor using a tapered POF coated with un-doped ZnO and Al-doped ZnO nanostructures

3.3.3 Sensing performance

Figure 3.4 shows the variation of the transmitted light from the tapered POF coated with Al-doped ZnO nanostructures at different doping concentration and the data of output voltages against the relative humidity, which were collected for 600 seconds. The change in the intensity of the transmitted light of the tapered POF coated with Al-doped ZnO nanostructures decreases linearly with relative humidity. It is found that at 1 mol %, the tapered POF has a sensitivity of 0.0172 mV % and a linearity of 97.5 %.

These two values are the best amongst the other doping concentrations that were tested in this experiment. Therefore, it can be concluded that tapered POF coated with Al doped ZnO nanostructures at 1 mol % exhibits better performance compared to 0.5, 3 and 5 mol % respectively.

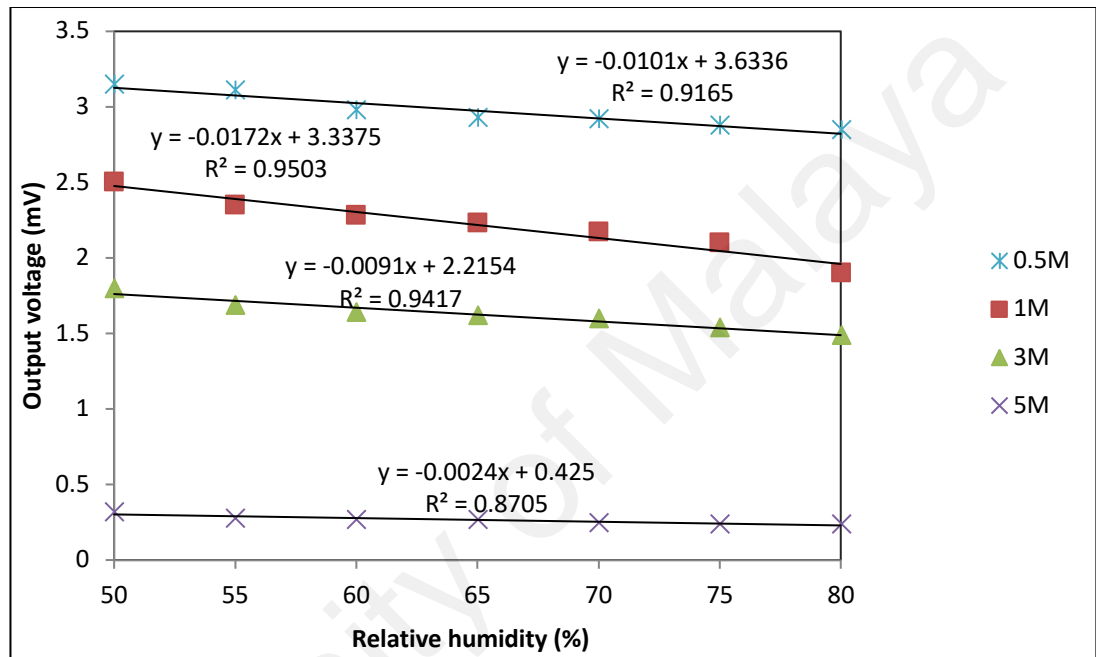


Figure 3.4: Output voltage against relative humidity for the proposed tapered POF with Al-doped ZnO nanostructure at different doping concentration

The tapered POF coated with Al-doped ZnO nanostructures at 1 mol 1% is then compared with un-doped ZnO by Batumalay et al. (2014) as shown in Figure 3.5. It can be observed that when ZnO is doped with Al, the sensitivity of the proposed sensors have improved as shown in Figure 3.5. According to Liu et al. (2012), the refractive index (RI) of ZnO composite varies from 1.698 to 1.718 with relative humidity change from 10 – 95%. The ZnO composite are exposed to an environment of humidity which causes rapid surface adsorption of water molecules. The optical properties of ZnO composite

surfaces are modulated by the surface adsorption of water molecules. The increase of water molecules being absorbed on ZnO composite results in an increase of relative humidity (Liu et al., 2012). The increasing water molecules cause an increase in both effective refractive index of surrounding medium and absorption coefficient of the ZnO composite surfaces and leads to larger leakage of light. In addition, according to Prajapati et al. (2013), when ZnO is doped with Al, refractive index will decrease. This decrement causes the graph to decrease; however, the performance of the sensor has enhanced, as shown in Figure 3.5. Doping can increase a current carrier in material, therefore when ZnO is doped with Al, there will be more electrons because Al atoms are ionized to Al^{3+} whereas Zn is ionized to Zn^{2+} (Md Sin et al., 2011). Thus, one free electron is produced from one Zn atom replacement. The increase in carrier concentration causing a decrease in the resistivity, hence more current can pass through the fiber and therefore yield a higher output voltage.

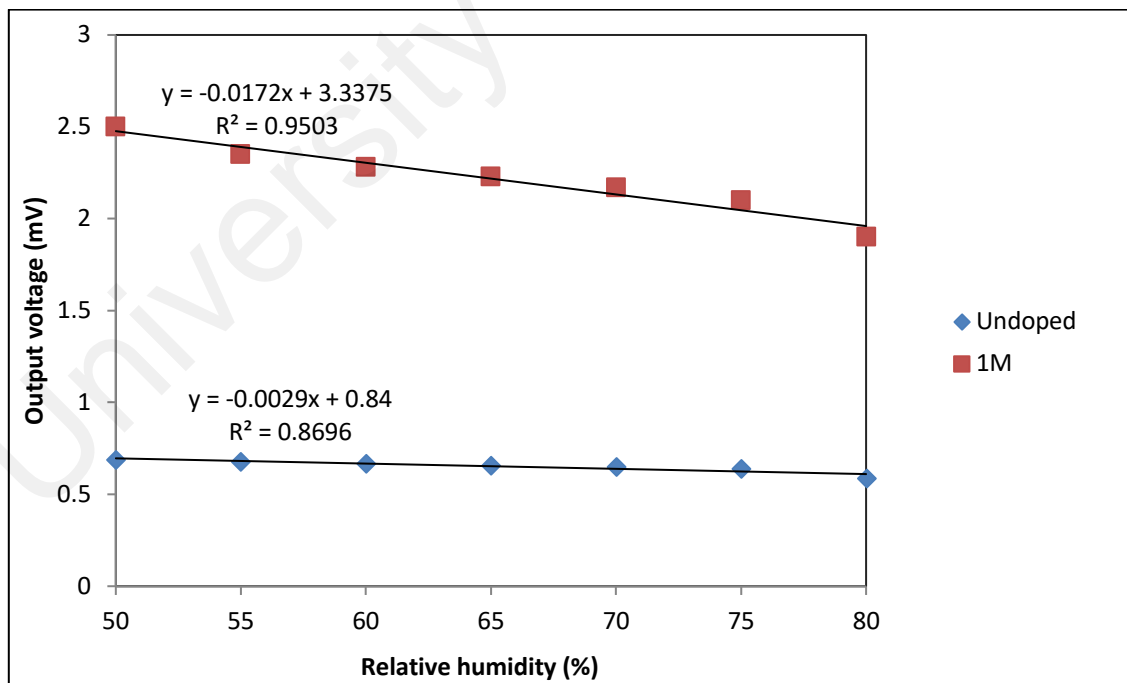


Figure 3.5: Output voltage against relative humidity for the proposed tapered POF with un-doped ZnO and Al-doped ZnO nanostructure

The performances of the proposed sensor are summarized in Table 3.1 and Table 3.2. Overall, the sensor is observed to be sufficiently stable with standard deviations of 0.0130 mV for Al-doped ZnO at concentration of 1 mol % as being recorded for the time duration of 600 s.

Sensitivity is a measurement obtained from the slope of the output characteristic curve. It is defined as the minimum input of physical parameter that will create a detectable output change. The sensitivity can be calculated using this formula:

$$\text{Sensitivity} = \frac{\text{Change in output voltage}}{\text{Corresponding change in \%RH}} \quad (3.1)$$

As shown in Figure 3.5, value of sensitivity can be obtained graphically. The transfer function shown is in term of the following equation:

$$y = mx + c \quad (3.2)$$

whereby m is the slope of the output characteristic curve. By comparing the values of m for both Al-doped ZnO and un-doped ZnO, Al-doped ZnO has higher value, which is 0.0172 mV/%, whereby un-doped ZnO is only 0.0029 mV/%. In comparison, it can be deduced that Al-doped ZnO has higher sensitivity than un-doped ZnO. Besides that, when ZnO is doped with Al, the limit of detection has also improved tremendously. The limit of detection (LOD) is calculated by dividing the standard deviation with the sensitivity, which indicates that the system is more efficient when the value of LOD is lower. Based on the calculation, it shows that when ZnO is doped with Al, the sensor is more stable with a value of 0.7558 %. These results show that the proposed sensor coated with

Al-doped ZnO nanostructures exhibits better performance in measuring the changes of relative humidity in real time.

Table 3.1: Performance of the proposed RH sensor at different doping concentration

Performances	0.5 mol %	1 mol %	3 mol %	5 mol %
Sensitivity (mV/%)	0.0101	0.0172	0.0091	0.0024
Linearity (%)	95.7	97.5	97	93.3

Table 3.2: The performance of the proposed RH sensor for un-doped ZnO and Al-doped ZnO

Performances	Undoped	1 mol %
Sensitivity (mV/%)	0.0029	0.0172
Linearity (%)	93.3	97.5
Standard deviation (mV)	0.0789	0.0130
Limit of detection (%)	13.84	0.7558

3.4 RH sensor employing tapered POF coated with seeded Al-Doped ZnO

A relative humidity sensor operating on intensity modulation principle is proposed and demonstrated using a tapered POF that is coated with seeded Al-doped ZnO nanostructures. The tapered POF was prepared based on chemical etching technique using acetone, de-ionized water and sandpaper. They have a stripped region waist diameter of 0.45 mm and the total length 10 mm, which is similar to the previous sensor. The preparation for ZnO nanostructures on the tapered fiber consists of two primary steps: First, the seed layer to grow the ZnO nanostructures on the fiber was developed using a simple manual dip coating technique. The seeded solution was prepared using zinc acetate dehydrate ($\text{Zn}(\text{CH}_3\text{COO})_2 \cdot 2\text{H}_2\text{O}$) as a precursor dissolved in isopropanol. In this experiment, 0.55 g zinc acetate dehydrate was mixed into 100 ml isopropanol. The solution was stirred at 60° C for 2 hours in ambient to yield a clear and homogenous solution. Then, the solution was cooled down to room temperature for the coating process. The fiber was manually dipped into the seeding solution and was dried at 60° C for 10 minutes to evaporate the solvent and to remove the organic residuals. This coating and drying method was repeated for 5 times to increase the thickness of the seed layer.

Subsequently, ZnO nanostructures/nanorods solution was prepared using zinc nitrate hexahydrate ($\text{Zn}(\text{NO}_3)_2 \cdot 6\text{H}_2\text{O}$) as the Zn precursor and hexamethylenetetramine (HMTA, $\text{C}_6\text{H}_{12}\text{N}_4$) as the reducing agent. Both chemicals were dissolved in deionized (DI) water at a concentration of 0.01 M. Al doped ZnO nanostructures/nanorods, aluminium nitrate nonahydrate ($\text{Al}(\text{NO}_3)_3 \cdot 9\text{H}_2\text{O}$) solution was added to the stock solution at concentrations of 0.5, 1, 3 and 5 mol % Al with respect to Zn. The solution was stirred at 60 °C for 2 hours to yield a clear and homogenous solution and left overnight for aging. The seeded tapered fiber was immersed in the stock solution for 15 hours to grow ZnO nanostructures/nanorods. Finally, the tapered fiber was dried at 60 °C for 1 hour. The fiber sensor was then characterized using Field Emission Scanning Electron Microscope

(FESEM) to investigate the morphology of the seeded Al-doped ZnO nanostructures tapered fiber.

Figure 3.6 shows the FESEM images of the Al doped ZnO nanostructures grown using seeded method. Compared with the images in Figure 3.2, it is shown that the morphology of ZnO changes and the nanorods become bigger and denser when the seeding method is employed as reported by Djurišić et al. (2010). The sensor probe behavior towards changes in relative humidity sensor based on the intensity modulation technique is then investigated using an experimental setup as shown in Figure 3.3.

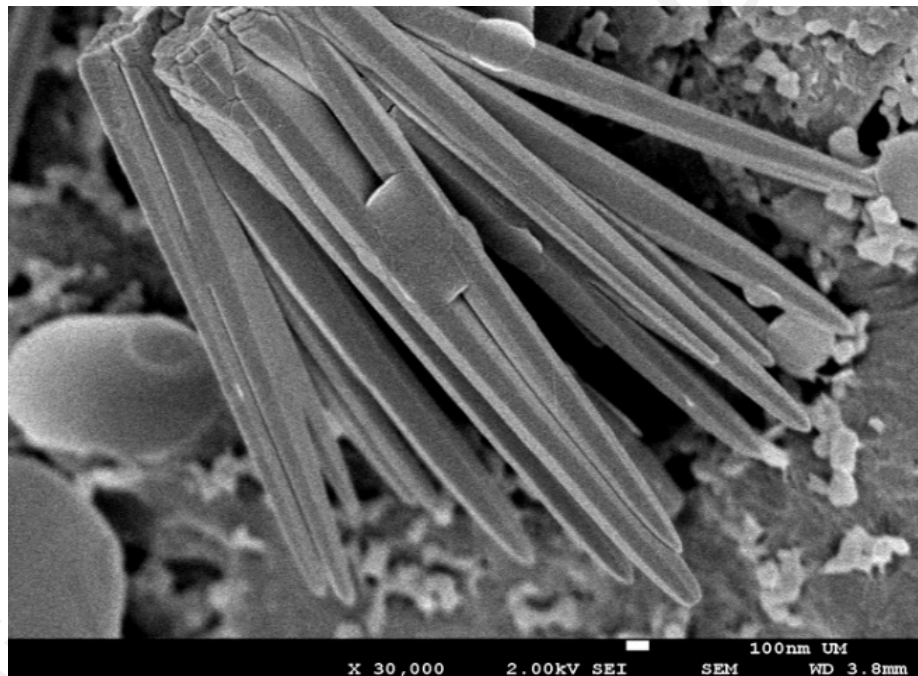


Figure 3.6: FESEM image of Al doped ZnO nanostructures obtained with seeding method

Figure 3.7 shows the outputs of the tapered POFs coated with Al-doped ZnO nanostructures at different doping concentrations against relative humidity, which were collected for 600 seconds. It can be inferred that the intensity of the transmitted light of the tapered POF decreases linearly with relative humidity. It is found that the POF coated

with ZnO structures with Al nitrate doping concentration of 1 mol % shows the best sensitivity and linearity of 0.0172 mV % and 97.5 % respectively. These are the best values offered by the tapered POF with seeded Al doped ZnO nanostructures.

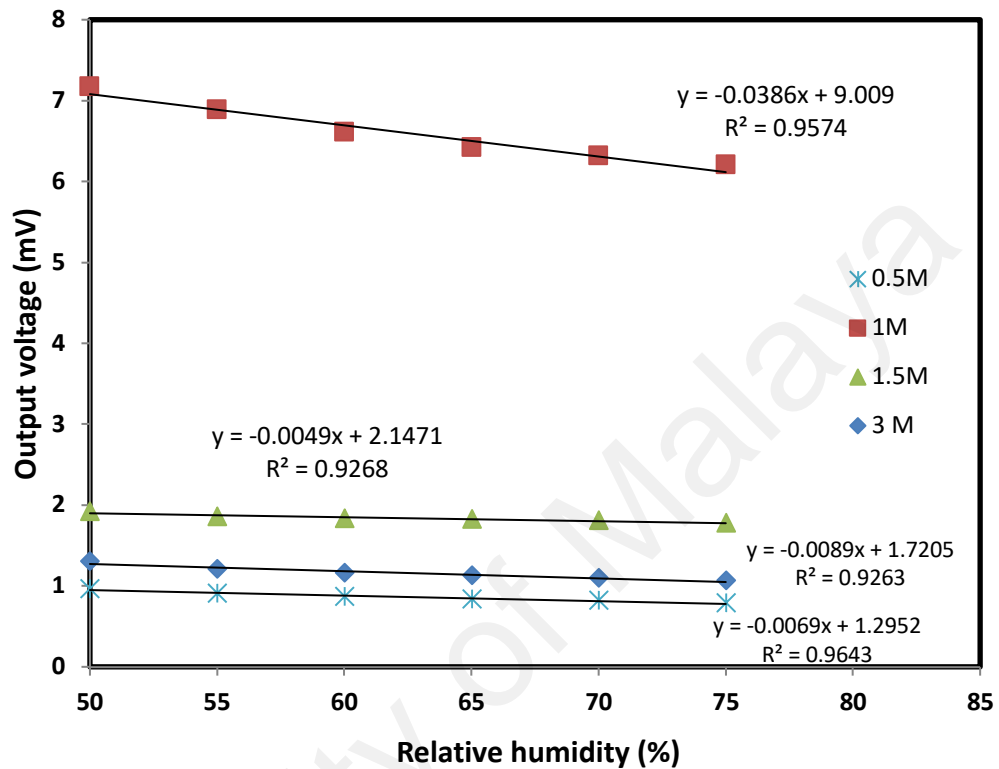


Figure 3.7: Output voltage against relative humidity for the proposed tapered POF with seeded Al-doped ZnO nanostructure at different doping concentration

The performance of the POF with seeded Al-doped ZnO nanostructures at 1 mol 1% is then compared with seeded un-doped ZnO by Batumalay et al. (2014) and non-seeded Al doped ZnO as shown in Figure 3.8. It can be observed that among the four tapered POF sensors, the one that is doped with Al with seeded method offers the best sensitivity of 0.0386 mV/%. According to Liu et al. (2012), the refractive index (RI) of ZnO composite varies from 1.698 to 1.718 with relative humidity change from 10 – 95%. When the ZnO composite is exposed to ambient humidity, rapid surface adsorption of water molecules occurs. The increase in water molecules absorbed by the ZnO coating

results in an increase in both effective RI of the coating and leakage of light (Liu et al., 2012a). In addition, according to Prajapati et al. (2013), when ZnO is doped with Al, its refractive index decreases. This reduction widens the difference in RI between the coating and water, thus enhancing the performance of the sensor, as indicated in Figure 3.8.

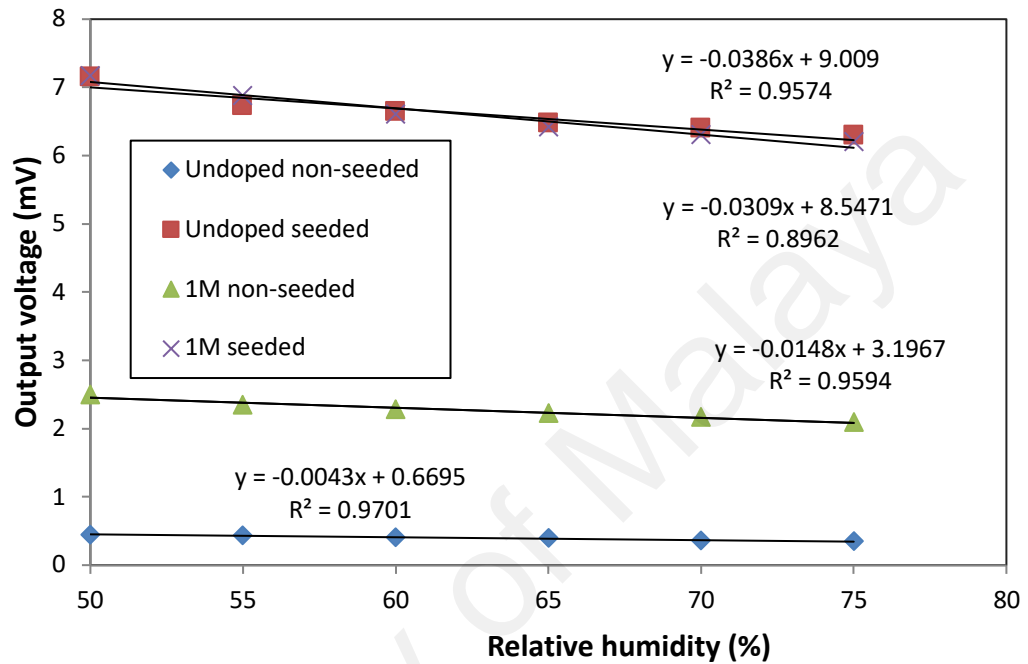


Figure 3.8: Output voltage against relative humidity for the proposed tapered POF with un-doped ZnO and Al-doped ZnO nanostructure (non-seeded method)

The performances of the proposed sensors with different concentrations of Al nitrate are summarized in Table 3.3. Overall, the outputs of the sensors are sufficiently stable with a sensitivity and linearity of 0.0386 mV/% and 97.84 %, respectively for seeded Al-doped ZnO at Al nitrate concentration of 1 mol % within a duration of 600 s. The sensor with seeded Al-doped ZnO has a higher sensitivity compared to the ones with un-doped seeded ZnO and non-seeded Al-doped ZnO at the same concentration as shown in Table 3.4. The performance of the proposed seeded RH sensor is also better than non-seeded sensor as shown in Table 3.5.

Table 3.3: The performance of the proposed RH sensor at different doping concentration

Performances	0.5 mol %	1 mol %	1.5 mol %	3 mol %
Sensitivity (mV/%)	0.0069	0.0386	0.0049	0.0089
Linearity (%)	98.2	97.84	96.27	96.24

Table 3.4: The comparison of performances between seeded ZnO and proposed RH sensor for seeded Al-doped ZnO

Performances	Undoped Seeded	Al-doped ZnO (1 mol %)
Sensitivity (mV/%)	0.0309	0.0386
Linearity (%)	94.67	97.84

Table 3.5: The comparison of performances between non-seeded and proposed seeded RH sensor for Al-doped ZnO

Performances	Non-seeded Al-Doped ZnO (1 mol%)	Seeded Al-Doped ZnO (1 mol %)
Sensitivity (mV/%)	0.0172	0.0386
Linearity (%)	95.05	97.84
Standard deviation (mV)	0.0130	0.0351
Limit of detection (%)	0.7558	0.909

3.5 Comparison with RH sensor employing silica microfiber coated with ZnO Nanostructures

In this section, the performance of the tapered POF based sensor is compared with another evanescent wave-based RH sensor employing a silica microfiber as a probe. The silica microfiber was fabricated from a standard single mode fiber (SMF) using a flame brushing technique. An oxy-butane burner was used as the heat source and the gas pressure was controlled at the lowest level of 5 psi to ensure that the convective air flow from flame is very low. Prior to tapering process, a small region of the fiber protective polymer buffer jacket was stripped and mounted onto a pair of motorized translation stages. During the tapering process, the fiber was being stretched out by pulling while heating by a moving torch to ensure the consistent heat is applied to the uncoated region of the fiber. The repeated heating process produced good uniformity of microfiber. ZnO nanostructures coating onto the silica microfiber was done using sol-gel immersion method as previously described.

The microfiber probe was then characterized using Field Emission Scanning Electron Microscope (FESEM) to investigate the morphology of ZnO nanostructures. The image is shown in Figure 3.9, which clearly shows the homogenous particles of ZnO nanostructures. The nanorod structure with hexagonal cross-section was not observed on the surface of microfiber.

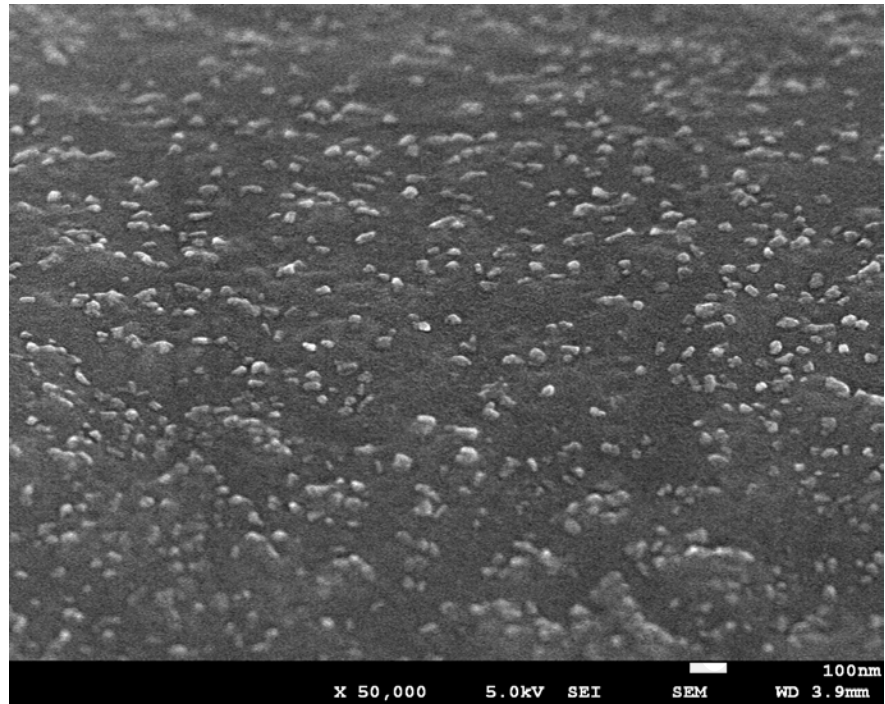


Figure 3.9: FESEM image of ZnO nanostructures coated on silica microfiber

Figure 3.10 shows the experimental setup to measure RH using a silica microfiber coated with ZnO nanostructures as a probe. As shown in the figure, ASE light from the Erbium-doped fiber amplifier (EDFA) is launched into the silica microfiber probe placed in a sealed chamber with a dish filled with saturated salt solution while monitoring the output spectrum using an OSA. The sealed chamber is constructed with a hole and the tapered silica microfiber is introduced through it into the sealed receptacle and suspended to saturated salt solutions in order to simulate different values of RH. In the experiment, the performance of the proposed sensor was calibrated for relative humidity ranging from 50 to 70 % using 1365 data logging humidity-temperature meter.

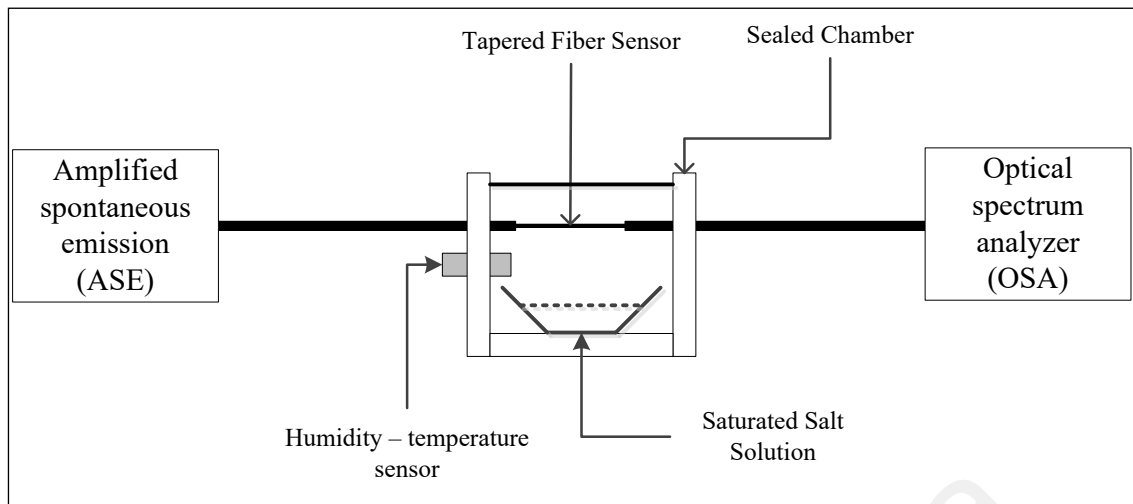


Figure 3.10: Experimental setup for the proposed RH sensor using a silica microfiber coated with ZnO nanostructures as a probe

Figure 3.11 shows the variation of the transmitted light from both tapered POF and silica microfiber coated with non-seeded ZnO nanostructures with data of output voltages against the RH. As shown in the figure, the tapered POF based sensor has a linearity of 97.61 % and sensitivity of 0.0222 mV/% while the linearity and the sensitivity of the silica microfiber-based sensor are 94.10 % and 0.0011 mV/% respectively. The working of the sensor is based on the refractive index changes. The variation of refractive index between core, cladding and sensitive material provides changes in the output voltage which has been discussed. When the tapered fiber is coated with sensitive material, it will act like an external stimulus, with a refractive index close to the effective index of the propagating modes along the fiber. When relative humidity increases, there will be more water molecules being absorbed by ZnO nanostructures, increasing the relative humidity and leads to larger leakage of light. The changes shown by both tapered fibers indicate that the ZnO coating has successfully functioned as a sensitive material and thus the performance of the sensor is significantly improved with the coating.

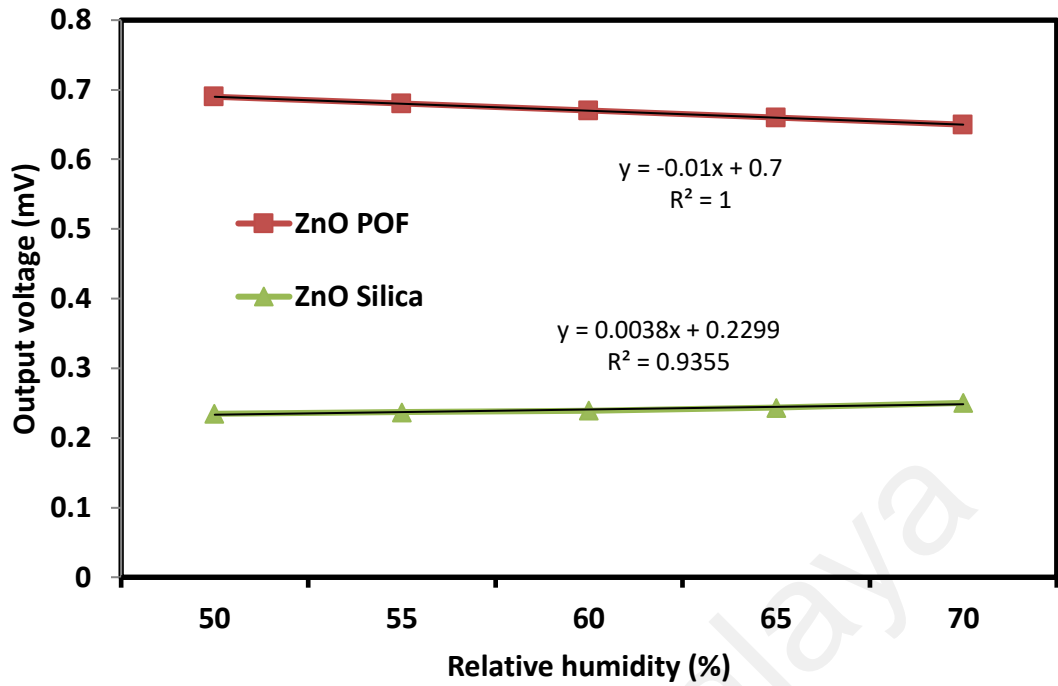


Figure 3.11: Output voltage against relative humidity for the proposed tapered POF and silica microfiber coated with non-seeded ZnO nanostructure

Figure 3.12 shows the variation of the transmitted light from both tapered POF and silica microfiber coated with seeded ZnO nanostructures with data of output voltages against the RH. As shown in the figure, the tapered POF based sensor has a linearity of 94.41 % and sensitivity has improved to of 0.176 mV/% while the linearity and the sensitivity of the silica microfiber-based sensor are 96.72 % and 0.0038 mV/% respectively. As reported by Liu et al. (2012), well-arrayed nanorods has large surface to volume ratio and the RI of ZnO composite changes from 1.698 to 1.718 as RH changes between 10 to 95%. When ZnO composite exposed to humid environment, it leads to rapid surface adsorption of water molecules and causes changes in optical properties. The RH value increases linearly with the amount water molecules being absorbed on ZnO composite and leads to larger leakage of light. Liu et al. (2012) also reported that the increasing water molecules cause an increase in both effective refractive index of surrounding medium and absorption coefficient of the ZnO composite surfaces and leads

to a larger leakage of light or losses. In addition, the interaction within the fiber and the target analyte results in refractive index change and as an approach for evanescent wave sensing. The higher the portion of evanescent wave travelling inside the fiber cause it to become more sensitive to physical ambience of its surrounding.

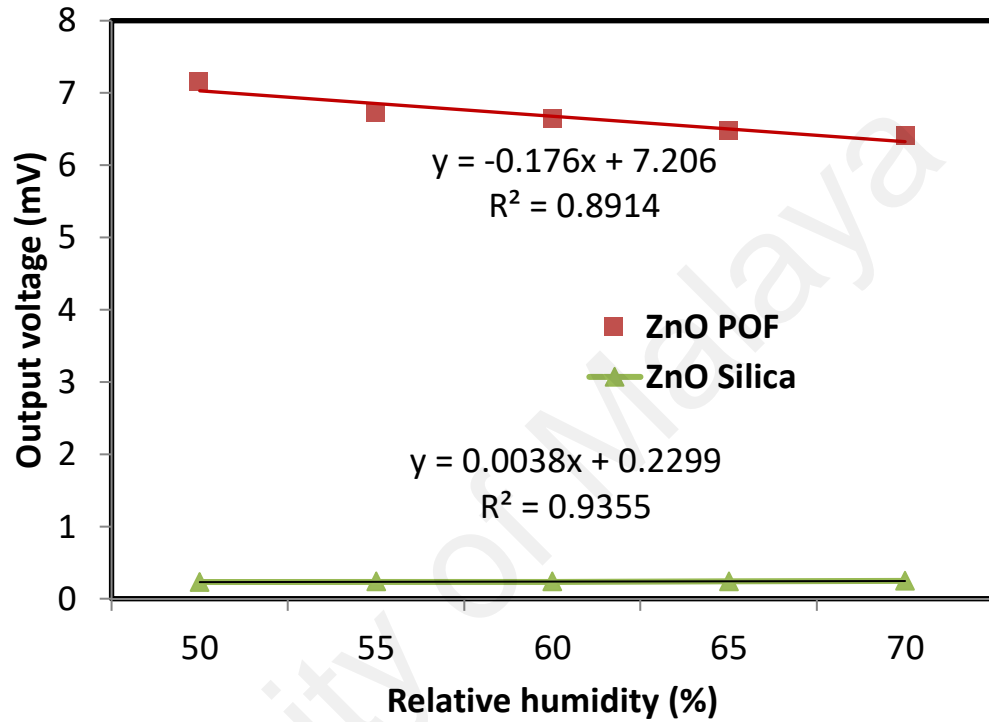


Figure 3.12: Output voltage against relative humidity for the proposed tapered POF and silica microfiber coated with seeded ZnO nanostructure

The performance comparison for both sensors is summarized in Table 3.6 and Table 3.7. As seen in the Table 3.6, tapered POF fiber coated with non-seeded ZnO has performed better as a RH sensor compared to that of silica microfiber. Tapered POF coated with non-seeded ZnO nanostructures exhibited better linearity and sensitivity with 97.61 % and 0.0222 mV/% respectively, while tapered silica microfiber coated with ZnO nanostructures shows linearity of 94.10 % and sensitivity of 0.0011 mV/%. Linearity is a measurement of a correlation coefficient, which is the reliability of linear relationship

between input and output parameter values. It provides the closest possible best fit to all data points on the curve. When the percentage of linearity is high or close to 100%, it shows that the measured sensitivity will not vary with input variable. Meanwhile, sensitivity is a measurement obtained from the slope of the output characteristic curve. It is defined as the minimum input of physical parameter that will create a detectable output change.

When the tapered fibers were coated with seeded ZnO nanostructures, sensitivities of the sensors have improved further, as shown in Table 3.7. It shows that sensitivity of tapered POF has increased from 0.0222 mV/% to 0.176 mV/% and sensitivity of tapered silica has improved from 0.0011 mV/% to 0.038 mV/%. However, tapered POF still performed better as a RH sensor when coated with seeded ZnO, compared to that of silica microfiber.

The differences in the obtained results are most probably due to the different tapering method applied to the fibers. The diameter of the POF core will not change when chemical etched method is applied in the tapering process and the coated ZnO nanostructures acted as external stimulus. The ZnO nanostructures on the tapered region play an important role by causing rapid adsorption of water molecules. Apart from that, the gradual process of the chemical etching enables much simpler monitoring of the waist diameter. In contrast, the flame brushing technique that was used to taper silica microfiber evenly reduced further the core and cladding diameters and altered the refractive index profile. Due to thinning of the core, light propagated through the tapered region will be more distorted. On the other hand, different methods of coating have shown different results to both of the tapered fibers. Seeded method has exhibited better performance as the sensitivities of proposed sensors have improved compared to the non-seeded method.

This probably due to more nanostructures were able to be formed as the dip and dry process produces the base for the ZnO nanostructures to grow.

Table 3.6: The performance comparison for both RH sensors with non-seeded ZnO

Performances	Tapered POF	Tapered Silica Microfiber
Sensitivity (mV/%)	0.0222	0.0011
Linearity (%)	97.61	94.10
Standard deviation (mV)	0.0356	0.0018

Table 3.7: The performance comparison for both RH sensors with seeded ZnO nanostructure

Performance	Tapered POF	Tapered Silica Microfiber
Sensitivity (mV/%)	0.176	0.0038
Linearity (%)	94.41	96.72
Standard deviation (mV)	0.2947	0.0061

3.6 Summary

A RH sensor has been successfully demonstrated using a tapered POF that is coated with Al-doped ZnO nanostructures. The sensor operates based on intensity modulation technique. The POF was tapered by chemical etching method whereby the fiber was immersed into acetone and polished by a sandpaper to reduce the fiber's waist diameter from 1 mm to about 0.4 - 0.5 mm. The tapered fiber was then coated with Al-doped ZnO nanostructures using sol-gel immersion method with different mol% of

Al nitrate that acts as a dopant. The 1 mol% of Al nitrate that used in the synthesis process exhibited better performance compared with the other doping concentrations. Then, results obtained for both undoped ZnO and 1 mol% of Al-doped ZnO were compared and investigated. The performance of 1 mol% of Al-doped ZnO demonstrated better linearity and sensitivity of 97.5% and 0.0172 mV/%, respectively, whereas the un-doped ZnO yielded linearity and sensitivity of 93.3% and 0.0029 mV/%, respectively.

A simple RH sensor is also demonstrated using a tapered POF with seeded Al-doped ZnO nanostructures. The tapered fiber was coated with seeded Al-doped ZnO nanostructures with various Al nitrate concentrations in mol %. It was observed that the morphology of ZnO changed with Al doping while the density of the nanorods improved with seeding. The density or the compactness of nanorods were observed by comparing the number of nanorods grown on the tapered fiber, for the same magnification size. The POF with seeded Al-doped ZnO with 1 mol % concentration exhibits a sensitivity of 0.0386 mV/% and a slope linearity of 97.84 %. This performance is superior to those recorded by un-doped and unseeded POF sensors.

The performance of the tapered POF sensor was also compared with the silica microfiber. The silica microfibers were fabricated using flame brushing techniques. In the experiment, both tapered fibers were then coated with zinc oxide (ZnO) nanostructures using sol-gel immersion on ZnO seeded and non-seeded fiber methods before it was used to sense relative humidity. It is found that the tapered POF coated with seeded ZnO performed better compared to tapered silica microfiber. The tapered POF coated with seeded ZnO based sensor has linearity and sensitivity of 94.41 % and 0.176 mV/%, respectively.

The proposed sensors provide numerous advantages, such as simplicity of design, low cost of production, higher mechanical strength, and is easier to handle compared with

silica fiber-optic. Results show that tapered POF with Al-doped ZnO nanostructures enables the increase in sensitivity of fiber for detection of changes in RH.

University of Malaya

CHAPTER 4

GROWTH OF ZINC OXIDE NANORODS ON TAPERED PLASTIC OPTICAL FIBERS VIA HYDROTHERMAL TECHNIQUE FOR RELATIVE HUMIDITY SENSOR

4.1 Introduction

Plastic optical fibers (POF) are large diameter, flexible and durable multimode fibers made from polymers, including polymethylmethacrylate (PMMA), polystyrene, polycarbonates and per-fluorinated materials. Most of the commercial POFs are made of PMMA with core diameter in mm range and step index profile with typical core and cladding indices of 1.49 and 1.41, respectively (Shin & Park, 2013). In recent years, POF has garnered many interests to researchers in developing and commercializing various applications due to its characteristics, such as greater flexibility and capability to resist impacts and variations (Zubia & Arrue, 2001). In addition, unlike silica-based fibers that will break under a strain of only 5%, POF will not break with strains over 50% (Gravina et al., 2009). This interesting physical and mechanical feature, together with the recent advances of polymer technology, enable POF to be used in various sensor designs. POF has several advantages over glass fiber as far as sensing applications are concerned, in that a number of enabling technologies has been made it possible. Furthermore, it can easily be used to enhance the performance of various sensors, using simple and inexpensive techniques and equipment, compared with those required for glass.

POFs have been employed in many sensor applications based on various techniques. For instance, by monitoring optical power attenuation caused by the refraction at the taper region of POF, the refractive index of the surrounding medium can

be sensed (Morisawa & Muto, 2012). Muhammad et al. (2013) reported that a simple sensor arrangement based on a tapered POF can be used to monitor salinity based on different concentration of sodium chloride (NaCl) in de-ionized water. Beres et al. (2011) has proposed POF based biosensor to detect cells in aqueous medium. POF also has been used to measure different concentrations of uric acid in de-ionized water, as reported by Batumalay et al. (2014).

As discussed in the previous chapter, humidity measurement has becoming an important issue in various areas of applications such as instrumentation, automated systems, agriculture and climatology. Hence, numerous sorts of humidity sensors are being fabricated and developed for industrial and laboratory applications. Wu et al. (2011) reported a fiber-optic interferometric humidity sensor based on silica/polymer microfiber knot resonators (SMKR/PMKR). The sensors were fabricated using silica/polymer microfibers without any humidity-sensitive coating. Batumalay et al. (2014) proposed a humidity sensor that employed hydrophilic gel (agarose) deposited on the tapered POF. The sensor was operated based on the intensity modulation technique. The agarose that was coated on the fiber acted as a sensing element, whereby it absorbed moisture from or to the ambience and altered the refractive index, thus, change its ability to modulate the intensity of light that propagates through the fiber. Chang et al., (2010) fabricated a humidity sensor using the randomly oriented nanowires bridged across two electrodes, with the growth of high-density single crystalline ZnO nanowires on patterned ZnO:Ga/SiO₂/Si templates. By measuring I–V characteristics of the fabricated device at 80 °C with 25%, 50%, 70%, 90% RH, it was found that resistance of the humidity sensor decreased monotonically with the increase of RH.

In the previous chapter, a humidity sensor was demonstrated using Al-doped ZnO nanostructures, which was coated onto tapered POF. Al-doped ZnO nanostructures coating was carried out using sol-gel immersion method for both seeded and non-seeded techniques, in order to grow ZnO nanostructures. In this chapter, a new humidity sensor is proposed and demonstrated using a tapered POF coated with ZnO nanorods, which was prepared using a hydrothermal technique, as a probe. ZnO nanorods was synthesized using modified hydrothermal techniques, in which pre-surface treatment procedure were done to achieve strong attachment of nanorods on the tapered POF. The tapered POF was prepared through chemical etching process as described in the previous chapter.

4.2 Tapered Plastic Optical Fiber

POF consists of core and cladding with refractive index of the core and cladding are 1.492 and 1.402 respectively. When light propagates along the fiber, the main guided field is confined in the core while the evanescent field in the cladding decays exponentially. For some sensing applications, the evanescent field needs to be exposed to the environment. However, penetration depth in optical fiber is far smaller than the cladding thickness and there is almost no interaction between the optical field and surrounding environment. This is due to the fact that optical fibers were originally made for low loss communication. In order to solve this issue, tapering is a good solution to enhance the interaction between the evanescent wave and surrounding target possible (Tian et al., 2011).

Tapering is a process where the waist diameter of the fiber is reduced. POF has a diameter of 1mm, and using the chemical etching method as discussed in the previous chapter, the waist diameter is reduced to ~0.45 to 0.50 mm, with a tapering length of

10 mm. Hence, the tapered fiber will consist of three adjoining segments: un-tapered fiber with a diameter of 1 mm, tapered transition with gradually changed diameter and taper waist with a diameter of ~ 0.5 mm, as shown by Figure 4.1. Figure 4.2 shows the microscope images of the original un-tapered and tapered POF.

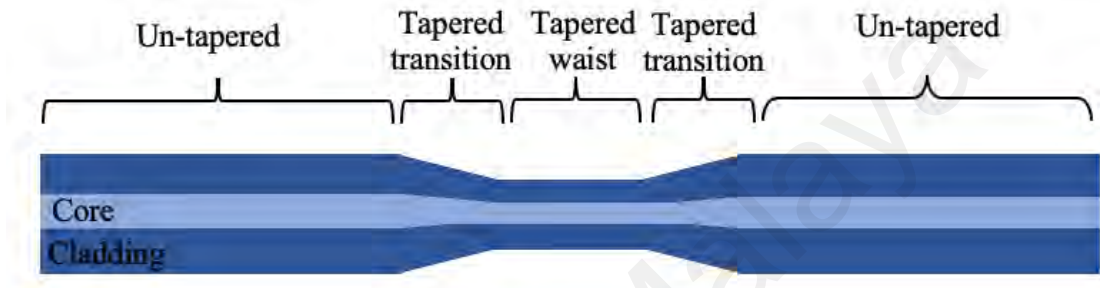


Figure 4.1: Schematic diagram of tapered fiber

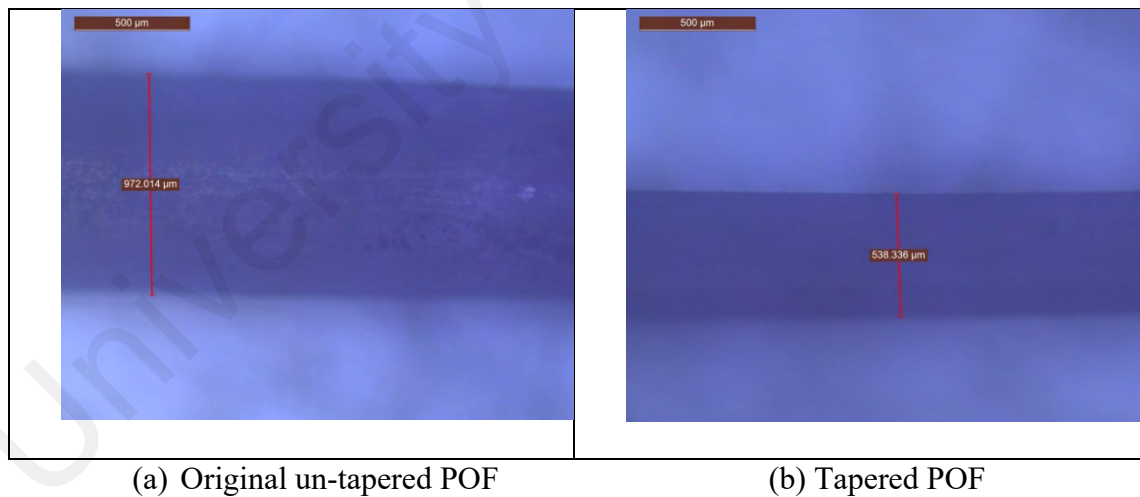


Figure 4.2: Microscope images of the (a) original un-tapered and (b) tapered POF

4.3 Synthesis of Zinc Oxide Nanorods on Tapered Plastic Optical Fiber

ZnO is a versatile functional material with rich family of nanostructures such as nanotubes, nanowires, nanorods, nanorings and so on which can be fabricated by different techniques. There are two main methods of preparing ZnO: metallurgical and chemical methods. Mechanochemical process, sol-gel method, controlled precipitation, solvothermal and hydrothermal methods are classified as chemical method. In this section, hydrothermal technique was applied in order to synthesize ZnO nanorods on tapered POF. This technique was chosen because it is able to provide a highly uniform growth of nanorod, low temperature process and less hazardous, which makes it a simple and environmentally friendly technique. For experimental purpose, four steps of hydrothermal technique were conducted, namely preparing seeding solution, POF core surface treatment, forming nucleation site on POF core, and annealing. The process of hydrothermal techniques is shown in Figure 4.3.

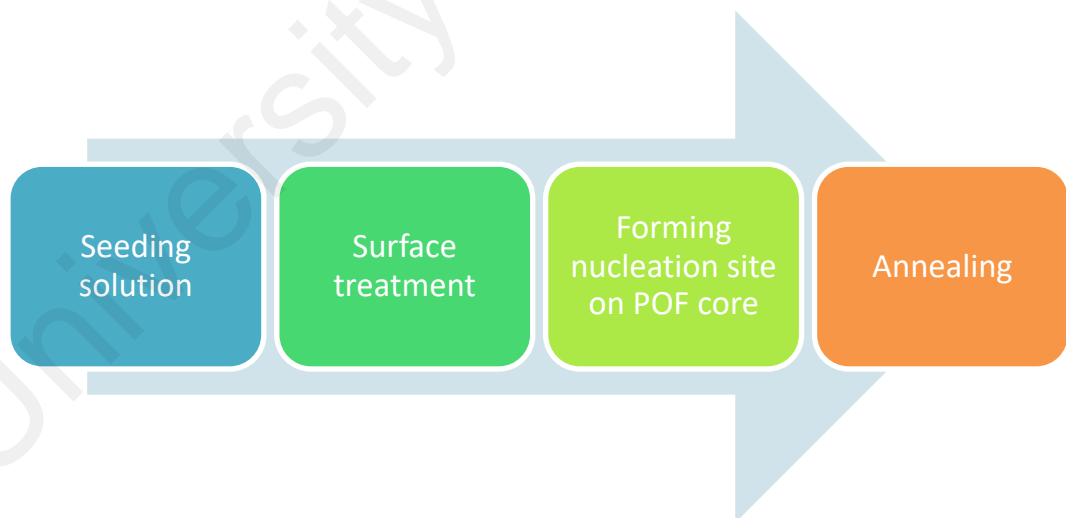


Figure 4.3: Hydrothermal techniques procedure for synthesis ZnO nanorods on tapered of POF

4.3.1 ZnO Seeding Procedure

Seeding procedure is an important process in the growing of ZnO nanorods on the tapered POF as the diameter, length, uniformity and density of the nanorods are dependent on this process. To prepare the seeding solution, ZnO nanoparticles and pH-controlled solution are required in order to synthesize ZnO seed particles. For ZnO nanoparticles solution, 0.0044 g of zinc acetate dehydrate [$\text{Zn}(\text{O}_2\text{CCH}_3)_2 \cdot 2\text{H}_2\text{O}$, Merck] were dissolved in 20 ml of ethanol to form 1 mM solution under slow stirring at temperature 50°C for 30 minutes and then, the solution was let cooled in the room temperature for 5 minutes. After that, 20 ml of ethanol was added into the zinc acetate solution, as shown in Figure 4.4.

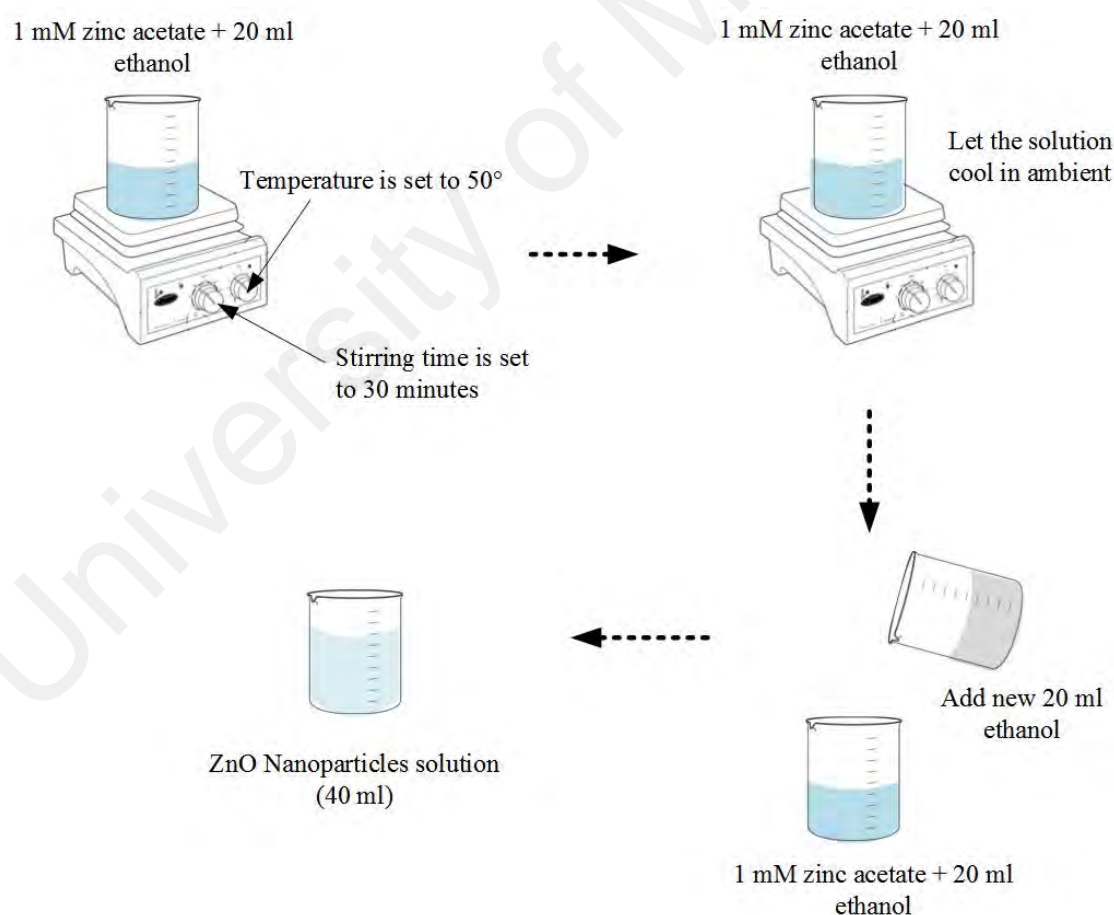


Figure 4.4: Process of the preparation of 1 mM ZnO nanoparticle solution

Through hydrothermal process, the properties of ZnO can be manipulated by the pH of ZnO nanoparticles solution. According to Zhang et al. (2004), pH can change the amount of ZnO nuclei and growth units. Alias et al. (2010) reported that when the pH of the ZnO nanoparticles solution increases, that is from acidic to alkaline, it enhances the growth of the ZnO film. Hence, in order to control the aqueous pH, a pH control solution was prepared. Sodium hydroxide (NaOH) was dissolved in 20 ml ethanol and the solution was then stirred slowly with temperature set to 50 °C in order to form 1 mM solution.

1 mM NaOH + 20 ml ethanol

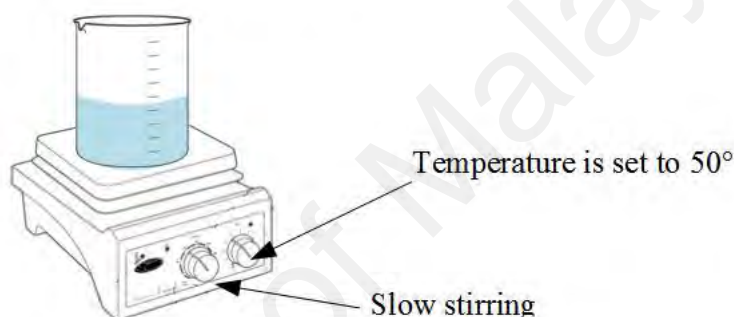


Figure 4.5: Preparation of the pH-controlled solution using NaOH

After 10 minutes, using 1 ml pipet, 20 ml of the pH control solution was added into the ZnO nanoparticles as shown in Figure 4.6. This is done to ensure that more hydroxyl ions OH^- in the seeding solution, as reported by Baruah & Dutta (2009). For every single drop of 1 ml pH control solution, the ZnO nanoparticles solution would be stirred slowly for a minute, and this process is repeated for 20 times. Then, the seeding solution was kept in a water bath at a temperature of 60 °C for 3 hours, resulted in an apparent change in the color of the solution that is from clear to milky solution. The pH can be observed from ~4 to ~9.

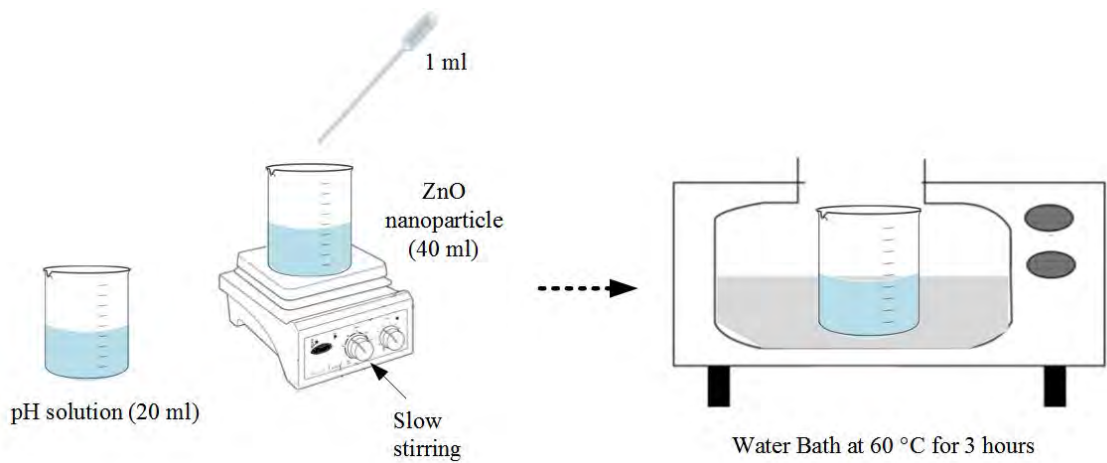


Figure 4.6: Alkaline process of ZnO nanoparticles solution by NaOH

4.3.2 Formation of Nucleation Site on POF

To form nucleation site on the tapered POF, two seeding methods were employed in order to ensure proper profile of ZnO nanorods growth on POF. The methods used are as follows:

(i) Dip and Dry

- i. Figure 4.7 shows that the samples of POF were dipped in the seeding solution for a minute and let dried on a hot plate for another minute. The temperature of the hot plate is set to 70 °C. This process was repeated for another 10 times and then the POFs were annealed at 70 °C for three hours.

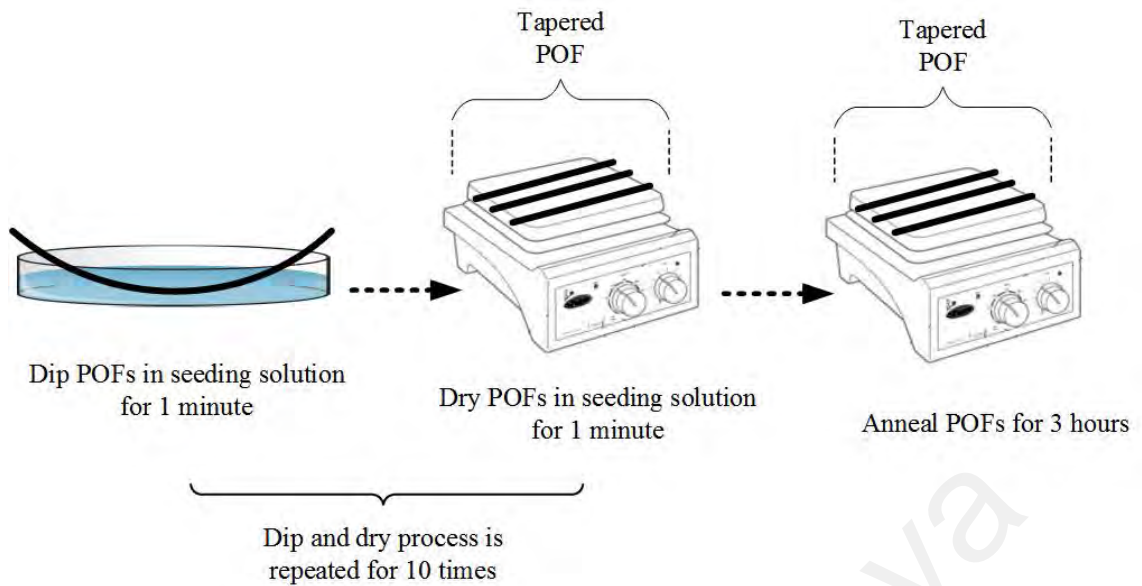


Figure 4.7: Dip and dry process

(ii) Drop and dry

Figure 4.8 shows the method of drop and dry. In this method, POFs were placed on a hot plate with a temperature set to 70 °C. Using micro pipet, 100µL of the seeding solution was dropped on the POFs, then the POFs were let dry for a minute. This process was repeated for another 10 times. After that, the POFs were annealed at 70 °C for three hours.

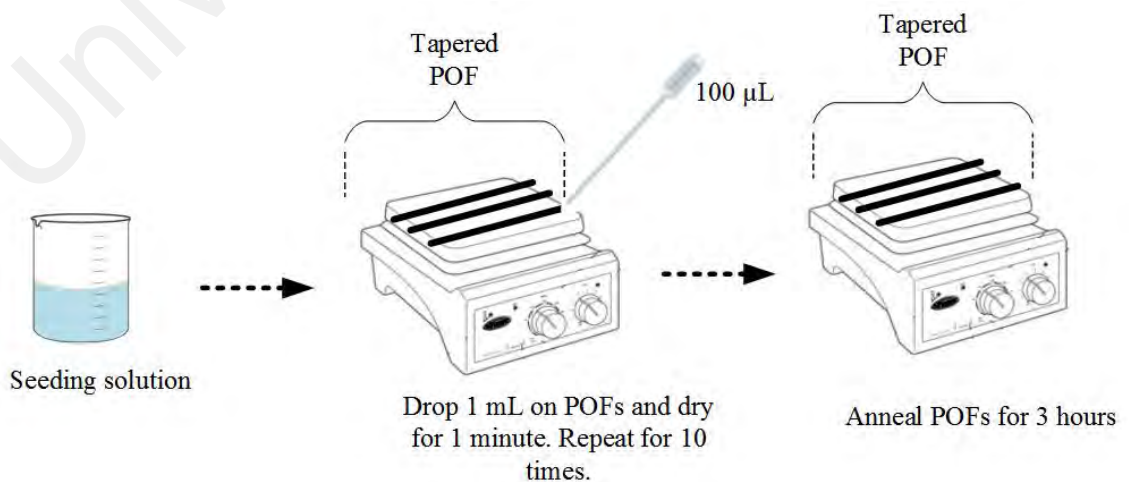


Figure 4.8: Drop and dry method in seeding process

4.3.3 Physical Characterization

Field Emission Scanning Electron Microscopy (FESEM)

The fiber sensor was characterized using Field Emission Scanning Electron Microscope (FESEM) to investigate the morphology of the seeded ZnO nanorods grown on the tapered fiber.

Figure 4.9 depicts the morphology of ZnO nanorods that were grown using hydrothermal method. It can be seen that the nanorods grew vertically, with an estimate diameter of 250 nm and a length of 600 nm. The distribution of the nanorods was much denser, unlike the ones grown using sol-gel method, as shown in Figure 4.10 (a) and (b). Figure 4.11 depicts the higher magnification of the FESEM image that shows each nanorod exhibits a hexagonal end facet. Baruah & Dutta (2009), Jiaqiang et al. (2006), Kim et al. (2011), Liu & Zeng (2003), and Liu et al. (2012) reported similar morphology of ZnO nanorods synthesized using hydrothermal method.

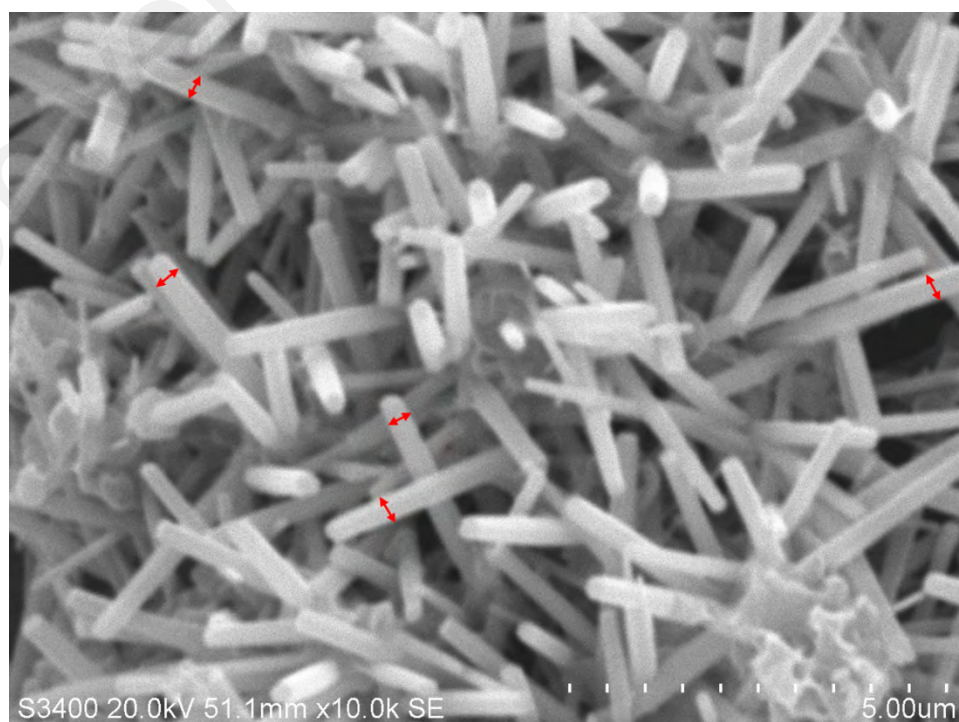
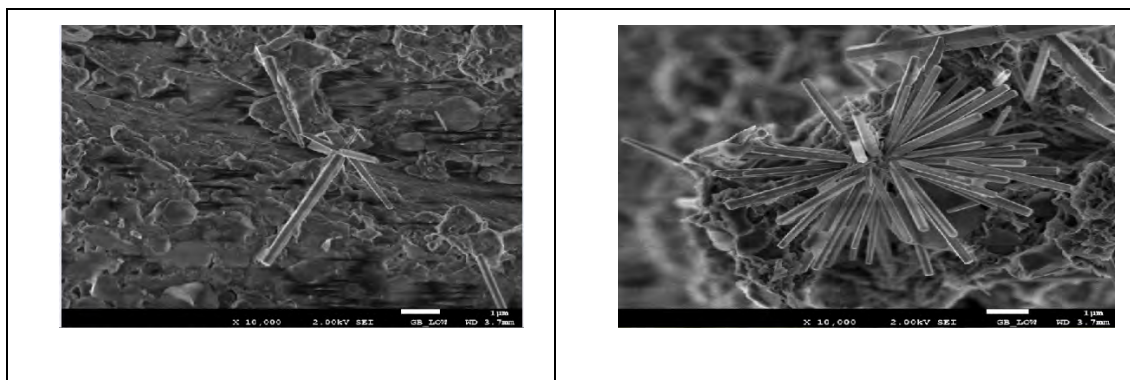


Figure 4.9: Morphology of ZnO nanorods



(a)

(b)

Figure 4.10: Morphology of ZnO nanostructures (a) non-seeded method (b) seeded method

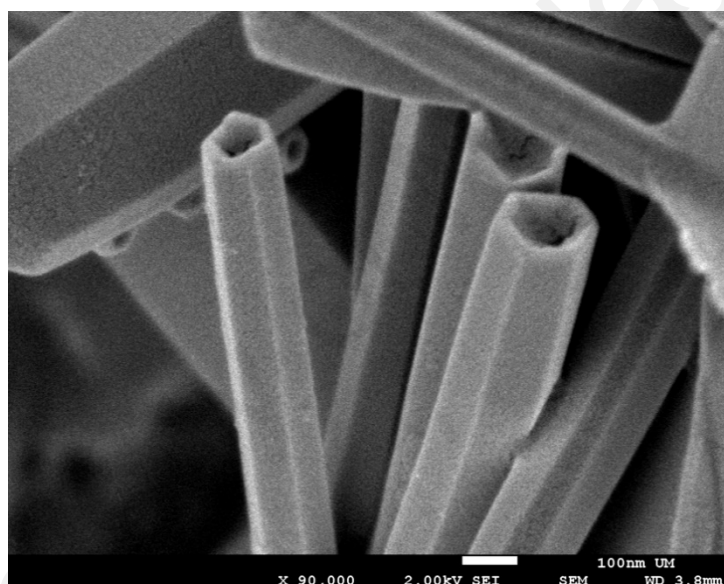


Figure 4.11: FESEM image of ZnO nanorods at higher magnification

4.4 Experimental Setup for the Humidity Sensor

The experimental setup for relative humidity sensor, employing the fabricated tapered POF coated with ZnO nanorods is as shown in Figure 4.12. The setup comprises of the following equipment: a light source, an external mechanical chopper, the proposed probe, a photo-detector, a lock-in amplifier and a computer. A helium neon (He-Ne) laser source is connected to the input port of the fiber while at the output port, a highly sensitive

photo-detector is used to convert the light to electrical signal. The light source used operates at a wavelength of 633 nm with an average output power of 5.5 mW. The external mechanical chopper is used to chop a frequency at 113 Hz, hence preventing the harmonics from the line frequency which is about 50 to 60 Hz, subsequently avoiding multiplication of 50 and 60 Hz. Besides that, the selected frequency is an acceptable value of output and stability. An increase to the value of chopper frequency causes the output voltage and stability to decrease.

In order to simulate different values of relative humidity, a dish of salt solution is placed in the sealed chamber. The sealed chamber is constructed with holes that are having an equivalent diameter with the tapered POF. The proposed sensor is then introduced through the holes and suspended in the sealed chamber. For this experiment, the achievable relative humidity is from 40 % to 85 % and the values were measured using 1365 data logging humidity-temperature meter. The output lights that were into the silicon photodetector (818 SL, Newport) will be converted to the electrical signal and this signal was then fed into the lock-in amplifier (SR-510, Stanford Research System), together with the reference signal of the mechanical chopper. The output that resulted from the lock-in amplifier was connected to a computer through an RS232 port interface and the signal was processed using Delphi software. The reference signal from the chopper was matched with the input electrical signal from the photo-diode. This allows a very sensitive detection system that will remove the noise generated by the laser source.

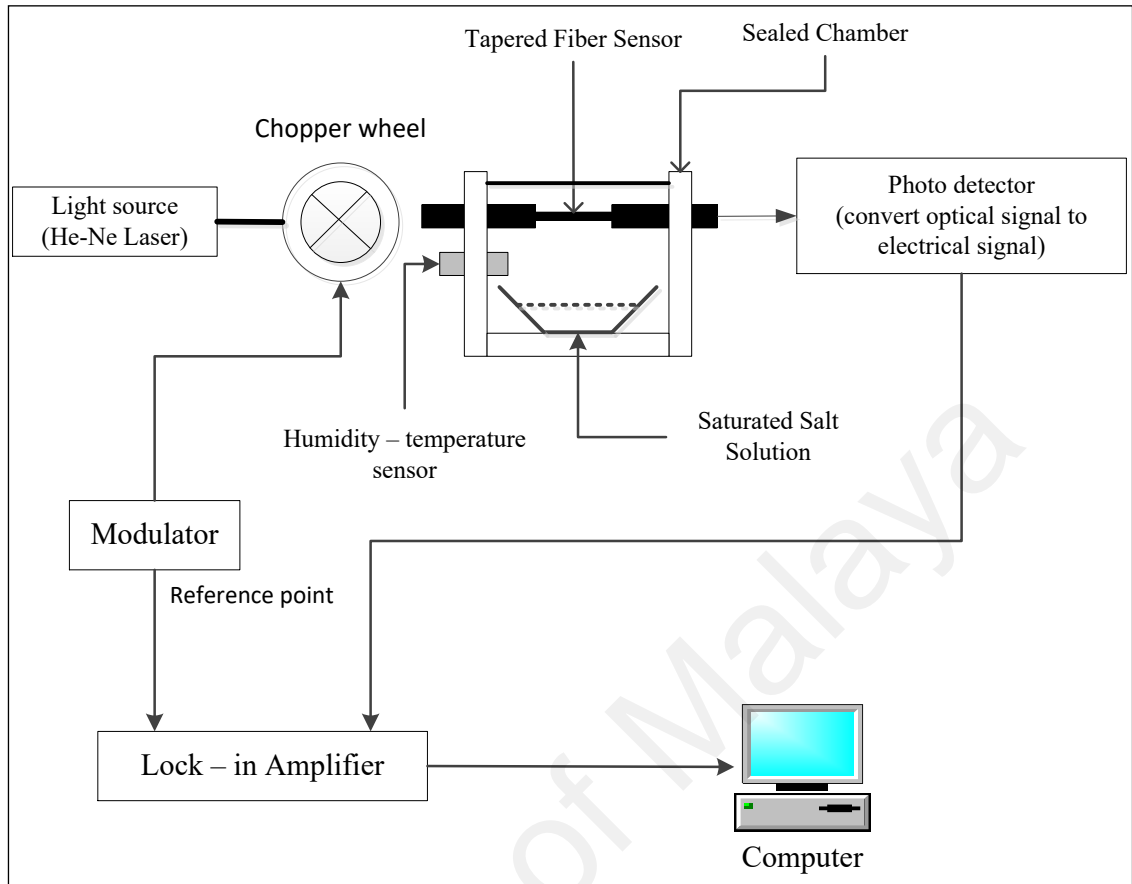


Figure 4.12: Schematic diagram for the proposed humidity sensor

4.5 Sensing performance

The sensing result of the transmitted light from the tapered POF coated with ZnO nanorods grown using hydrothermal method against relative humidity is as shown in Figure 4.13. The initial value of the humidity level is set to 40 % by passing dry air to the chamber. Then, the light intensity was recorded at this humidity level with a lock-in amplifier. The saturated salt solution in the sealed chamber simulated different values of relative humidity. All these measurements were recorded at a stable room temperature. The maximum achievable relative humidity level for this experiment was 85 %.

It can be observed that the change in the intensity of the transmitted light decreases linearly with RH. According to Liu et al. (2012), the effective refractive index (RI) of ZnO composite varies from 1.698 to 1.718 with RH change from 10-95%. When the ZnO nanorods are exposed to humid environment, rapid surface adsorption of water molecules on ZnO nanorods occur, as ZnO nanorods have dry air on the surface. The optical properties of the ZnO nanorod surfaces are modulated by the surface adsorption of water molecules on the ZnO nanorods. As the relative humidity increases, more water molecules will be absorbed on the ZnO nanorod surfaces. The increasing water molecules cause an increase in both effective refractive index of the surrounding medium and absorption coefficient of the ZnO nanorod surfaces, which leads to a larger leakage and absorption of light.

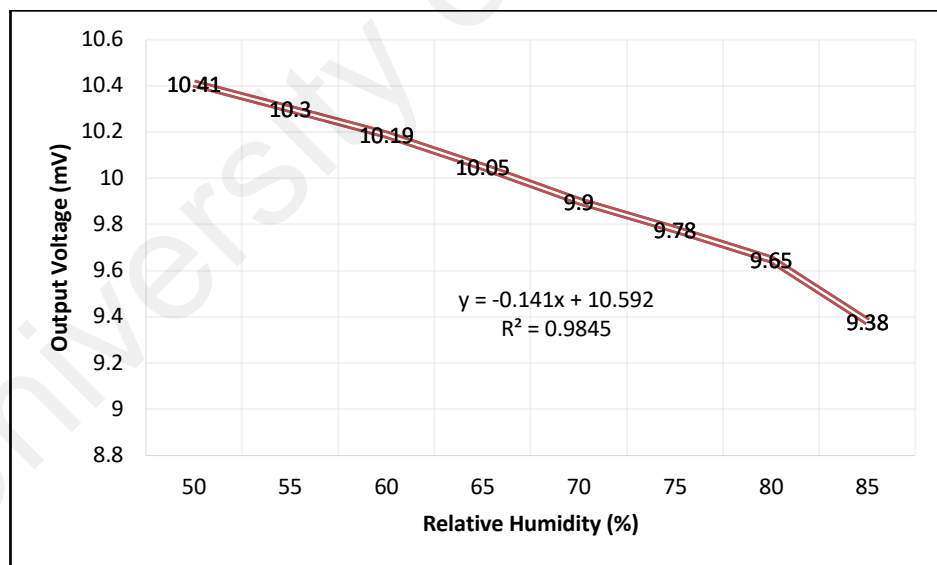


Figure 4.13: Output voltage against relative humidity for the proposed tapered POF with ZnO nanorods

From the graph, the transfer function for the output voltage versus relative humidity is obtained as follows for the sensor with ZnO nanorods.

$$y = 0.141x - 10.59 \quad (4.1)$$

Figure 4.14 depicts the comparison of different methods in growing the ZnO nanostructures: non-seeded and seeded ZnO nanostructures using sol-gel method and ZnO nanorods using hydrothermal method. For sol-gel method, the sensitivity for ZnO non-seeded and seeded are 0.0057 %/mV and 0.0258 %/mV and linearity of 91.67 % and 95.42 % respectively. It shows that the ZnO seeded sol-gel method has better performance. However, when tapered POF, coated with ZnO nanorods using hydrothermal technique, the performance of the proposed sensor has improved significantly, with a sensitivity of 0.0295 %/mV and a slope of linearity of 98.38 % respectively. Evidently, hydrothermal method yields the best sensor performance compared to sol-gel method.

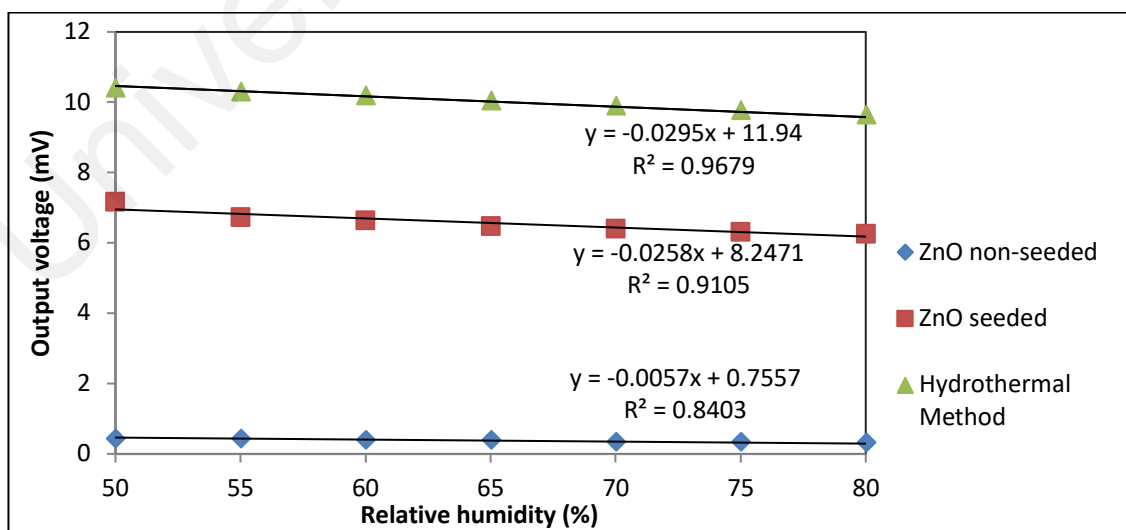


Figure 4.14: Performance of proposed sensor for both sol-gel and hydrothermal method

From the above graph, the transfer function for the output voltage versus relative humidity (from 50% to 80%) for different methods used to grow ZnO were obtained and compared.

For growing ZnO using hydrothermal method, the transfer function is

$$y = 0.0295x - 11.94 \quad (4.2)$$

and for non-seeded ZnO nanorods using sol-gel method, the transfer function is

$$y = 0.0057x - 0.7557 \quad (4.3)$$

while for seeded ZnO using the same sol-gel method, the transfer function obtained is

$$y = 0.0258x - 8.2471 \quad (4.4)$$

The methods employed in producing ZnO nanostructures affect the performance of the proposed sensor. As shown in Figure 4.10 (a) for non-seeded method, the morphology of the ZnO layer were unstructured suggesting the growth of layers comprising of nanoparticles. The seeded method improved the ZnO nanostructures whereby more dense nanostructures were observed. In hydrothermal method, higher density distribution of ZnO nanorods were obtained, hence higher adsorption of water molecules.

The performance characteristic of the proposed sensor is summarized in Table 4.1. The sensor is observed to be sufficiently stable for RH changes as the measurement is taken within 100 s for the probe obtained by non-seeded, seeded and

hydrothermal processes, respectively. These results show that the tapered POF with ZnO nanostructures is capable for RH detection. It is also found that the seeding approach improves the sensitivity and linearity of the sensor.

Table 4.1: The comparison of performances between sol – gel and hydrothermal method for growing ZnO

Performance	Sol – gel method		Hydrothermal method
	ZnO non-seeded	ZnO seeded	ZnO
Sensitive Material	ZnO non-seeded	ZnO seeded	ZnO
Sensitivity (mV/%)	0.0029	0.0258	0.0295
Linearity (%)	93.3	95.42	98.38

4.6 Summary

An enhanced RH sensor by employing hydrothermal method to coat ZnO on tapered POF has been successfully demonstrated. The POF is tapered using chemical etching method, whereby the waist diameter of the fiber, which is 1 mm, is reduced to ~ 0.45 to 0.5 mm by repeated polishing using sandpaper. The length of the tapered region is kept to ~ 10 mm. ZnO nanorods that were coated on the tapered POF were synthesized using hydrothermal method, as this method is able to provide a highly uniform growth of nanorod, low temperature process and less hazardous. There were four steps of hydrothermal technique that were conducted, namely preparing seeding solution, POF core surface treatment, forming nucleation site on POF core, and annealing. In preparing seeding solution, ZnO nanoparticles solution, which is zinc acetate dehydrate

[Zn(O₂CCH₃)₂·2H₂O, Merck] and for pH-controlled solution, NaOH were used. To enable the amount of ZnO nuclei and growth units to be changed, the seeding solution was kept in a water bath for 3 hours. To form nucleation site on the tapered POF, two seeding methods were employed, namely dip and dry and drop and dry. These methods were done to ensure proper profile of ZnO nanorods growth on POF. Then, the POFs were annealed 70 °C for three hours. From the FESEM images, it was evident that the morphology of ZnO grown using hydrothermal method were denser and more distributed on the tapered POF. In addition, the ZnO nanorods grew vertically with hexagonal end facet. The proposed sensor was used to measure the changes in relative humidity. The experimental setup consisted of light source, an external mechanical chopper, the proposed probe, a highly sensitive photo-detector, a lock-in amplifier and a computer. The sensor operates based on intensity modulation technique. From the data collected, the proposed sensor exhibited a sensitivity of 0.0295 %/mV with a slope of linearity of 98.38 % respectively. When compared to the previous method used in growing ZnO, which is the sol-gel method, hydrothermal method has shown an enhancement in both the sensitivity and linearity. Apart from that, the method used also provides more advantages such as environmentally friendly as well energy saving and economical.

CHAPTER 5

POLYMER MICROFIBER COATED WITH ZNO NANOSTRUCTURES FOR HUMIDITY SENSING

5.1 Introduction

Optical microfibers have gained tremendous interest in recent years as promising components for subwavelength waveguiding and nanophotonic devices (Jiang et al., 2007; Lim et al., 2011). This is due to a number of interesting optical properties of these devices, which can be used to develop low-cost, miniaturized and all-fiber based optical devices for various applications. For instance, they have been attracting considerable attention in physical, chemical, and biological sensors due to their unique geometry with low dimension and large surface-to-volume ratio and their versatility for electrical and optical detection. Furthermore, the higher portion of the evanescent field is travelling inside the cladding in the microfiber and thus the travelling wave characteristics becoming more sensitive to the physical ambience of its surrounding (Harith et al., 2015; Ismael et al., 2013; Rahman et al., 2011). Previously, many works have been reported on silica microfiber for various applications (Jiang et al., 2007; Liu et al., 2012; Vienne et al., 2007; Wu et al., 2011). Compared with the silica and glass counterparts, polymer optical microfibers may also play a key role in several rapidly developing areas of broadband communications because of their mechanical flexibility, lightweight, low cost, chemical specificities, tunable properties, easier process, and integration (Yang et al., 2008).

To date, polymer-based microfibers or nanowires have been achieved by various techniques such as chemical synthesis (Cui et al., 2006), electro-spinning (Li & Xia,

2004), nano-lithography (Noy et al., 2002) and mechanical drawing (Nain et al., 2006). Chemical synthesis and nano-lithography are quite complicated and requires expensive facilities. Electrospinning is only for microfiber mat fabrication but not for a single microfiber structure. The simplest and cheapest technique is based on mechanical drawing where the microfiber is normally drawn from solvated liquid polymer. In this technique, the main concerns are on the nature of solvent and concentration of polymers. Typical polymer's solvent are volatile organic compound which poses serious health risk to frontline worker.

In chapters 3 and 4, relative humidity (RH) sensor has been proposed and demonstrated using plastic optical fiber (POF) coated with zinc oxide nanostructures. In this chapter, we demonstrate new RH sensors using a Polymethyl methacrylate (PMMA) polymer microfiber coated with ZnO nanostructure as a probe. An eco-friendly and simple drawing method is used to fabricate the polymer microfibers. PMMA is selected as the polymer waveguiding material in the experiment because of its high mechanical strength, good dimensional stability, good weather resistance, and natural transparent above deep ultraviolet. In a rubber like state, PMMA possess a weak restoring force and will deform significantly under stress (Nain et al., 2006) and thus microfiber can be easily fabricated by the proposed direct drawing technique.

5.2 Fabrication and characterization of PMMA microfiber

A PMMA microfiber was fabricated using a molten PMMA in conjunction with the direct drawing technique. Figure 5.1 shows the step by step process, which uses a heating plate to melt PMMA and keep the temperature constant during the fiber drawing process. For the polymer to maintain a desirable viscosity level, the temperature of the heating plate should be controlled within the temperature range, between the glass

transition temperature and the melting temperature of polymer and should be kept constant. As the glass transition temperature (T_g) of PMMA ranges from 85 to 165 °C, the heating plate temperature was kept at round 115°C during the fiber drawing. First, a tapered silica fiber with a diameter of about 125 μm is being used and its tip is immersed into the molten PMMA. Then the fiber tip is retracted from the molten polymer with a speed of 0.1–1 m/s, leaving a PMMA microfiber extending between the molten PMMA and the tip. The extended PMMA microfiber is quickly quenched in air and finally, a bare PMMA microfiber is formed. The microfiber diameter can be controlled by the pulling speed and viscosity of the polymer (which depends on the hot plate temperature). Microfibers produced by this technique are uniform in diameter over a long length with good flexibility.

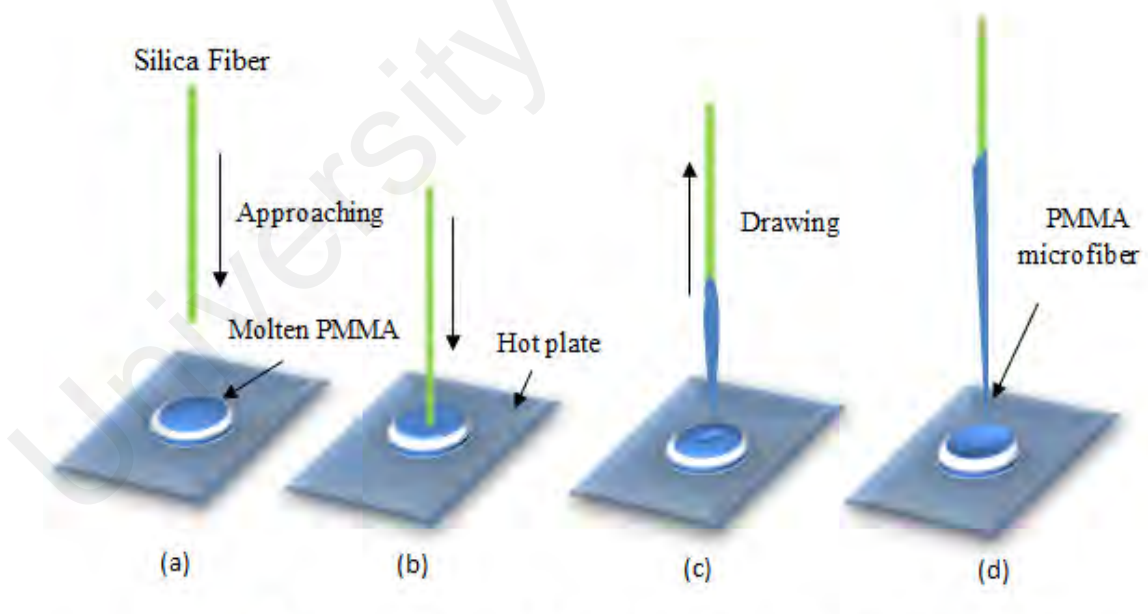


Figure 5.1: Schematic illustration of the polymer microfiber fabrication by direct drawing method from molten PMMA. (a) A cylindrical silica fiber is approaching the molten PMMA (b) The fiber tip is immersed into the molten PMMA (c) The fiber conglutinated PMMA is being drawn out. (d) A PMMA microfiber is formed

It was found that PMMA microfibers were easier to be fabricated when the viscosity of the PMMA is at optimum level. The attainable diameter of the microfiber reduces as the viscosity of the PMMA increases. Figure 5.2 shows the microscope image of the fabricated PMMA microfiber. As shown in Figure 5.2(a), the microfiber can be easily formed between the molten PMMA and the fiber tip using the proposed direct drawing technique. During the drawing process, a He-Ne 632 nm laser is launched into the microfiber for easier monitoring. As the microfiber surface is relatively smooth, the leakage of light (Figure 5.2(b)) is probably due to bending, dust and transition region rather than surface roughness. The fabricated microfibers can be easily bent and curled, offering a wide range of optical sensors applications. It exhibits high uniformity, smooth surface and can be drawn up to the length of 500 mm long.

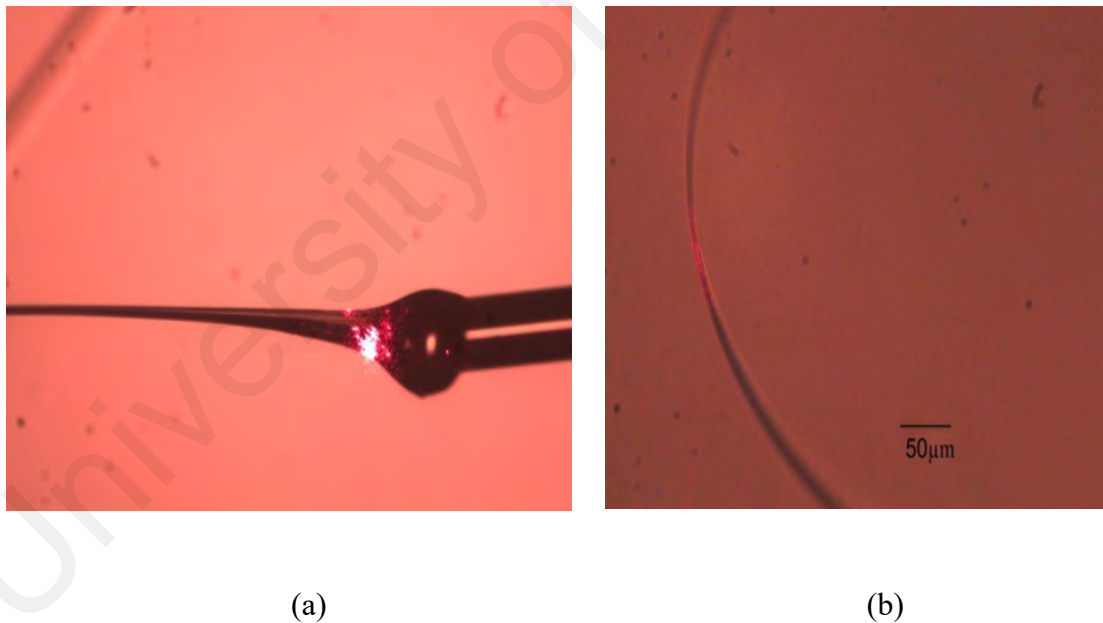


Figure 5.2: Microscope image of the fabricated PMMA microfiber (a) PMMA microfiber is formed between the molten PMMA and the fiber tip (b) the middle part of the PMMA microfiber as a 632 nm laser is launched into the microfiber

Figure 5.3 illustrates the fabricated microfibers with three different waist diameters, which were obtained by varying the temperature of the heating plate and the speed of drawing. The excellent diameter uniformity and sidewall smoothness make the microfiber suitable for low-loss optical wave guiding and sensing. PMMA microfibers with diameters ranged from 9 to 13 μm and lengths up to few centimeters have been drawn by this method. The transmission loss of the fabricated microfiber is investigated for three different diameters; 9, 11 and 13 μm . Optical wave guiding in a single PMMA microfiber is implemented by an evanescent coupling method as shown in Figure 5.4. As shown in Figure 5.4, a silica microfiber with a diameter of about 4 μm , which was fabricated by using the flame brushing technique is fixed at a fiber holder at two ends of the PMMA microfiber. The PMMA microfiber is then placed in parallel and close contact with these silica microfibers. Due to the strong evanescent coupling between the PMMA microfiber and the silica microfiber, light can be efficiently launched into and picked up from the PMMA microfiber within a few micrometers' overlap. The transmitted light power against the PMMA microfiber length is investigated for all PMMA samples. The result is shown in Figure 5.5.



Figure 5.3: PMMA microfibers with three different waist diameters (a) 9 μm (b) 11 μm and (c) 13 μm

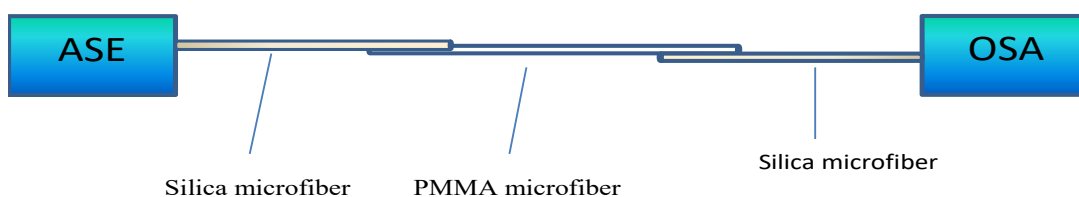


Figure 5.4: Schematic diagram of an optical waveguiding in a single PMMA microfiber with two ends coupled with silica microfibers

As seen in Figure 5.5, the transmitted power reduces linearly with the increase of the microfiber length. The microfiber loss is obtained at 0.16 dB/mm, 0.12 dB/mm and 0.11 dB/mm for the microfiber diameters of 9 μm , 11 μm and 13 μm , respectively. It shows that the microfiber loss increases with the reduction of its diameter. This is due to the amount of light travelling inside the cladding, which increases for smaller diameters. Some portion of the light leaks out the fiber as loss.

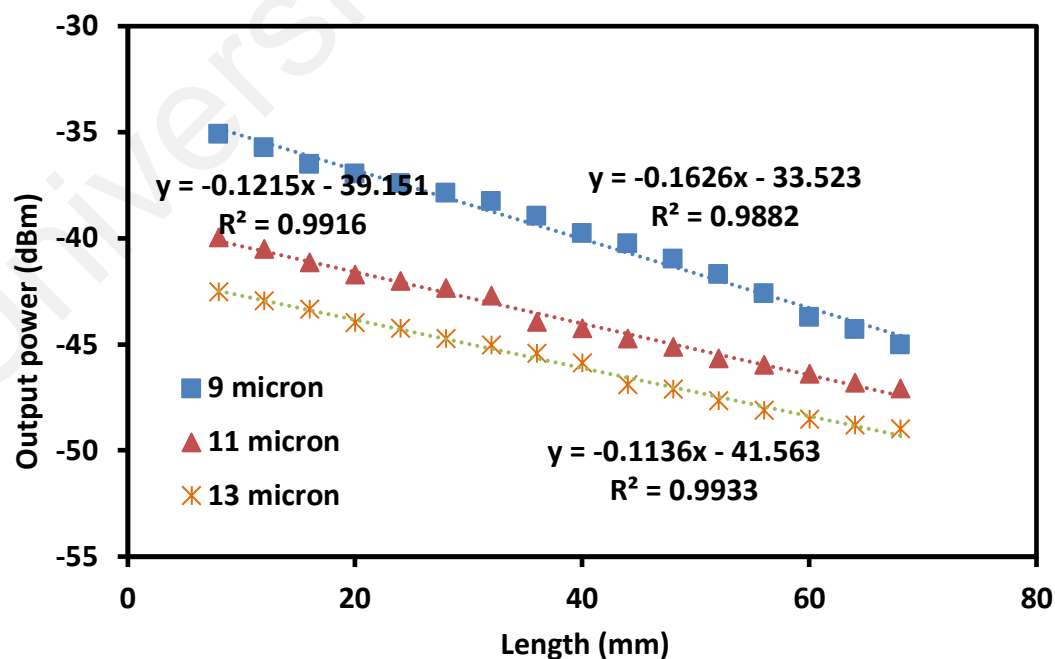


Figure 5.5: The transmitted output power from the PMMA microfiber against its length

5.3 PMMA microfiber for relative humidity sensor

PMMA microfibers, inherited from the perm-selective nature and biocompatibility of polymer materials, could also offer a number of highly attractive advantages for sensing applications. For example, gas molecules to be detected can be either selectively bound to their surface or diffused into the polymer matrix, which may be difficult for other materials such as semiconductor nanowires or glass microfibers. ZnO is an interesting, applicable, biocompatible, biosafe material, hence the advantages of incorporating them as sensing elements are manifold. ZnO has potential benefit for biophotonics, exhibits excellent electrochemical activity and can be grown on any substrate at low temperatures (Willander & Nur, 2011). Growing ZnO nanostructure on flat substrates has been extensively demonstrated in various platforms such as glass, silica and aluminium foil (Lee et al., 2006; Umar et al., 2007; Wei et al., 2005). It has been reported in the previous chapters that ZnO nanostructure enhances the interaction of fiber guided light for humidity sensor. In this section, a PMMA microfiber was coated with ZnO nanostructure for detecting changes in relative humidity (RH). The ZnO nanostructure coated on the microfiber induce changes to the optical properties in response to an external stimulus. Here, a PMMA microfiber was fabricated by direct drawing the solvated polymer as discussed in the previous section. The smooth morphology of PMMA microfibers make them suitable for low loss optical wave guiding and sensing.

5.3.1 Preparation of sensor probe

At first, the PMMA microfiber with a diameter of 9 μm was fabricated by using a one-step process as illustrated in Figure 5.1. The ZnO nanostructure coating was prepared onto the microfiber using an improved sol-gel method. In the process, the seed layer was

deposited onto the PMMA microfiber to grow the ZnO nanostructures using a simple manual dip coating technique. The seeded solution was prepared by dissolving zinc acetate dehydrate ($\text{Zn}(\text{CH}_3\text{COO})_2 \cdot 2\text{H}_2\text{O}$) as a precursor in isopropanol with a molarity of 0.025 M. The solution was stirred at 60 °C for 2 hours at ambient temperature to yield a clear and homogenous solution. Then, the solution was cooled down to room temperature for the coating process. The microfiber was manually dipped into the seeding solution and dried at 30 °C to evaporate the solvent repeatedly for 5 times to increase the thickness of the fiber during the coating and drying process. Subsequently, the growing solution was prepared by dissolving 0.01 M zinc nitrate hexahydrate ($\text{Zn}(\text{NO}_3)_2 \cdot 6\text{H}_2\text{O}$) and 0.01 M hexamethylenetetramine (HMTA) in 100 ml deionized water. The deposition process of ZnO nanostructure on the fibers was performed using sol-gel immersion method by suspending the ZnO fibers in the growing solution at 30 °C for 2 hours. The microfiber was then characterized using Field Emission Scanning Electron Microscope (FESEM) to investigate the morphology of the ZnO nanostructure coated onto the PMMA microfiber. Figure 5.6 shows the FESEM image of the ZnO nanostructure grown on PMMA microfiber.

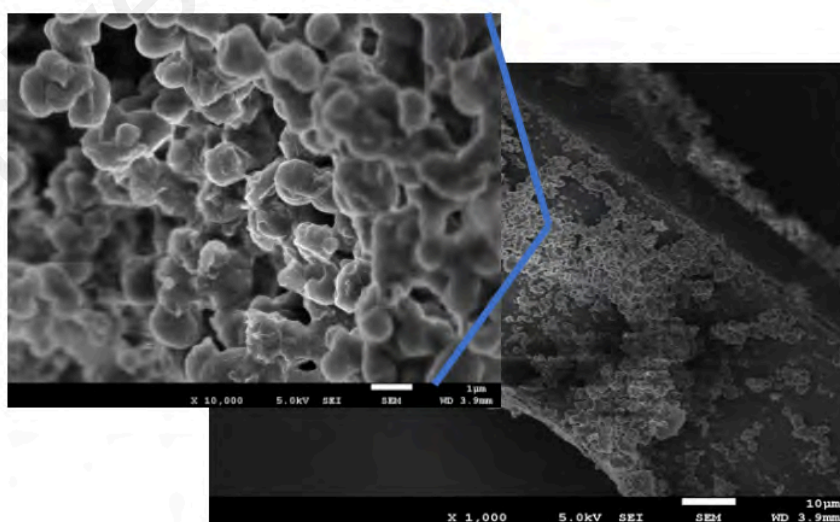


Figure 5.6: FESEM image of ZnO nanostructure coated on PMMA microfiber

5.3.2 Experimental setup for the RH measurement

The setup used to measure relative humidity using the fabricated PMMA microfiber coated with ZnO nanostructure is displayed in Figure 5.7. The amplified spontaneous emission (ASE) light from the Erbium-doped fiber amplifier (EDFA) was launched onto the microfiber probe placed in a sealed chamber with a dish filled with saturated salt solution. Relative humidity depends on the amount of moisture of the surrounding; therefore, salt solution was placed in the sealed chamber in order to simulate the different values of relative humidity until the equilibrium relative solution of the salt solution is achieved, which is around 80 %RH. The transmitted light and wavelength shift are measured by the optical spectrum analyzer (OSA, Anritsu MS9710C). In the experiment, the performance of the proposed sensor was investigated for various relative humidity levels, ranging from 50%RH to 80%RH. The humidity was measured using the Omega RH-21C temperature-relative humidity meter with a resolution of 0.1%RH.

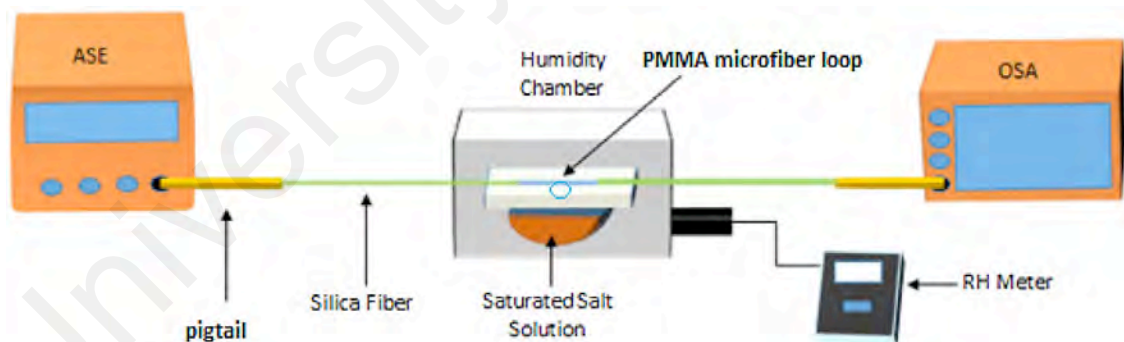


Figure 5.7: Experimental setup for humidity sensor using PMMA microfiber

5.3.3 Performance of the RH sensor

Figure 5.8 shows the variation of the output power of the ASE with relative humidity. In the experiment, the humidity is increased from 50 % to 80 % by putting the salt solution inside the humidity chamber. It is observed that the output power decreases from -22.43 dBm to -27.87 dBm as the humidity is increased from 50 % to 80 %. Evidently, the performance of the sensor is enhanced after being coated with ZnO nanostructure, as shown in Figure 5.8. The ZnO nanostructure composite surfaces are modulated by the surface absorption of water molecules. This is because the increase of water molecules being absorbed by the ZnO nanostructure composite results in an increase of relative humidity (Liu et al., 2012). According to Liu et al. (2012), the effective refractive index (RI) of ZnO composite varies from 1.698 to 1.718 as the relative humidity changes from 10 to 95 %. The increase in water molecules being absorbed by ZnO layer increases the RI of the effective coating of the fiber which leads to a larger leakage of light. This, in turn has improved the performance of the PMMA microfiber coated with ZnO nanostructure.

Figure 5.9 shows the repeatability of the sensors. Throughout the experiment, it is evident that the performance of the sensor is enhanced after being coated with ZnO nanorods due to its ability to absorb more water. As the relative humidity level varies from 50 % to 80 %, the output power of the microfiber sensor decreases linearly with a maximum sensitivity, linearity and resolution of 0.1791 dBm/%, 96 % and 2.1 %, respectively. The performance of the humidity sensors with and without ZnO nanostructure coating are summarized in Table 5.1. It is shown that sensitivity of the sensor has improved from 0.1191 dBm/% to 0.1791 dBm/% with the coating. As a comparison, the coating of ZnO on the PMMA microfiber also improved the sensor's resolution by a factor of 1.84. The measurement for resolution is achieved by dividing the standard deviation of repeated measurements with the sensitivity of the sensor.

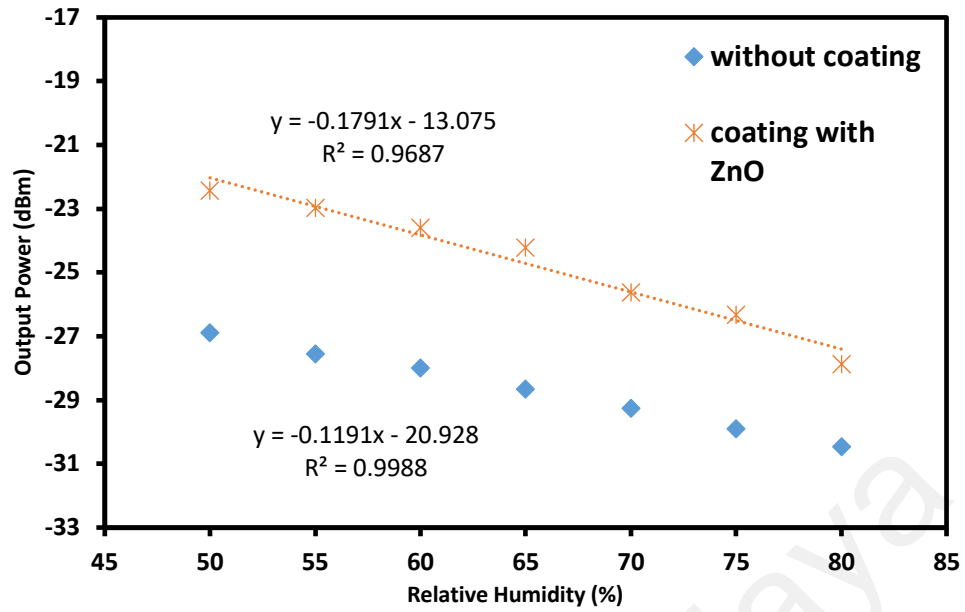


Figure 5.8: Output power against relative humidity for PMMA microfiber with and without ZnO nanostructure coating

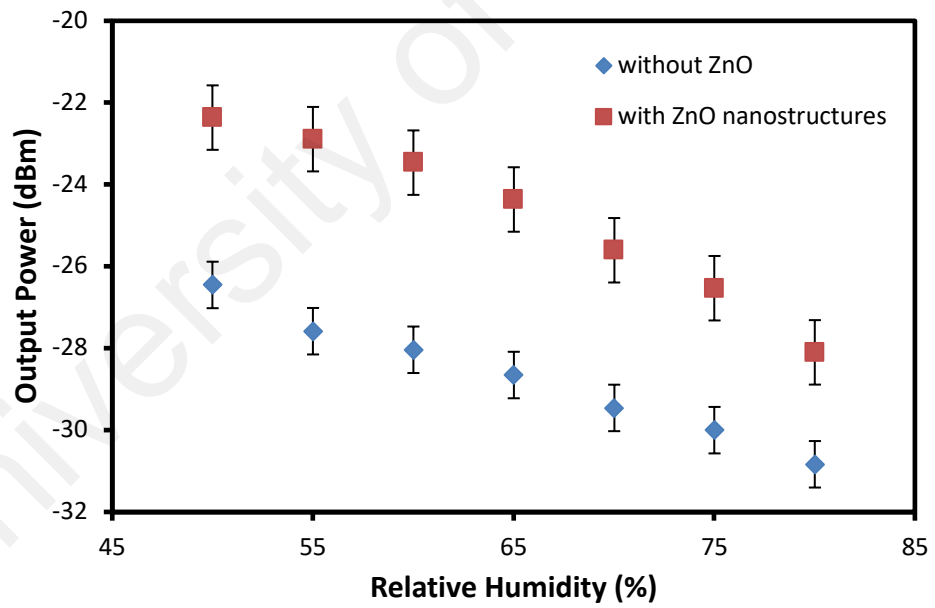


Figure 5.9: Repeatability of the sensors

Table 5.1: Performance of the humidity sensor using PMMA microfiber with and without ZnO nanostructures coating

Parameters	Coated ZnO nanostructure	Uncoated PMMA
Resolution (%)	2.1	3.87
Standard Deviation (dBm)	0.384	0.46
Linearity	More than 96%	More than 99%
Sensitivity (dBm/%)	0.1791	0.1191
Linear Range (%)	50-80	50-80

5.4 PMMA microfiber-based humidity sensor with ZnO nanorods coating

In this section, the PMMA microfiber was coated with ZnO nanorods for detecting the changes in the relative humidity. The ZnO nanorods coating on the microfiber induces changes to the optical properties in response to an external stimulus. In the experiment, a PMMA microfiber was fabricated using a molten PMMA in conjunction with the direct drawing technique (Figure 5.1). The fabricated microfiber with a diameter of about 9 μm was selected as the polymer wave guiding material due to its high mechanical strength, good dimensional stability, good weather resistance, and its natural transparency above the deep ultraviolet region

As for the ZnO nanorods, the seed layer was deposited onto the fiber to grow the ZnO nanorods using a simple manual dip coating technique. The seeded solution was prepared by dissolving zinc acetate dehydrate ($\text{Zn}(\text{CH}_3\text{COO})_2 \cdot 2\text{H}_2\text{O}$) as a precursor in isopropanol with a molarity of 0.025 M. The solution was stirred at 60°C

for 2 hours at ambient temperature to yield a clear and homogenous solution. Then, the solution was cooled down to room temperature for the coating process. The fiber was manually dipped into the seeding solution and dried at 30°C to evaporate the solvent. This process was repeated 5 times until the desired thickness of the fiber was achieved. Subsequently, the growing solution was prepared by dissolving 0.01 M zinc nitrate hexahydrate ($\text{Zn}(\text{NO}_3)_2 \cdot 6\text{H}_2\text{O}$) and 0.01 M hexamethylenetetramine (HMTA) in 100 ml deionized water. The deposition process of the ZnO nanorods on the PMMA microfiber was performed using the sol-gel immersion method by suspending the fiber in the growing solution at 30°C for 2 hours.

The PMMA microfiber was then characterized using Field Emission Scanning Electron Microscope (FESEM) to investigate the morphology of the coated ZnO nanorods as shown in Figure 5.10. As highlighted in the diagram, there are apparent structures of nanorods with hexagonal end facet. Similar morphology of ZnO nanorods have been reported by Baruah & Dutta (2009), Jiaqiang et al. (2006), Kim et al. (2011), and Liu & Zeng (2003). It can also be observed that although the ZnO nanorods are dispersive, their diameters and lengths are rather uniform.

Figure 5.11 shows the output power of the ASE against relative humidity for PMMA microfiber without ZnO coating for three different runs. The figure shows that as the level of relative humidity increases, the output power from the OSA decreases, giving a directly proportional relationship of the output power against the level of the relative humidity. The sensitivity and linearity of the linear function for the first, second and third runs are 0.1168 dBm/% and 98 %; 0.1069 dBm/% and 90 %; and 0.1322 dBm/% and 97 %, respectively. The sensitivity refers to slope of the linear curve whereas the linearity measures the maximum deviation in the output signal value of a linear transfer function. Linearity is measured using the correlation coefficient, R,

which is a measure of the reliability of the linear relationship between the input and output parameter values. The linear reliability increases as R approaches 1. R can be calculated by obtaining the square root of R^2 as depicted in the figure. The highest standard deviation obtained for the three different runs was obtained at 0.368 dBm.

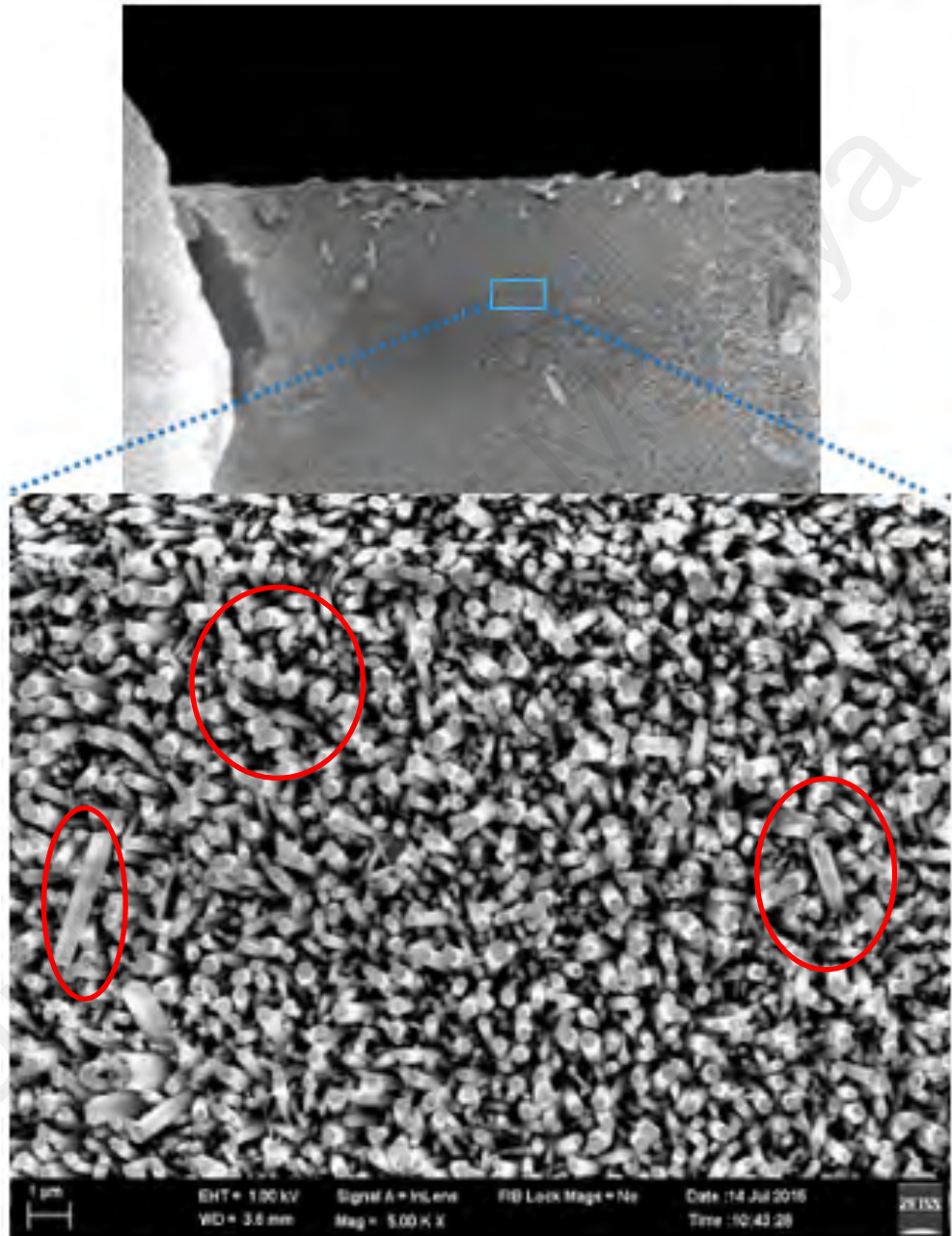


Figure 5.10: FESEM image of the PMMA microfiber coated with ZnO nanorods

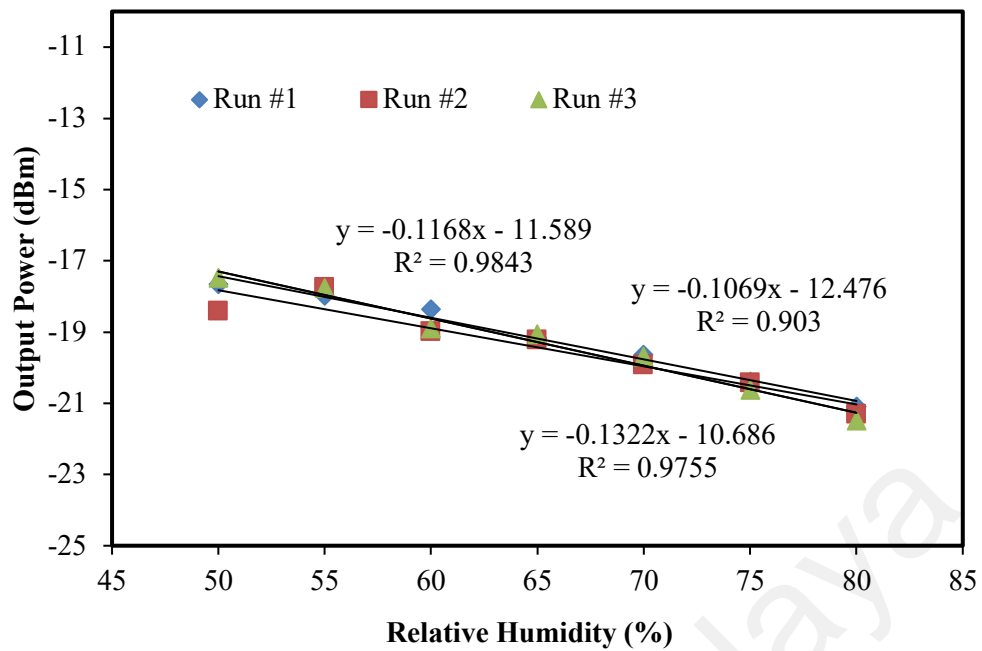


Figure 5.11: The output power of the ASE against relative humidity for PMMA microfiber without ZnO nanorods coating for three different runs

Figure 5.12 shows the linear function of the output signal against the relative humidity for the PMMA microfiber with ZnO nanorods coating. As the humidity is increased from 50 % to 80 %, the output power decreases where the sensitivity and linearity of the linear function for the first, second and third run are 0.1809 dBm/% and 97 %; 0.1964 dBm/% and 98 %; and 0.2159 dBm/% and 98 %, respectively. Throughout the experiment, it is evident that the performance of the sensor is enhanced after being coated with ZnO nanorods. These ZnO nanorods absorb more water and increase the sensitivity of the sensor. The ZnO nanorods is a hydrophilic material and water molecules can be easily absorbed by the ZnO layer of the PMMA microfiber in a humid environment. A lot of factors come into play during the growth of the ZnO, like the concentration of the chemical bath, temperature, duration of growth, pH, etc. (Baruah & Dutta, 2009; Zhao et al., 2014), which directly affect the final morphology of the rods grown using the hydrothermal method. The increase in water molecules

being absorbed by ZnO layer increases the refractive index of the effective coating of the fiber which leads to a larger leakage of light (Liu et al., 2012). This induces an additional mass on the surface which influences the transmission characteristics of the PMMA microfiber. The increase in the water molecules in higher humidity levels increases both the effective index of the surrounding medium and the absorption coefficient of the ZnO composite, justifying the improved performance of the microfiber coated with ZnO nanorods. The nanorods produce a larger surface area compared to the conventional nanostructure. This justifies the improved performance with ZnO nanorods compared to that of the conventional nanostructures.

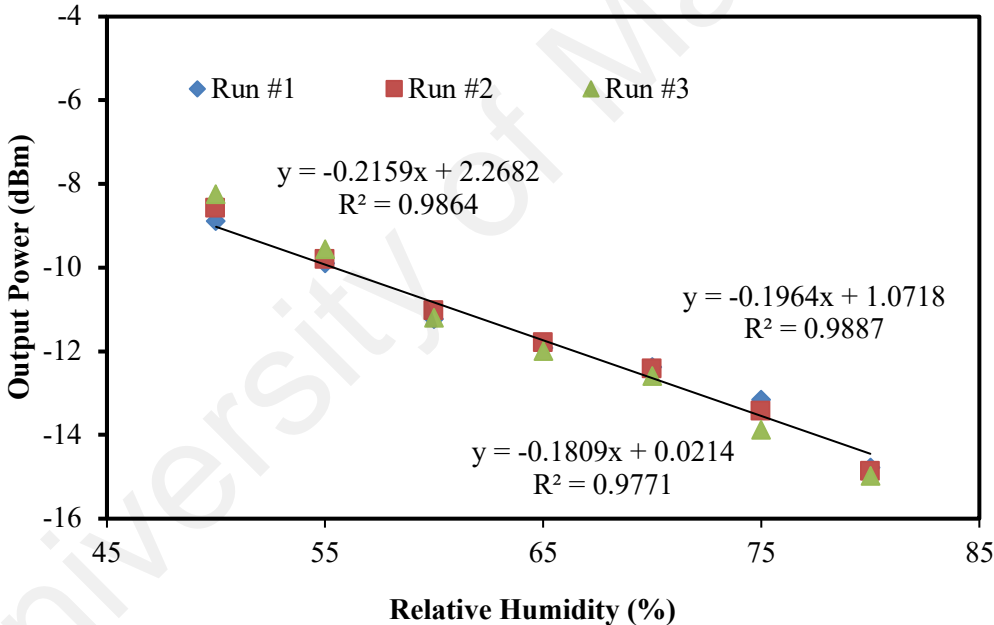


Figure 5.12: The output power of the ASE against relative humidity for PMMA microfiber coated with ZnO nanorods coating for three different runs

The comparison of the sensor performance with and without the ZnO coating is depicted in Figure 5.14. A ZnO nanorod sensor exploits enhanced surface area and thus, the surface activity. Absorption of the molecules on the nanorods can be detected through

the variation of the nanorods' properties, such as photoluminescence, electrical conductivity, vibration frequency, mass, etc. Throughout the experiment, it is evident that the performance of the sensor is enhanced after being coated with ZnO nanorods due to its ability to absorb more water. The same observation was made by Yun et al. (2008). The performance characteristic of the humidity sensor with and without the ZnO nanorods coating is summarized in Table 5.2. Overall, the sensor is observed to be sufficiently stable with standard deviations of 0.497 dBm and 0.368 dBm for the uncoated and ZnO nanorods coated PMMA microfiber, respectively.

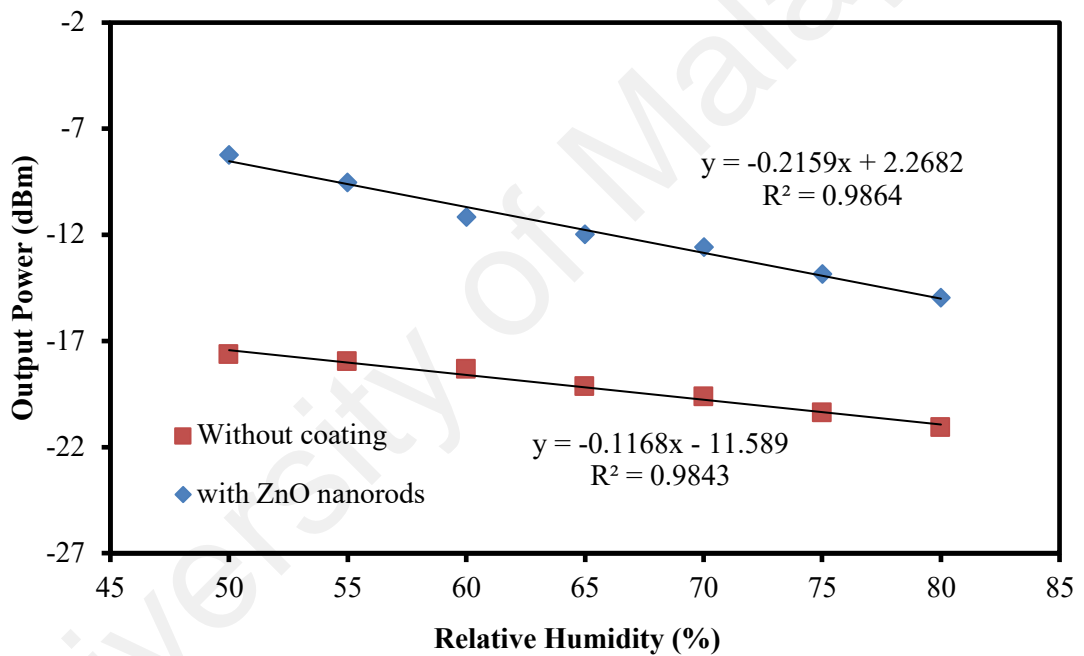


Figure 5.13: Output power against relative humidity for PMMA microfiber with and without ZnO nanorods coating

Table 5.2: Performance of the humidity sensor using PMMA microfiber with and without ZnO nanorods coating

Parameters	Coated ZnO nanorods	Uncoated PMMA
Resolution (%)	1.7	4.25
Standard Deviation (dBm)	0.368	0.497
Linearity	More than 98%	More than 98%
Sensitivity (dBm/%)	0.2159	0.1168
Linear Range (%)	50-80	50-80

5.5 Summary

In this chapter, we have successfully fabricated a PMMA microfiber using a direct drawing technique for measuring the changes of relative humidity from 50 % to 80 %. Based on the results, the PMMA microfiber with ZnO nanostructures coating exhibits better performance than the one without coating, in measuring the changes of relative humidity. The output intensity of the PMMA coated with ZnO nanorods decreases linearly with relative humidity. Its sensitivity, linearity and resolution are 0.1791 dBm/%RH, more than 96 % and 0.384 %RH, respectively. The obtained results signify that the output power from the OSA is directly related to the changes in the relative humidity.

The PMMA microfiber coated with ZnO nanorods is also proposed and demonstrated for the monitoring of relative humidity. The results showed an increase in the sensitivity of the sensor with the additional coating of ZnO nanorods on the surface of the PMMA microfiber. The working mechanism of the device is based on the observed

decrement in the transmission of the sensor that was carefully placed in a sealed chamber. It is observed that the transmission of the microfiber with ZnO nanorods coating decreases linearly with the increase of humidity. The maximum sensitivity, linearity and resolution of the proposed sensor are 0.2159 dBm/%, 98% and 0.368%, respectively. The ZnO nanorods coating was obtained by combining the sol gel with the hydrothermal growing technique. This sensor is highly suitable for continuous monitoring of relative humidity in compact areas.

University of Malaya

CHAPTER 6

CONCLUSION AND FUTURE WORKS

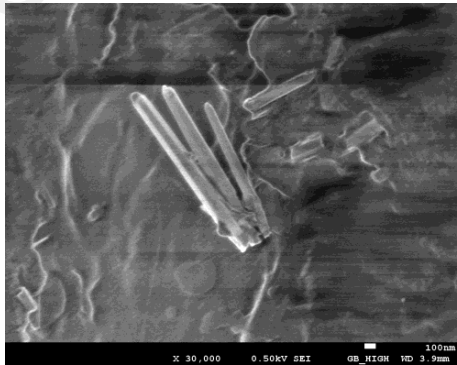
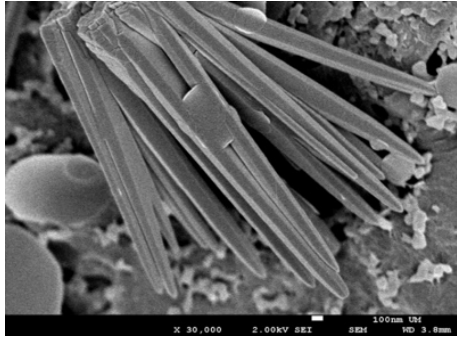
6.1 Conclusion

Plastic optical fiber (POF) has been overshadowed by glass optical fiber due to its characteristic such as high loss during transmission. However, POF stands out for their greater flexibility and resistance to impacts and vibrations, immunity to electromagnetic interferences, as well as greater coupling of light from the light source to the fiber. These merits enable POF to be employed in wider applications. In addition, with the recent advancement in polymer technology, POF has been an attractive to sensor design. When POF is fabricated to have reduced waist diameter via tapering process, it opens up to more sensing applications because tapered POF allows more interaction with physical ambience of the surroundings due to its higher interaction with evanescent field. One of the fundamental and important parameters in sensors is the refractive index measurement, as it is frequently demonstrated as an approach for evanescent wave sensing. Any change in the optical or structural characteristic of the chemical will provoke a change in the effective index of the optical fiber, hence, changing its transmission properties. Whilst tapered region is coated with sensitive materials with different refractive index, the sensitivity of the sensor will be enhanced.

In this work, synthetization of Al-doped ZnO has been achieved by mixing the aqueous solution using zinc nitrate hexahydrate ($\text{Zn}(\text{NO}_3)_2 \cdot 6\text{H}_2\text{O}$) as the Zn precursor and hexamethylenetetramine (HMTA, $\text{C}_6\text{H}_{12}\text{N}_4$) as the reducing agent. Both chemicals were dissolved in deionized (DI) water at a concentration of 0.01 M. Then, aluminium nitrate nonahydrate ($\text{Al}(\text{NO}_3)_3 \cdot 9\text{H}_2\text{O}$) solution was added to the stock solution at concentrations

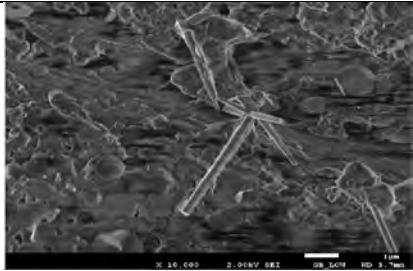
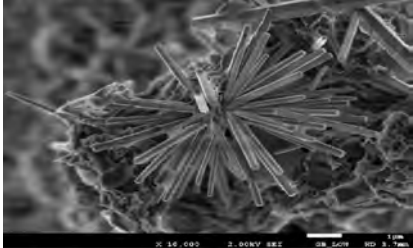
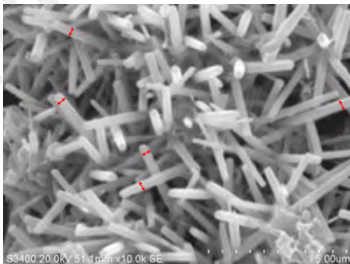
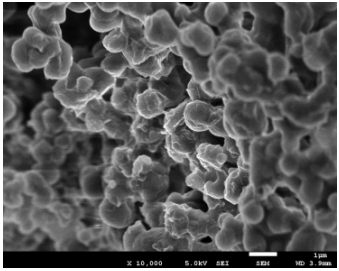
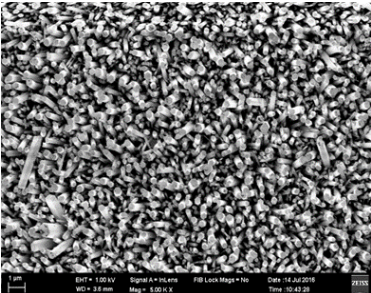
of 0.5, 1, 3 and 5 mol % Al with respect to Zn. The solution was stirred at 60 °C for 2 hours to yield a clear and homogenous solution and left overnight for aging. Subsequently, the seeded solution was prepared using zinc acetate dehydrate ($\text{Zn}(\text{CH}_3\text{COO})_2 \cdot 2\text{H}_2\text{O}$) as a precursor dissolved in isopropanol. 0.55 g zinc acetate dehydrate was mixed into 100 ml isopropanol. The solution was stirred at 60° C for 2 hours in ambient to yield a clear and homogenous solution. Then, the solution was cooled down to room temperature for the coating process. The changes of morphologies for Al-doped ZnO, when synthesized using different techniques of sol-gel method, for both seeded and non-seeded can be observed using Field Emission Scanning Electron Microscope (FESEM) and tabulated as shown by Table 6.1.

Table 6.1: Morphologies Al-Doped ZnO for different synthetization methods

Method		Tapered POF
Sol-gel	Non-seeded	
	Seeded	

Secondly, the synthesis of ZnO has been achieved by using different techniques, namely sol-gel and hydrothermal method. In sol-gel process, the seeded solution was prepared by dissolving zinc acetate dehydrate ($\text{Zn}(\text{CH}_3\text{COO})_2 \cdot 2\text{H}_2\text{O}$) as a precursor in isopropanol with a molarity of 0.025 M. The solution was stirred at 60 °C for 2 hours at ambient temperature to yield a clear and homogenous solution. Then, the solution was cooled down to room temperature for the coating process. Next, growing solution was prepared by dissolving 0.01 M zinc nitrate hexahydrate ($\text{Zn}(\text{NO}_3)_2 \cdot 6\text{H}_2\text{O}$) and 0.01 M hexamethylenetetramine (HMTA) in 100 ml deionized water. As for hydrothermal method, the process consists of four steps, namely preparing seeding solution, POF core surface treatment, forming nucleation site on POF core, and annealing. For ZnO nanoparticles solution, 0.0044 g of zinc acetate dehydrate [$\text{Zn}(\text{O}_2\text{CCH}_3)_2 \cdot 2\text{H}_2\text{O}$, Merck] were dissolved in 20 ml of ethanol to form 1 mM solution under slow stirring at temperature 50 °C for 30 minutes and then, the solution was let cooled in the room temperature for 5 minutes, and 20 ml of ethanol was added into the zinc acetate solution. Then, sodium hydroxide (NaOH) was dissolved in 20 ml ethanol in order to control the aqueous pH and the solution was then stirred slowly, hence, forming a 1 mM solution. The different morphologies of ZnO synthesized using the sol-gel and hydrothermal can be observed using Field Emission Scanning Electron Microscope (FESEM) and is organized as shown by Table 6.2.

Table 6.2: Morphologies of ZnO for different synthetization methods

Fiber	Method		Morphology
Plastic optical fiber (POF)	Sol-gel	Non-seeded	
		Seeded	
	Hydrothermal		
PMMA Microfiber	Sol-Gel	Non-seeded	
		Seeded	

Thirdly, a relative humidity sensor has been successfully developed by employing tapered POF and polymer microfiber that is coated with ZnO nanostructures. The POF used has an overall cladding diameter of 1 mm, while PMMA microfiber has a diameter of about 9 μm . For former fiber, the fiber is tapered using chemical etching method and direct drawing method is used to fabricate the latter. To investigate the performance of the proposed sensors, the output parameter against different value of relative humidity was recorded (refer Appendix A for the sample of data). The data were then plotted and analyzed graphically, and performance of the sensor can be deduced from the slope and R-squared function respectively. Sensitivity is a measurement obtained from the slope of the output characteristic curve, which is defined as the minimum input of physical parameter that will create a detectable output change. Meanwhile, R-square value measures a correlation coefficient, which is the reliability of linear relationship between input and output parameter values. It provides the closest possible best fit to all data points on the curve. When the percentage of linearity is high or close to 100%, it shows that the measured sensitivity will not vary with input variable. The data was further analyzed (refer Appendix B for sample of statistical analysis) in order to determine standard deviation and limit of detection. There is no difference to the output voltage as the standard deviation value falls into the acceptable limit, justifying the performance of the sensor. The overview of the results for the proposed sensors using POF and PMMA are presented in Table 6.3 and 6.4 respectively.

Table 6.3: Overview of the results for the proposed sensors using POF

Method		Sol-Gel				Hydrothermal
Sensitive material		Non-seeded ZnO	Seeded ZnO	Non-seeded Al-doped ZnO	Seeded Al-doped ZnO	ZnO
Performance	Sensitivity (mV/%)	0.0029	0.0258	0.0172	0.0386	0.0295
	Linearity (%)	93.3	95.42	97.5	97.84	98.38

Table 6.4: Overview of the results for the proposed sensors using PMMA Microfiber

Method		Sol-Gel			
Microfiber Fiber		Silica		PMMA	
Sensitive material		Non-seeded ZnO	Seeded ZnO	Non-seeded ZnO	Seeded ZnO
Performance	Sensitivity (mV/%)	0.0011	0.0038	0.1791	0.2159
	Linearity (%)	94.10	96.72	> 96	> 98

For the proposed sensor, sensing is based on the refractive index of the fiber, as the change in refractive index provides as an approach of the evanescent wave sensing. The sensitive material that is coated on the tapered region acts like a new cladding layer with a refractive index close to effective index of the propagating modes along the fiber. The optical properties of ZnO nanostructures are modulated by the surface adsorption of water molecules. When the ZnO nanostructures are exposed to humid environment, rapid surface adsorption of water molecules occur, as they have dry air on the surface. As the relative humidity increases, more water molecules will be absorbed on the ZnO nanostructures surfaces. The increasing water molecules cause an increase in both effective refractive index of the surrounding medium and absorption coefficient of the

ZnO nanostructures or nanorod surfaces, which leads to a larger leakage and absorption of light.

Therefore, the proposed sensors show that tapered fiber coated with ZnO that act like a sensitive material can be applied as a relative humidity sensor.

6.2 Recommendation for future work

The proposed sensors are able to be applied as relative humidity sensor. Nevertheless, the sensor can be improved further in future. One of the improvements that can be made is to enhance the synthesizing of ZnO nanostructures. Depending on the precursors used, as well as the synthesis conditions, there are other different synthesizing methods that can be explored, such as mechanochemical and precipitation process. ZnO is an element with the widest possible nanostructures, therefore, with the appropriate method, other nanostructures can be obtained that might improve the performance of the sensor. This is because, different surface morphologies will have different surface to volume ratio, thus different sensor performance. The more O ions or biomolecules are adsorbed on the surface of ZnO nanostructures, the higher the sensitivity of the sensor will be. As such, more comprehensive study can be done in future to leverage on this property of ZnO so that better performance of sensor that are more reliable and stable can be explored.

REFERENCES

- Ahuja, D., & Parande, D. (2012). Optical sensors and their applications. *Journal of Scientific Research and Reviews*, 1(5), 060-068.
- Alder, T., Stohr, A., Heinzelmann, R., & Jager, D. (2000). High-efficiency fiber-to-chip coupling using low-loss tapered single-mode fiber. *IEEE Photonics Technology Letters*, 12(8), 1016-1018.
- Ali, S. M. U., Ibupoto, Z. H., Kashif, M., Hashim, U., & Willander, M. (2012). A potentiometric indirect uric acid sensor based on ZnO nanoflakes and immobilized uricase. *Sensors*, 12(3), 2787-2797.
- Alias, S. S., Ismail, A. B., & Mohamad, A. A. (2010). Effect of pH on ZnO nanoparticle properties synthesized by sol-gel centrifugation. *Journal of Alloys and Compounds*, 499(2), 231-237.
- Arya, S. K., Saha, S., Ramirez-Vick, J. E., Gupta, V., Bhansali, S., & Singh, S. P. (2012). Recent advances in ZnO nanostructures and thin films for biosensor applications. *Analytica chimica acta*, 737, 1-21.
- Ascorbe, J., Corres, J., Arregui, F., & Matias, I. (2017). Recent developments in fiber optics humidity sensors. *Sensors*, 17(4), 893.
- Baratto, C., Todros, S., Faglia, G., Comini, E., Sberveglieri, G., Lettieri, S., ... & Maddalena, P. (2009). Luminescence response of ZnO nanowires to gas adsorption. *Sensors and Actuators B: Chemical*, 140(2), 461-466.
- Bariain, C., Matias, I. R., Romeo, I., Garrido, J., & Laguna, M. (2000). Detection of volatile organic compound vapors by using a vapochromic material on a tapered optical fiber. *Applied Physics Letters*, 77(15), 2274-2276.
- Baruah, S., & Dutta, J. (2009). Effect of seeded substrates on hydrothermally grown ZnO nanorods. *Journal of sol-gel science and technology*, 50(3), 456.
- Batumalay, M., Harith, Z., Rafaie, H. A., Ahmad, F., Khasanah, M., Harun, S. W., ... & Ahmad, H. (2014). Tapered plastic optical fiber coated with ZnO nanostructures for the measurement of uric acid concentrations and changes in relative humidity. *Sensors and Actuators A: Physical*, 210, 190-196.
- Batumalay, M., Lokman, A., Ahmad, F., Arof, H., Ahmad, H., & Harun, S. W. (2013). Tapered plastic optical fiber coated with HEC/PVDF for measurement of relative humidity. *IEEE Sens. J*, 13(12), 4702-4705.
- Beres, C., de Nazaré, F. V. B., de Souza, N. C. C., Miguel, M. A. L., & Werneck, M. M. (2011). Tapered plastic optical fiber-based biosensor—tests and application. *Biosensors and Bioelectronics*, 30(1), 328-332.
- Bilro, L., Alberto, N., Pinto, J. L., & Nogueira, R. (2012). Optical sensors based on plastic fibers. *Sensors*, 12(9), 12184-12207.

- Bohnert, K., Gabus, P., Nehring, J., Brandle, H., & Brunzel, M. G. (2007). Fiber-optic current sensor for electrowinning of metals. *Journal of lightwave technology*, 25(11), 3602-3609.
- Bognitzki, M., Czado, W., Frese, T., Schaper, A., Hellwig, M., Steinhart, M., ... & Wendorff, J. H. (2001). Nanostructured fibers via electrospinning. *Advanced Materials*, 13(1), 70-72.
- Brambilla, G., Finazzi, V., & Richardson, D. J. (2004). Ultra-low-loss optical fiber nanotapers. *Optics Express*, 12(10), 2258-2263.
- Carotta, M. C., Cervi, A. D., Di Natale, V., Gherardi, S., Giberti, A., Guidi, V., ... & Calestani, D. (2009). ZnO gas sensors: a comparison between nanoparticles and nanotetrapods-based thick films. *Sensors and Actuators B: Chemical*, 137(1), 164-169.
- Cennamo, N., D'Agostino, G., Galatus, R., Bibbò, L., Pesavento, M., & Zeni, L. (2013). Sensors based on surface plasmon resonance in a plastic optical fiber for the detection of trinitrotoluene. *Sensors and Actuators B: Chemical*, 188, 221-226.
- Chang, S. P., Chang, S. J., Lu, C. Y., Li, M. J., Hsu, C. L., Chiou, Y. Z., ... & Chen, I. C. (2010). A ZnO nanowire-based humidity sensor. *Superlattices and Microstructures*, 47(6), 772-778.
- Chen, D., Jiao, X., & Cheng, G. (1999). Hydrothermal synthesis of zinc oxide powders with different morphologies. *Solid State Communications*, 113(6), 363-366.
- Chen, G. Y., Newson, T. P., & Brambilla, G. (2013). Optical microfibers for fast current sensing. *Optical Fiber Technology*, 19(6), 802-807.
- Chiu, Y. S., Tseng, C. Y., & Lee, C. T. (2012). Nanostructured EGFET pH sensors with surface-passivated ZnO thin-film and nanorod array. *IEEE Sensors Journal*, 12(5), 930-934.
- Choopun, S., Tubtimtae, A., Santhaveesuk, T., Nilphai, S., Wongrat, E., & Hongstith, N. (2009). Zinc oxide nanostructures for applications as ethanol sensors and dye-sensitized solar cells. *Applied Surface Science*, 256(4), 998-1002.
- Coleman, V. A., & Jagadish, C. (2006). *Zinc oxide bulk, thin films and nanostructures*. UK, Elsevier, 1-5.
- Conforti, G., Brenci, M., Mencaglia, A., & Mignani, A. G. (1989). Fiber optic vibration sensor for remote monitoring in high power electric machines. *Applied optics*, 28(23), 5158-5161.
- Corres, J. M., Arregui, F. J., & Matías, I. R. (2007). Sensitivity optimization of tapered optical fiber humidity sensors by means of tuning the thickness of nanostructured sensitive coatings. *Sensors and Actuators B: Chemical*, 122(2), 442-449.
- Corres, J. M., Arregui, F. J., & Matias, I. R. (2006). Design of humidity sensors based on tapered optical fibers. *Journal of Lightwave Technology*, 24(11), 4329-4336.

- Corres, J. M., Matias, I. R., Hernaez, M., Bravo, J., & Arregui, F. J. (2008). Optical fiber humidity sensors using nanostructured coatings of SiO₂ nanoparticles. *IEEE Sensors Journal*, 8(3), 281-285.
- Cui, T., Cui, F., Zhang, J., Wang, J., Huang, J., Lü, C., ... & Yang, B. (2006). From monomeric nanofibers to PbS nanoparticles/polymer composite nanofibers through the combined use of γ -irradiation and gas/solid reaction. *Journal of the American Chemical Society*, 128(19), 6298-6299.
- Djurišić, A. B., Ng, A. M. C., & Chen, X. Y. (2010). ZnO nanostructures for optoelectronics: material properties and device applications. *Progress in quantum electronics*, 34(4), 191-259.
- Eggleton, B. J., Kerbage, C., Westbrook, P. S., Windeler, R. S., & Hale, A. (2001). Microstructured optical fiber devices. *Optics Express*, 9(13), 698-713.
- Elosua, C., Matias, I., Barriain, C., & Arregui, F. (2006). Volatile organic compound optical fiber sensors: A review. *Sensors*, 6(11), 1440-1465.
- Erol, A., Okur, S., Comba, B., Mermer, Ö., & Arıkan, M. C. (2010). Humidity sensing properties of ZnO nanoparticles synthesized by sol-gel process. *Sensors and Actuators B: Chemical*, 145(1), 174-180.
- Farahani, H., Wagiran, R., & Hamidon, M. (2014). Humidity sensors principle, mechanism, and fabrication technologies: a comprehensive review. *Sensors*, 14(5), 7881-7939.
- Fidanboyly, K. A., & Efendioglu, H. S. (2009, May). Fiber optic sensors and their applications. In *5th International Advanced Technologies Symposium (IATS'09)* (Vol. 6).
- Fortunato, E., Gonçalves, A., Pimentel, A., Barquinha, P., Gonçalves, G., Pereira, L., ... & Martins, R. (2009). Zinc oxide, a multifunctional material: from material to device applications. *Applied Physics A*, 96(1), 197-205.
- Fulati, A., Usman Ali, S. M., Riaz, M., Amin, G., Nur, O., & Willander, M. (2009). Miniaturized pH sensors based on zinc oxide nanotubes/nanorods. *Sensors*, 9(11), 8911-8923.
- Gao, P. X., Mai, W., & Wang, Z. L. (2006). Superelasticity and nanofracture mechanics of ZnO nanohelices. *Nano letters*, 6(11), 2536-2543.
- Gao, W., & Li, Z. (2009). Nanostructures of zinc oxide. *International Journal of Nanotechnology*, 6(3-4), 245-257.
- Gaston, A., Lozano, I., Perez, F., Auza, F., & Sevilla, J. (2003). Evanescent wave optical-fiber sensing (temperature, relative humidity, and pH sensors). *IEEE Sensors Journal*, 3(6), 806-811.
- Ghatak, A., & Thyagarajan, K. (1998). *An introduction to fiber optics*. Cambridge university press.

- Gholamzadeh, B., & Nabovati, H. (2008). Fiber optic sensors. *World Academy of Science, Engineering and Technology*, 42(3), 335-340.
- Gravina, R., Testa, G., & Bernini, R. (2009). Perfluorinated plastic optical fiber tapers for evanescent wave sensing. *Sensors*, 9(12), 10423-10433.
- Gu, F. X., & Tong, L. M. (2008, November). Polymer single-nanowire for optical humidity sensing. In *Optical Fiber Sensors Conference, 2008. APOS'08. 1st Asia-Pacific* (pp. 1-3). IEEE.
- G Gupta, B. D. (2001). A novel probe for a fiber optic humidity sensor. *Sensors and Actuators B: Chemical*, 80(2), 132-135.
- Haidekker, M. A., Akers, W. J., Fischer, D., & Theodorakis, E. A. (2006). Optical fiber-based fluorescent viscosity sensor. *Optics letters*, 31(17), 2529-2531.
- Heo, Y. W., Norton, D. P., Tien, L. C., Kwon, Y., Kang, B. S., Ren, F., ... & LaRoche, J. R. (2004). ZnO nanowire growth and devices. *Materials Science and Engineering: R: Reports*, 47(1-2), 1-47.
- Hernández-Romano, I., Monzón-Hernández, D., Moreno-Hernández, C., Moreno-Hernandez, D., & Villatoro, J. (2015). Highly sensitive temperature sensor based on a polymer-coated microfiber interferometer. *IEEE Photonics Technology Letters*, 27(24), 2591-2594.
- Huang, J., Dai, Y., Gu, C., Sun, Y., & Liu, J. (2013). Preparation of porous flower-like CuO/ZnO nanostructures and analysis of their gas-sensing property. *Journal of Alloys and Compounds*, 575, 115-122.
- Irawati, N., Rahman, H. A., Ahmad, H., & Harun, S. W. (2017). A PMMA microfiber loop resonator based humidity sensor with ZnO nanorods coating. *Measurement*, 99, 128-133.
- Ismaeel, R., Lee, T., Ding, M., Belal, M., & Brambilla, G. (2013). Optical microfiber passive components. *Laser & Photonics Reviews*, 7(3), 350-384.
- Jiang, G., Shi, R. F., & Garito, A. F. (1997). Mode coupling and equilibrium mode distribution conditions in plastic optical fibers. *IEEE Photonics Technology Letters*, 9(8), 1128-1130.
- Jiang, X., Song, Q., Xu, L., Fu, J., & Tong, L. (2007). Microfiber knot dye laser based on the evanescent-wave-coupled gain. *Applied physics letters*, 90(23), 233501.
- Jiang, X., Tong, L., Vienne, G., Guo, X., Tsao, A., Yang, Q., & Yang, D. (2006). Demonstration of optical microfiber knot resonators. *Applied Physics Letters*, 88(22), 223501.
- Jiaqiang, X., Yuping, C., Daoyong, C., & Jianian, S. (2006). Hydrothermal synthesis and gas sensing characters of ZnO nanorods. *Sensors and Actuators B: Chemical*, 113(1), 526-531.

- Jindal, R., Tao, S., Singh, J. P., & Gaikwad, P. (2002). High dynamic range fiber optic relative humidity sensor. *Optical Engineering*, 41(5), 1093-1097.
- Kharaz, A., & Jones, B. E. (1995). A distributed optical-fibre sensing system for multi-point humidity measurement. *Sensors and Actuators A: Physical*, 47(1-3), 491-493.
- Kobyakov, A., Sauer, M., & Chowdhury, D. (2010). Stimulated Brillouin scattering in optical fibers. *Advances in optics and photonics*, 2(1), 1-59.
- Kou, J. L., Feng, J., Wang, Q. J., Xu, F., & Lu, Y. Q. (2010). Microfiber-probe-based ultrasmall interferometric sensor. *Optics letters*, 35(13), 2308-2310.
- Kersey, A. D. (1996). A review of recent developments in fiber optic sensor technology. *Optical fiber technology*, 2(3), 291-317.
- Khijwania, S. K., Srinivasan, K. L., & Singh, J. P. (2005). An evanescent-wave optical fiber relative humidity sensor with enhanced sensitivity. *Sensors and Actuators B: Chemical*, 104(2), 217-222.
- Kim, H., Horwitz, J. S., Qadri, S. B., & Chrisey, D. B. (2002). Epitaxial growth of Al-doped ZnO thin films grown by pulsed laser deposition. *Thin Solid Films*, 420, 107-111.
- Kim, Y. J., Yoon, A., Kim, M., Yi, G. C., & Liu, C. (2011). Hydrothermally grown ZnO nanostructures on few-layer graphene sheets. *Nanotechnology*, 22(24), 245603.
- Kim, Y. J., Yoo, H., Lee, C. H., Park, J. B., Baek, H., Kim, M., & Yi, G. C. (2012). Position - and morphology - controlled ZnO nanostructures grown on graphene layers. *Advanced Materials*, 24(41), 5565-5569.
- Kołodziejczak-Radzimska, A., & Jesionowski, T. (2014). Zinc oxide—from synthesis to application: a review. *Materials*, 7(4), 2833-2881.
- Kong, X. Y., & Wang, Z. L. (2004). Polar-surface dominated ZnO nanobelts and the electrostatic energy induced nanohelices, nanosprings, and nanospirals. *Applied physics letters*, 84(6), 975-977.
- Kronenberg, P., Rastogi, P. K., Giaccari, P., & Limberger, H. G. (2002). Relative humidity sensor with optical fiber Bragg gratings. *Optics letters*, 27(16), 1385-1387.
- Kuang, J. H., Chen, P. C., & Chen, Y. C. (2010). Plastic optical fiber displacement sensor based on dual cycling bending. *Sensors*, 10(11), 10198-10210.
- Leal-Junior, A. G., Frizera, A., & Pontes, M. J. (2018). Dynamic compensation technique for POF curvature sensors. *Journal of Lightwave Technology*, 36(4), 1112-1117.
- Lee, H., Inoue, Y., Kim, M., Ren, X., & Kim, I. (2018). Effective Formation of Well-Defined Polymeric Microfibers and Nanofibers with Exceptional Uniformity by Simple Mechanical Needle Spinning. *Polymers*, 10(9), 980.

- Lee, J. H., Leu, C., Chung, Y. W., & Hon, M. H. (2006). Fabrication of ordered ZnO hierarchical structures controlled via surface charge in the electrophoretic deposition process. *Nanotechnology*, 17(17), 4445.
- Lee, S. T., Aneeshkumar, B., Radhakrishnan, P., Vallabhan, C. P. G., & Nampoore, V. P. N. (2002). A microbent fiber optic pH sensor. *Optics Communications*, 205(4-6), 253-256.
- Leung, A., Shankar, P. M., & Mutharasan, R. (2007). A review of fiber-optic biosensors. *Sensors and Actuators B: Chemical*, 125(2), 688-703.
- Li, D., & Xia, Y. (2004). Electrospinning of nanofibers: reinventing the wheel?. *Advanced materials*, 16(14), 1151-1170.
- Li, E., Wang, X., & Zhang, C. (2006). Fiber-optic temperature sensor based on interference of selective higher-order modes. *Applied physics letters*, 89(9), 091119.
- Lim, K. S., Harun, S. W., Damanhuri, S. S. A., Jasim, A. A., Tio, C. K., & Ahmad, H. (2011). Current sensor based on microfiber knot resonator. *Sensors and Actuators A: Physical*, 167(1), 60-62.
- Lin, J., Ding, B., & Yu, J. (2010). Direct fabrication of highly nanoporous polystyrene fibers via electrospinning. *ACS applied materials & interfaces*, 2(2), 521-528.
- Liu, B., & Zeng, H. C. (2003). Hydrothermal synthesis of ZnO nanorods in the diameter regime of 50 nm. *Journal of the American Chemical Society*, 125(15), 4430-4431.
- Liu, Y., Zhang, Y., Lei, H., Song, J., Chen, H., & Li, B. (2012). Growth of well-arrayed ZnO nanorods on thinned silica fiber and application for humidity sensing. *Optics express*, 20(17), 19404-19411.
- Lou, J., Wang, Y., & Tong, L. (2014). Microfiber optical sensors: A review. *Sensors*, 14(4), 5823-5844.
- Lupan, O., Emelchenko, G. A., Ursaki, V. V., Chai, G., Redkin, A. N., Gruzintsev, A. N., ... & Heinrich, H. (2010). Synthesis and characterization of ZnO nanowires for nanosensor applications. *Materials Research Bulletin*, 45(8), 1026-1032.
- Ma, S., Li, R., Lv, C., Xu, W., & Gou, X. (2011). Facile synthesis of ZnO nanorod arrays and hierarchical nanostructures for photocatalysis and gas sensor applications. *Journal of hazardous materials*, 192(2), 730-740.
- MacCraith, B. D., McDonagh, C. M., O'keeffe, G., McEvoy, A. K., Butler, T., & Sheridan, F. R. (1995). Sol-gel coatings for optical chemical sensors and biosensors. *Sensors and Actuators B: Chemical*, 29(1-3), 51-57.
- Madathil, A. N. P., Vanaja, K. A., & Jayaraj, M. K. (2007, September). Synthesis of ZnO nanoparticles by hydrothermal method. In *Nanophotonic Materials IV* (Vol. 6639, p. 66390J). International Society for Optics and Photonics.

- Major, C., Nemeth, A., Radnoczi, G., Czigany, Z., Fried, M., Labadi, Z., & Barsony, I. (2009). Optical and electrical characterization of aluminium doped ZnO layers. *Applied Surface Science*, 255(21), 8907-8912.
- Md Sin, N. D., Fuad Kamel, M., Alip, R. I., Mohamad, Z., & Rusop, M. (2011). The electrical characteristics of aluminium doped zinc oxide thin film for humidity sensor applications. *Advances in Materials Science and Engineering*, 2011.
- Megelski, S., Stephens, J. S., Chase, D. B., & Rabolt, J. F. (2002). Micro- and nanostructured surface morphology on electrospun polymer fibers. *Macromolecules*, 35(22), 8456-8466.
- Mehta, A., Mohammed, W., & Johnson, E. G. (2003). Multimode interference-based fiber-optic displacement sensor. *IEEE Photonics Technology Letters*, 15(8), 1129-1131.
- Muhammad, M. Z., Jasim, A. A., Ahmad, H., Arof, H., & Harun, S. W. (2013). Non-adiabatic silica microfiber for strain and temperature sensors. *Sensors and Actuators A: Physical*, 192, 130-132.
- Mondal, S. B. S. R., Bhattacharyya, S. R., & Mitra, P. (2013). Effect of Al doping on microstructure and optical band gap of ZnO thin film synthesized by successive ion layer adsorption and reaction. *Pramana*, 80(2), 315-326.
- Morisawa, M., & Muto, S. (2012). Plastic optical fiber sensing of alcohol concentration in liquors. *Journal of Sensors*, 2012.
- Mridha, S., & Basak, D. (2007). Aluminium doped ZnO films: electrical, optical and photoresponse studies. *Journal of Physics D: Applied Physics*, 40(22), 6902.
- Nagata, J., Honma, S., Morisawa, M., & Muto, S. (2008, January). Development of polymer optical waveguide-type alcohol sensor. In *Advanced Materials and Devices for Sensing and Imaging III* (Vol. 6829, p. 682920). International Society for Optics and Photonics.
- Nain, A. S., Wong, J. C., Amon, C., & Sitti, M. (2006). Drawing suspended polymer micro-/nanofibers using glass micropipettes. *Applied Physics Letters*, 89(18), 183105.
- Noy, A., Miller, A. E., Klare, J. E., Weeks, B. L., Woods, B. W., & De Yoreo, J. J. (2002, November). Fabrication of luminescent nanostructures by dip-pen nanolithography. In *Nanoscale Optics and Applications* (Vol. 4809, pp. 249-255). International Society for Optics and Photonics.
- Ong, Y. S., Kam, W., Harun, S. W., & Zakaria, R. (2015). Fabrication of polymer microfiber through direct drawing and splicing of silica microfiber via vapor spray and flame treatment. *Applied Optics*, 54(13), 3863-3867.
- Otsuki, S., Adachi, K., & Taguchi, T. (1998). A novel fiber-optic gas-sensing configuration using extremely curved optical fibers and an attempt for optical humidity detection. *Sensors and Actuators B: Chemical*, 53(1-2), 91-96.

- Özgür, Ü., Alivov, Y. I., Liu, C., Teke, A., Reshchikov, M. A., Doğan, S., ... & Morkoç, H. (2005). A comprehensive review of ZnO materials and devices. *Journal of applied physics*, 98(4), 11.
- Ozgur, U., Hofstetter, D., & Morkoc, H. (2010). ZnO devices and applications: a review of current status and future prospects. *Proceedings of the IEEE*, 98(7), 1255-1268.
- Peters, K. (2010). Polymer optical fiber sensors—a review. *Smart materials and structures*, 20(1), 013002.
- Polynkin, P., Polynkin, A., Peyghambarian, N., & Mansuripur, M. (2005). Evanescent field-based optical fiber sensing device for measuring the refractive index of liquids in microfluidic channels. *Optics letters*, 30(11), 1273-1275.
- Prajapati, C. S., Kushwaha, A., & Sahay, P. P. (2013). Effect of Al dopants on the structural, optical and gas sensing properties of spray-deposited ZnO thin films. *Materials Chemistry and Physics*, 142(1), 276-285.
- Qi, Q., Zhang, T., Yu, Q., Wang, R., Zeng, Y., Liu, L., & Yang, H. (2008). Properties of humidity sensing ZnO nanorods-base sensor fabricated by screen-printing. *Sensors and Actuators B: Chemical*, 133(2), 638-643.
- Qin, Y., Wang, X., & Wang, Z. L. (2008). Microfibre–nanowire hybrid structure for energy scavenging. *Nature*, 451(7180), 809.
- Qiu, Y., & Yang, S. (2007). ZnO Nanotetrapods: Controlled Vapor - Phase Synthesis and Application for Humidity Sensing. *Advanced Functional Materials*, 17(8), 1345-1352.
- Rahman, H. A., Harun, S. W., Yasin, M., Phang, S. W., Damanhuri, S. S. A., Arof, H., & Ahmad, H. (2011). Tapered plastic multimode fiber sensor for salinity detection. *Sensors and Actuators A: Physical*, 171(2), 219-222.
- Rajan, G., Liu, B., Luo, Y., Ambikairajah, E., & Peng, G. D. (2013). High sensitivity force and pressure measurements using etched singlemode polymer fiber Bragg gratings. *IEEE Sensors Journal*, 13(5), 1794-1800.
- Rao, B. G., Mukherjee, D., & Reddy, B. M. (2017). Novel approaches for preparation of nanoparticles. In *Nanostructures for Novel Therapy* (pp. 1-36).
- Renganathan, B., Sastikumar, D., Gobi, G., Yogamalar, N. R., & Bose, A. C. (2011). Nanocrystalline ZnO coated fiber optic sensor for ammonia gas detection. *optics & laser technology*, 43(8), 1398-1404.
- Ridhuan, N. S., Razak, K. A., Lockman, Z., & Aziz, A. A. (2012). Structural and morphology of ZnO nanorods synthesized using ZnO seeded growth hydrothermal method and its properties as UV sensing. *PloS one*, 7(11), e50405.
- Rosolem, J. B., Dini, D. C., Penze, R. S., Florida, C., Leonardi, A. A., Loichate, M. D., & Durelli, A. S. (2013). Fiber optic bending sensor for water level monitoring: development and field test: a review. *IEEE Sensors Journal*, 13(11), 4113-4120.

- Schmidt-Mende, L., & MacManus-Driscoll, J. L. (2007). ZnO–nanostructures, defects, and devices. *Materials today*, 10(5), 40-48.
- Shi, L., Chen, X., Liu, H., Chen, Y., Ye, Z., Liao, W., & Xia, Y. (2006). Fabrication of submicron-diameter silica fibers using electric strip heater. *Optics express*, 14(12), 5055-5060.
- Shin, J. D., & Park, J. (2013). Plastic optical fiber refractive index sensor employing an in-line submillimeter hole. *IEEE Photon. Technol. Lett*, 25(19), 1041-1135.
- Stiebeiner, A., Garcia-Fernandez, R., & Rauschenbeutel, A. (2010). Design and optimization of broadband tapered optical fibers with a nanofiber waist. *Optics express*, 18(22), 22677-22685.
- Sun, Z., Liao, T., Dou, Y., Hwang, S. M., Park, M. S., Jiang, L., ... & Dou, S. X. (2014). Generalized self-assembly of scalable two-dimensional transition metal oxide nanosheets. *Nature communications*, 5, 3813.
- Tai, W. P., & Oh, J. H. (2002). Humidity sensing behaviors of nanocrystalline Al-doped ZnO thin films prepared by sol–gel process. *Journal of Materials Science: Materials in Electronics*, 13(7), 391-394.
- Tereshchenko, A., Bechelany, M., Viter, R., Khranovskyy, V., Smyntyna, V., Starodub, N., & Yakimova, R. (2016). Optical biosensors based on ZnO nanostructures: advantages and perspectives. A review. *Sensors and Actuators B: Chemical*, 229, 664-677.
- Tennyson, R. C., Mufti, A. A., Rizkalla, S., Tadros, G., & Benmokrane, B. (2001). Structural health monitoring of innovative bridges in Canada with fiber optic sensors. *Smart materials and Structures*, 10(3), 560.
- Tian, Y., Wang, W., Wu, N., Zou, X., & Wang, X. (2011). Tapered optical fiber sensor for label-free detection of biomolecules. *Sensors*, 11(4), 3780-3790.
- Tian, Z., Yam, S. S., & Loock, H. P. (2008). Refractive index sensor based on an abrupt taper Michelson interferometer in a single-mode fiber. *Optics letters*, 33(10), 1105-1107.
- Umar, A., Kim, B. K., Kim, J. J., & Hahn, Y. B. (2007). Optical and electrical properties of ZnO nanowires grown on aluminium foil by non-catalytic thermal evaporation. *Nanotechnology*, 18(17), 175606.
- Vienne, G., Li, Y., & Tong, L. (2007). Effect of host polymer on microfiber resonator. *IEEE Photonics Technology Letters*, 19(18), 1386-1388.
- Vohra, S. T., Bucholtz, F., & Kersey, A. D. (1991). Fiber-optic dc and low-frequency electric-field sensor. *Optics letters*, 16(18), 1445-1447.
- Wang, C., Chen, H., & Ma, J. (2011, July). The fiber-optic evanescent wave fluorescence sensor with a novel sensing architecture for determining penicillin G. In *Electronics and Optoelectronics (ICEOE), 2011 International Conference on* (Vol. 3, pp. V3-12). IEEE.

- Wang, J. X., Sun, X. W., Wei, A., Lei, Y., Cai, X. P., Li, C. M., & Dong, Z. L. (2006). Zinc oxide nanocomb biosensor for glucose detection. *Applied Physics Letters*, 88(23), 233106.
- Wang, J. X., Sun, X. W., Yang, Y., Huang, H., Lee, Y. C., Tan, O. K., & Vayssieres, L. (2006). Hydrothermally grown oriented ZnO nanorod arrays for gas sensing applications. *Nanotechnology*, 17(19), 4995.
- Wang, L., Kang, Y., Liu, X., Zhang, S., Huang, W., & Wang, S. (2012). ZnO nanorod gas sensor for ethanol detection. *Sensors and Actuators B: Chemical*, 162(1), 237-243.
- Wang, Z. L. (2004). Nanostructures of zinc oxide. *Materials today*, 7(6), 26-33.
- Wang, Y., Yeow, J. T., & Chen, L. Y. (2008, November). Synthesis of aligned zinc oxide nanorods for humidity sensing. In *Sensing Technology, 2008. ICST 2008. 3rd International Conference on* (pp. 670-673). IEEE.
- Wei, M., Zhi, D., & MacManus-Driscoll, J. L. (2005). Self-catalysed growth of zinc oxide nanowires. *Nanotechnology*, 16(8), 1364.
- Wei, Y., Li, Y., Liu, X., Xian, Y., Shi, G., & Jin, L. (2010). ZnO nanorods/Au hybrid nanocomposites for glucose biosensor. *Biosensors and Bioelectronics*, 26(1), 275-278.
- Willander, M., Nur, O., Fakhar-e-Alam, M., Sadaf, J. R., Israr, M. Q., Sultana, K., ... & Asif, M. H. (2011, March). Applications of zinc oxide nanowires for biophotonics and bio-electronics. In *Oxide-based Materials and Devices II* (Vol. 7940, p. 79400F). International Society for Optics and Photonics.
- Wo, J., Wang, G., Cui, Y., Sun, Q., Liang, R., Shum, P. P., & Liu, D. (2012). Refractive index sensor using microfiber-based Mach-Zehnder interferometer. *Optics letters*, 37(1), 67-69.
- Wolchover, N. A., Luan, F., George, A. K., Knight, J. C., & Omenetto, F. G. (2007). High nonlinearity glass photonic crystal nanowires. *Optics express*, 15(3), 829-833.
- Wolfbeis, O. S. (2005). Materials for fluorescence-based optical chemical sensors. *Journal of Materials Chemistry*, 15(27-28), 2657-2669.
- Wu, Y., Zhang, T., Rao, Y., & Gong, Y. (2011). Miniature interferometric humidity sensors based on silica/polymer microfiber knot resonators. *Sensors and Actuators B: Chemical*, 155(1), 258-263.
- Xiong, F. B., Zhu, W. Z., Meng, X. G., Lin, H. F., Huang, X. H., & Huang, Y. Q. (2013). Monitor light water concentration in deuterium oxide by evanescent absorption sensor. *Optik-International Journal for Light and Electron Optics*, 124(15), 2008-2012.
- Xu, F., Horak, P., & Brambilla, G. (2007). Optical microfiber coil resonator refractometric sensor. *Optics Express*, 15(12), 7888-7893.

- Xu, F., Pruneri, V., Finazzi, V., & Brambilla, G. (2008). An embedded optical nanowire loop resonator refractometric sensor. *Optics express*, 16(2), 1062-1067.
- Yadav, T. K., Narayanaswamy, R., Bakar, M. A., Kamil, Y. M., & Mahdi, M. A. (2014). Single mode tapered fiber-optic interferometer based refractive index sensor and its application to protein sensing. *Optics express*, 22(19), 22802-22807.
- Yakimova, R., Selegård, L., Khranovskyy, V., Pearce, R., Lloyd Spetz, A., & Uvdal, K. (2012). ZnO materials and surface tailoring for biosensing. *Frontiers in bioscience (Elite edition)*, 4(1), 254-278.
- Yang, Q., Jiang, X., Gu, F., Ma, Z., Zhang, J., & Tong, L. (2008). Polymer micro or nanofibers for optical device applications. *Journal of applied polymer science*, 110(2), 1080-1084.
- Yeo, T. L., Sun, T., & Grattan, K. T. V. (2008). Fibre-optic sensor technologies for humidity and moisture measurement. *Sensors and Actuators A: Physical*, 144(2), 280-295.
- Yoon, M. S., Park, S., & Han, Y. G. (2012). Simultaneous measurement of strain and temperature by using a micro-tapered fiber grating. *Journal of Lightwave Technology*, 30(8), 1156-1160.
- Yuan, J., & El-Sherif, M. A. (2003). Fiber-optic chemical sensor using polyaniline as modified cladding material. *IEEE sensors journal*, 3(1), 5-12.
- Zhang, C., Zhang, W., Webb, D. J., & Peng, G. D. (2010). Optical fibre temperature and humidity sensor. *Electronics Letters*, 46(9), 643-644.
- Zhang, H., Yang, D., Ma, X., Ji, Y., Xu, J., & Que, D. (2004). Synthesis of flower-like ZnO nanostructures by an organic-free hydrothermal process. *Nanotechnology*, 15(5), 622.
- Zhang, Y., Lin, B., Tjin, S. C., Zhang, H., Wang, G., Shum, P., & Zhang, X. (2010). Refractive index sensing based on higher-order mode reflection of a microfiber Bragg grating. *Optics express*, 18(25), 26345-26350.
- Zhang, Y., Yu, K., Jiang, D., Zhu, Z., Geng, H., & Luo, L. (2005). Zinc oxide nanorod and nanowire for humidity sensor. *Applied Surface Science*, 242(1-2), 212-217.
- Zhao, X., Li, M., & Lou, X. (2014). Sol-gel assisted hydrothermal synthesis of ZnO microstructures: Morphology control and photocatalytic activity. *Advanced Powder Technology*, 25(1), 372-378.
- Zhao, Z., Lei, W., Zhang, X., Wang, B., & Jiang, H. (2010). ZnO-based amperometric enzyme biosensors. *Sensors*, 10(2), 1216-1231.
- Tian, Z., & Yam, S. S. H. (2009). In-line abrupt taper optical fiber Mach-Zehnder interferometric strain sensor. *IEEE Photonics Technology Letters*, 21(3), 161-163.

Zubia, J., & Arrue, J. (2001). Plastic optical fibers: An introduction to their technological processes and applications. *Optical fiber technology*, 7(2), 101-140.

University of Malaya

LIST OF PUBLICATIONS AND PAPERS PRESENTED

Papers Published:

1. **Harith, Z.**, Batumalay, M., Irawati, N., Harun, S. W., & Ahmad, H. (2019, January). Polymer Microfiber Coated with ZnO for Humidity Sensing. In *Journal of Physics: Conference Series* (Vol. 1151, No. 1, p. 012019). IOP Publishing.
2. **Harith, Z.**, Batumalay, M., Irawati, N., Harun, S. W., Arof, H., & Ahmad, H. (2017). Relative humidity sensor employing tapered Plastic Optical Fiber coated with seeded Al-Doped ZnO. *Optik-International Journal for Light and Electron Optics*.
3. Lokman, A., Arof, H., Harun, S. W., **Harith, Z.**, Rifaie, H. A., & Nor, R. M. (2016). Optical Fiber Relative Humidity Sensor Based on Inline Mach–Zehnder Interferometer with ZnO Nanowires Coating. *Sensors Journal, IEEE*, 16(2), 312-316.
4. **Harith, Z.**, Irawati, N., Rifaie, H. A., Batumalay, M., Harun, S. W., Nor, R. M., & Ahmad, H. (2015). Tapered plastic optical fiber coated with Al-Doped ZnO nanostructures for detecting relative humidity. *IEEE Sensors Journal*, 15(2), 845-849.
5. **Harith, Z.**, Irawati, N., Batumalay, M., Rifaie, H. A., Yun II, G., Harun, S. W., & Ahmad, H. (2015). Relative humidity sensor employing optical fibers coated with ZnO nanostructures. *Indian Journal of Science and Technology*, 8(35).
6. Lokman, A., Harun, S. W., **Harith, Z.**, Rifaie, H. A., Nor, R. M., & Arof, H. (2015). Inline Mach–Zehnder interferometer with ZnO nanowires coating for the measurement of uric acid concentrations. *Sensors and Actuators A: Physical*, 234, 206-211.
7. Batumalay, M., **Harith, Z.**, Rifaie, H. A., Ahmad, F., Khasanah, M., Harun, S. W., & Ahmad, H. (2014). Tapered plastic optical fiber coated with ZnO nanostructures for the measurement of uric acid concentrations and changes in relative humidity. *Sensors and Actuators A: Physical*, 210, 190-196.